DEFENSE TECHNICAL INFORMATION CENTER

Information for the Defense Community

DTIC® has determined on 10/5/2010 that this Technical Document has the Distribution Statement checked below. The current distribution for this document can be found in the DTIC® Technical Report Database.

☑ **DISTRIBUTION STATEMENT A.** Approved for public release; distribution is unlimited.

☐ **© COPYRIGHTED**; U.S. Government or Federal Rights License. All other rights and uses except those permitted by copyright law are reserved by the copyright owner.

☐ **DISTRIBUTION STATEMENT B.** Distribution authorized to U.S. Government agencies only (fill in reason) (date of determination). Other requests for this document shall be referred to (insert controlling DoD office)

☐ **DISTRIBUTION STATEMENT C.** Distribution authorized to U.S. Government Agencies and their contractors (fill in reason) (date of determination). Other requests for this document shall be referred to (insert controlling DoD office)

☐ **DISTRIBUTION STATEMENT D.** Distribution authorized to the Department of Defense and U.S. DoD contractors only (fill in reason) (date of determination). Other requests shall be referred to (insert controlling DoD office).

☐ **DISTRIBUTION STATEMENT E.** Distribution authorized to DoD Components only (fill in reason) (date of determination). Other requests shall be referred to (insert controlling DoD office).

☐ **DISTRIBUTION STATEMENT F.** Further dissemination only as directed by (inserting controlling DoD office) (date of determination) or higher DoD authority.

Distribution Statement F is also used when a document does not contain a distribution statement and no distribution statement can be determined.

☐ **DISTRIBUTION STATEMENT X.** Distribution authorized to U.S. Government Agencies and private individuals or enterprises eligible to obtain export-controlled technical data in accordance with DoDD 5230.25; (date of determination). DoD Controlling Office is (insert controlling DoD office).

SPACE. TELECOMMUNICATIONS AND RADIOSCIENCE LABORATORY

STARLAB
DEPARTMENT OF ELECTRICAL ENGINEERING / SEL
STANFORD UNIVERSITY • STANFORD, CA 94305

INTERACTION WITH THE LOWER IONOSPHERE OF ELECTROMAGNETIC PULSES FROM LIGHTNING: HEATING, ATTACHMENT, IONIZATION, AND OPTICAL EMISSIONS

Yuri Nicholaevich Taranenko

September, 1993

INTERACTION WITH THE LOWER IONOSPHERE OF ELECTROMAGNETIC PULSES FROM LIGHTNING: HEATING, ATTACHMENT, IONIZATION, AND OPTICAL EMISSIONS

A DISSERTATION
SUBMITTED TO THE DEPARTMENT OF ELECTRICAL ENGINEERING
AND THE COMMITTEE ON GRADUATE STUDIES
OF STANFORD UNIVERSITY
IN PARTIAL FULFILLMENT OF THE REQUIREMENTS
FOR THE DEGREE OF
DOCTOR OF PHILOSOPHY

By
Yuri Nicholaevich Taranenko
September, 1993

I certify that I have read this dissertation and that in my opinion it is fully adequate, in scope and quality, as a dissertation for the degree of Doctor of Philosophy.

Umran S. Inan (Principal Advisor)

I certify that I have read this dissertation and that in my opinion it is fully adequate, in scope and quality, as a dissertation for the degree of Doctor of Philosophy.

Timothy F. Bell

I certify that I have read this dissertation and that in my opinion it is fully adequate, in scope and quality, as a dissertation for the degree of Doctor of Philosophy.

Dwight G. Nishimura

Approved for the University Committee on Graduate Studies:

To my family

Abstract

A typical lightning discharge produces an intense 20 gigawatt electromagnetic (EM) pulse of 50 to 150 μs duration. A significant portion of this energy propagates upward where it interacts with the ambient electrons in the collisional lower ionosphere. In the present work the Boltzmann kinetic equation for electrons and Maxwell's equations for the EM fields are self-consistently solved to simulate the interaction of lightning radiated EM pulses with the lower ionosphere. Results indicate that attachment, ionization, and optical emissions produced in this interaction are sufficient to explain 'early' subionospheric VLF signal perturbations and airglow brightening observed simultaneously with lightning. This model also provides the basis for the quantitative evaluation of a wide variety of electrodynamic and chemical processes in the ionosphere which occur in response to the energy released in lightning discharges. Under nighttime conditions, individual pulses with peak amplitudes of 10–20 V/m (normalized to 100 km free space distance) produce changes in electron density of 1–30% of the ambient while a sequence of such pulses leads to more than 100 % modification at altitudes between 85 and 92 km. Among the optical emissions, the most promising for observations are the 1st (red) and 2nd (blue) positive bands of N_2, which emit at rates of 7×10^7 and 10^7 $cm^{-3}s^{-1}$ at ~92 km respectively for a 20 V/m EM pulse. The height integrated intensities of the emissions reach 4×10^7 and 6×10^6 R, last for ~50 μs and produce 1,200 and 200 Rayleigh-seconds for zenith observations.

Preface

The three years I spent at Stanford were the most interesting and exciting years of my life. Learning opportunities and means to achieve scientific results are really superb at this Farm. Working at the STAR Laboratory fulfilled my childhood and adolescent dreams about interstellar space exploration. In a sense I worked with problems that are not related to stars themselves but I was moved by the same feeling that someone might have when looking at a mysterious wonder, like a star or the world itself.

However, my greatest admiration goes to the people whom I met and worked with at Stanford and in the neighbourhood. Their integrity, generosity, and understanding of problems of someone who arrived to a new country were such a cheerful experience during these years.

I am very thankful to my advisor Prof. Umran Inan and to my associate advisor Dr. Tim Bell for their trust in me as a potential student that allowed me to cross the ocean, for introducing me to a problem that resulted in this thesis, and for their guidance in solving it. I am also thankful to them for helping me solve numerous everyday problems which I and my family encountered during these three years. I am very impressed by their unique combination in seeing new and exciting scientific problems and finding ways of solving them in the real world. Their enthusiasm in going through all the challenges of scientific exploration is an example I would like to follow.

I appreciate collaborations with Prof. Leonid Kazovsky from whom I learned about the importance of a clear scientific presentation and with Prof. Peter Sturrock who showed me the importance of an ability for deep physical insight.

I am thankful to Professors Bob Helliwell, Martin Walt, Ron Bracewell, and Dr. Vikas Sonwalker for reviewing my papers before they were submitted for publication and making a lot of suggestions for their improvements.

I would like to express my gratitude to Professors Fabian Pease and Greg Kovacs for taking time in spite of their busy schedules and serving on the committee for my Ph.D. defense and to Prof. Dwight Nishimura for serving as the third reader at a very critical time prior to the beginning of a new academic year when it seemed to me that almost every Professor in the Department was busy or out of town.

I express my delight in writing this manuscript using TeX macros written by Dr. Bill Burgess and I am very thankful to him for saving me a lot of valuable time.

I am grateful for discussions on various topics and help I got from Prof. Oscar Buneman, Prof. Don Carpenter, Prof. Tony Fraser-Smith, Jerry Yarbrough, Bill Trabucco, and present and former students of the VLF group: Lee Poulsen, Bill Burgess, Sean Lev_Tov, Juan Rodriguez, Jasna Ristić-Djurović, Sasha Draganov, Viktor Pasko, Steve Cummer, Dave Lauben, Thomas Mielke, Dave Shafer, Steve Reising, Alan Brown, Chris Regan, Mark Danielson, Darren Hakeman, and Chem Lin.

I am grateful to Mr. Tom Sege and Mrs. Dorothy Sege, Mr. Bob Thorburn and Mrs. Jean Thorburn, Mr. Jaroslav Merkelo and Mrs. Stefanie Merkelo, Mr. Vitaly Vizyr and Mrs. Vira Vizyr, Mr. Henry Milcharski and Mrs. Lyalya Milcharski, Mr. Mike Sullivan and Mrs. Oksana Sullivan who generously supported me and my family in many different ways during these three years that made my living and working at Stanford much less frustrating and more effective than it would be otherwise.

This thesis would not be possible without the experience and background which I have acquired working back in Kyiv and Moscow with Prof. Nicholai Kotsarenko, Dr.

Gennadii Burlak, and Dr. Vitaly Chmyrev whom I thank for the time and efforts they spent for me. Also I am grateful to Dr. Vitaly Chmyrev for introducing me to Prof. Umran Inan and Dr. Tim Bell at a crucial point at the beginning of the long road which finalized in this Ph.D. thesis.

I want to express many thanks to Mrs. June Hua Wang and Mrs. Jenny Xu who helped me a lot with their secretarial work during these years.

I dedicate this thesis to my mother Svetlana and my father Nicholai Taranenko, my wife Nina, my daughter Christina, my mother-in-law Raisa and my father-in-law Leonid Zarubin, and to other members of my family whose contribution is beyond words and without whom I would not be what I am now.

YURI N. TARANENKO

Stanford, California
September 25, 1993

This research was supported by the National Aeronautics and Space Administration under grant NAGW-2871 to Stanford University.

Contents

Tables

Illustrations

1

Introduction

On the average, approximately 100 lightning discharges occur per second over our planet, in approximately 2000 thunderstorm centers which are active at any given time [*Chambers*, 1967]. The EM power radiated by a cloud-to-ground return lightning stroke may on the average be 20 GW lasting for $\sim$100 μs (Section 1.1). The cumulative effects of these electrical discharges influence many aspects of human life and the global atmospheric environment. Among the prominent lightning effects which we hear of in daily news broadcasts are the disturbances in power and communication systems, ignition of forest fires, and even sometimes direct injuries and death caused by cloud-to-ground lightning discharges. Lightning also influences atmospheric electric currents [e.g., *Tzur and Roble*, 1985; *Uman*, 1987; p. 8], charged particle populations in the magnetosphere [e.g., *Voss et al.*, 1984; *Burgess and Inan.*, 1993], and the radio environment in the Earth-ionosphere waveguide [e.g., *Uman*, 1987; p. 110; *Lewinstein.*, 1976].

The purpose of this research is to consider a new form of electrodynamic, thermal and aeronomic coupling of electromagnetic (EM) energy originating in lightning discharges to the mesosphere and the lower ionosphere. This new means of coupling was discovered in the course of recent measurements of ionospheric disturbances associated with lightning-induced electron precipitation (LEP) from the magnetosphere [*Inan et al.*, 1988]. The latter is now a well known means by which the lower ionosphere is regularly disturbed (secondary ionization, x-rays, light emissions, and heating) as energetic radiation belt

electrons precipitate as a result of magnetospheric interactions with lightning-generated whistler waves [*Inan et al.*, 1990, and references therein]. The new form of direct coupling considered in the present work is a completely different process and involves the intense heating of the lower ionospheric electrons by EM fields produced by lightning discharges which in turn leads to the production of secondary ionization and optical emissions [*Inan et al.*, 1991; *Taranenko et al.*, 1992].

1.1 CHARACTERISTICS OF LIGHTNING DISCHARGES

In this section we review the known parameters of EM pulses from lightning discharges that are important in the course of our study. More details on general characteristics and phenomenology of lightning discharges can be found in *Uman* [1987].

Lightning is a transient electrical discharge which extends through the atmosphere for several kilometers. The most common cause of lightning is the separation of electrical charges associated with rainfall. There are different types of lightning, e.g., discharges within the thunderstorm cloud (intracloud (IC) discharges), commonly seen cloud-to-ground (CG) discharges, and cloud-to-cloud (CC) lightning. Obviously, the directional pattern of the radiated EM fields depends on the orientation of the discharge. In our model we consider the one dimensional (upward) propagation of EM pulses and restrict ourselves only to general comments on the dependence of our results on the orientation and spatial structure of the discharge. It is important to note that our one dimensional model does nevertheless quantitatively account for all electrodynamic aspects of the interaction of the lightning EM pulses with the ionosphere. As discussed later in Section 5.1.1, 3-D modeling would be needed to determine the horizontal extent of the disturbed ionospheric region as well as its location with respect to the causative IC or CG discharges.

A typical CG lightning flash that lowers negative electric charge to the ground has a time duration of about half a second and consists of several stages [*Uman*, 1987; p. 10]: the *preliminary breakdown* occurs within the cloud, the *stepped leader* initiates the

first return stroke in a flash by propagating from cloud to ground in a series of discrete steps; the *attachment process* of the stepped leader begins when the negatively charged leader tip nears the ground and the electric field terminating on sharp objects exceeds the breakdown value of air and one or more upward-moving discharges are initiated from the objects; after the attachment process the first *return stroke* occurs, which is a ground potential wave that propagates continuously upward along the previously ionized and charged leader path (channel), producing a peak current near the ground of typically 30 kA. Successive return strokes of lower intensities may occur if, after the first return stroke, additional charge is available to the top of the channel. The time between successive return strokes in a flash is usually several tens of milliseconds.

Although our model of coupling of EM pulses from lightning to the lower ionosphere is applicable to different types of lightning discharges, the pulse shapes and intensities used in this work are mostly representative of EM pulses originating during a lightning return stroke. These EM fields have an oscillatory character and typical durations of 50–150 μs with peak electric field amplitudes of up to 50 V/m [*Uman*, 1987; p. 110] measured at horizontal distances of 100 km from the flash (designated here as E_{100}). In two series of comprehensive measurements, the mean amplitude for CG flashes was found to be $E_{100} \simeq 8.8$ to 11.2 V/m, with amplitudes greater than 20 V/m occuring $\sim$3 to 8 % of the time [*Krider and Guo*, 1983]. Examples of electric field waveforms radiated by lightning return strokes are shown in Figure 1.1.

The less than 150 μs duration for the first return stroke is short in comparison with the total duration of a complete lightning flash, which is closer to $\sim$500 ms [*Uman*, 1987; p. 13]. However, the largest electric current, EM power, and brightest optical emissions are generated by the lightning channel during the time period of the first return stroke [*Uman*, 1987; p. 110].

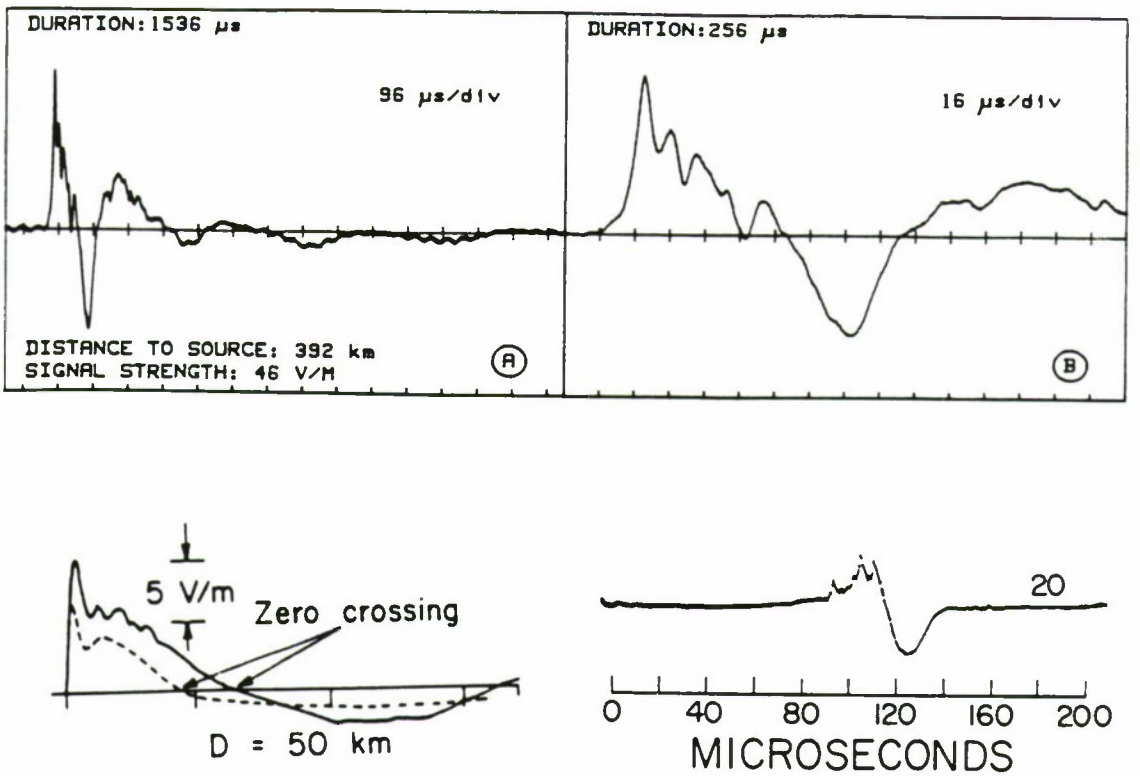

Fig. 1.1. Examples of different electric field forms radiated by lightning. The upper panel shows the electric field of a positive CG discharge [*Brook et al.*, 1989], the bottom left panel shows the electric field of a negative CG discharge [*Lin et al.*, 1979] (the scale is 50 μs per division, the solid line corresponds to the first and dotted line to the subsequent strokes), the bottom right panel shows the electric field of an IC discharge [*Weidman and Krider*, 1979].

1.2 OVERVIEW OF PREVIOUS WORK

If an electric field of E_{100} >16 V/m amplitude were to reach the ionosphere at 100 km altitude, where the energetic electron mean free path is about a meter [e.g., *Rees*, 1989; Appendix 1, and p. 273] and the ionization potential is about 16 eV [e.g., *Rees*, 1989; p. 273], it would cause avalanche ionization of neutrals. This simple consideration illustrates the potential for direct ionization of the lower ionosphere and stimulation of optical emissions by lightning radiated fields. On the other hand, it is important to note that the EM pulse would be attenuated on its way upward to 100 km altitude as a result of its interaction with the increasingly dense electron population so that the quantitative

consequences of the processes at the important altitudes of 80 – 100 km would depend on the amount of the radiated energy which reaches these altitudes where it can significantly influence the electrons. Thus, a self consistent evaluation of the electrodynamic coupling of a lightning generated EM pulse to the lower ionosphere, properly accounting for the energy losses, the evolution of the electron distribution, and the space-time evolution of the EM pulse, is needed in order to make a quantitative assessment of the consequences of the interaction of the EM pulse with the lower ionosphere.

The possibility of ionization of the lower ionosphere by lightning was considered earlier. *C. T. R. Wilson* [1925] evaluated the generation of electric discharges and ionization at altitudes of 60 km stimulated by the electrostatic dipole moment of thunderstorm clouds. *Bailey and Martyn* [1934] made a quantitative evaluation of ionization due to the electron acceleration by a strong EM wave in the lower ionosphere, and concluded that electron density increases of up to 6.5 times that of the ambient can be produced by EM fields from lightning. In their work, *Bailey and Martyn* [1934] did not consider the attenuation of the EM wave as it propagates through the collisional and highly conductive lower ionosphere and showed that a broad range of extra ionization would occur at the E region ($\sim$100 km) altitudes due to electric fields of 0.4 to 15.5 V/m and pulse durations up to 1 ms. However, our results (Chapter 3) show that the electric field amplitude at 100 km of a typical lightning EM pulse is not sufficient to produce ionization and that the region of perturbed ionization lies at $\sim$90 km. We also find that the dominant mechanism of heating and ionization is the process neglected by *Bailey and Martyn* [1934], namely the absorption of the wave power due to its interaction with the collisional lower ionosphere. In spite of these early theoretical works and some early experimental evidence (in the form of increased E region electron density during thunderstorms) obtained at about the same time [e.g., *Appleton and Naismith*, 1933], most contemporary researchers were unaware of the possibilities of ionization of the lower ionosphere produced by lightning EM energy released in the lower atmosphere. Techniques for electron kinetic modeling of the collisional ionosphere were developed years ago [e.g., *Gurevich*, 1978] and have

been extensively applied to VHF radar ionization of the upper atmosphere and the generation of artificial ionospheric mirrors [*Short et al.*, 1990; *Tsang et al.*, 1991]. However, these techniques were not applied to the interaction of EM pulses from lightning with the lower ionosphere. The application to this problem of oversimplified models (e.g., [*Kucherov and Nikolaenko*, 1979]) considering sharp ionospheric bounderies and a fluid description of electrons resulted in underestimations of the resultant heating of electrons leading to negative conclusions about possible ionization by EM energy from lightning.

The first contemporary evidence for direct upward coupling of lightning energy to the lower ionosphere was in the form of 'early' or 'fast' perturbations (sometime called 'early' or 'fast' Trimpi events) of subionospheric VLF transmitter signals. The 'early' events occur $<$ 50 ms after radio atmospherics [*Armstrong*, 1983] or CG lightning [*Inan et al.*, 1988*a*], while the 'fast' events are unusually rapid ($<$ 50 ms) amplitude changes [*Inan et al.*, 1988*a*, *b*]. Examples of 'early'/'fast' VLF perturbations, observed in direct association with lightning, are shown in Figure 1.2. Neither the 'early' nor the 'fast' aspects of these events are consistent with LEP events which are known to produce subionospheric VLF perturbations with similar signatures. VLF changes associated with LEP events follow the causative lightning with a 0.3–1.5 s delay and onset durations are typically 0.5–2.0 s [*Inan et al.*, 1990]. The lack of any such measured delay in the 'early' events is indicative of a process in which lightning directly disturbs the ionosphere lying above [*Inan et al.*, 1991]. The observed recovery times of 'early'/'fast' events are 10—100 s, indicating that a change in the lower ionospheric electron density is probably involved. In recent experimental work [*Inan et al.*, 1993] CG lightning flashes correlated with simultaneous (within 20 ms) subionospheric VLF wave perturbations were found to be within $<$60 km of the perturbed VLF Great Circle Paths and CG flashes with measured first stroke amplitudes as low as E_{100} = 6 V/m were associated with detectable VLF perturbations.

The direct upward coupling of lightning energy to the lower ionosphere is also consistent with observations from the Space Shuttle [*Boeck et al.*, 1992] of transient airglow

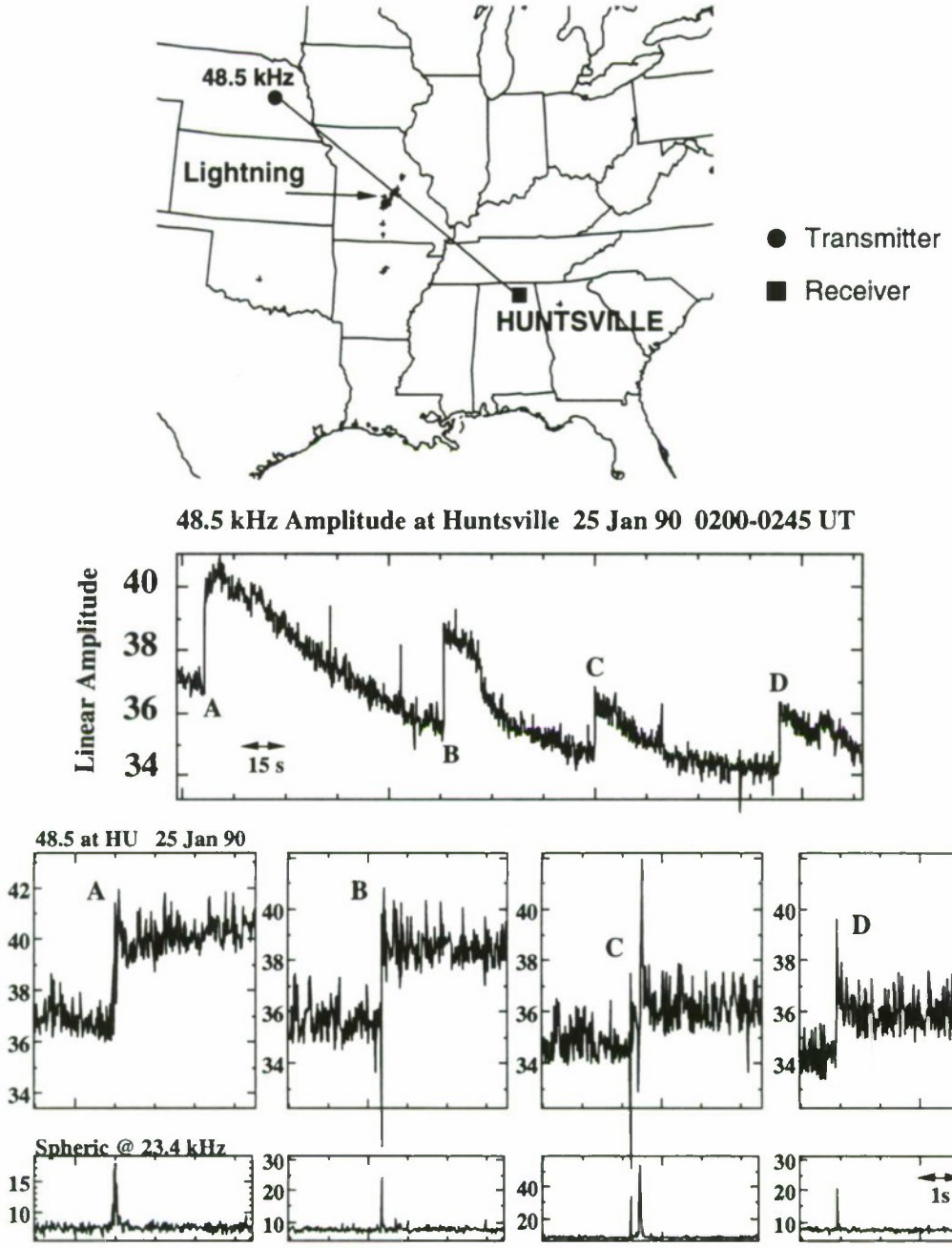

Fig. 1.2. Examples of 'early' and 'fast' VLF signal perturbations interpreted as lightning-induced heating and ionization events [*Inan et al.*, 1993]. The top of the figure shows the map of the region with transmitter (48.5 kHz), receiver at Huntsville, and a thunderstorm on the path (+'s indicate locations of individual CG flashes). The top panel shows an example of the observed VLF subionospheric signals. The lower two panels show details of the signal perturbations and simultaneous spheric observations.

brightening over a thunderstorm center, measured using a television video camera sensitive to visible light from 360 to 720 nm with peak sensitivity at 440 nm. The authors report that there were no luminous discharges connecting the airglow luminosity transient to the thunderstorm below. Only a single example of airglow brightening, reproduced in Figure 1.3, was observed during the Mission STS-41 flight on October 7, 1990. The field of view was scanned by the camera starting at the bottom of each figure and ending above the airglow image. The frame rate resulted in a time resolution of 1/60 of a second.

The *first* frame shows the ocean, the horizon, and the ambient airglow layer above the horizon. The *second* frame shows a brightly glowing arc within the airglow region above the horizon. According to the description by *Boeck et al.* [1992], the region of enhanced luminosity was 10 to 20 km thick and about 500 km in apparent horizontal extent. The airglow brightened to a level about twice that of the background airglow. At the time of the flash, the region where the cloud flash would appear in the next field was already saturated by the reflection of moonlight from the cloud bank. However, the authors identified the weak begining of illumination from the lightning flash in this frame. Under these conditions, a lightning flash would be recorded as an increase in the area that was saturated. Also, the time interval between the recording of the cloud and the airglow images was about 1 ms, long enough to allow a stroke to have occurred before the scan arrived at the airglow but after the image of the clouds was taken. The *third* frame shows a very large increase in the brightness of the same lightning flash accompanied by a decrease in intensity of the airglow transient. The authors conclude that the image of the 'blooming' clouds leaves the impression of a discharge of large horizontal extent. The *fourth* frame shows the airglow transient diminishing in intensity while the cloud luminosity remains high but decreases from maximum intensity. *Boeck et al.* [1992] concluded that the decay time constant of the optical airglow transient was of the order of 10 ms, in the range of decay constants characteristic of the video camera.

The possible heating of ionospheric electrons by VLF radiation from lightning was first suggested by *Inan* [1990] in a paper concerning a recent observation of ionospheric

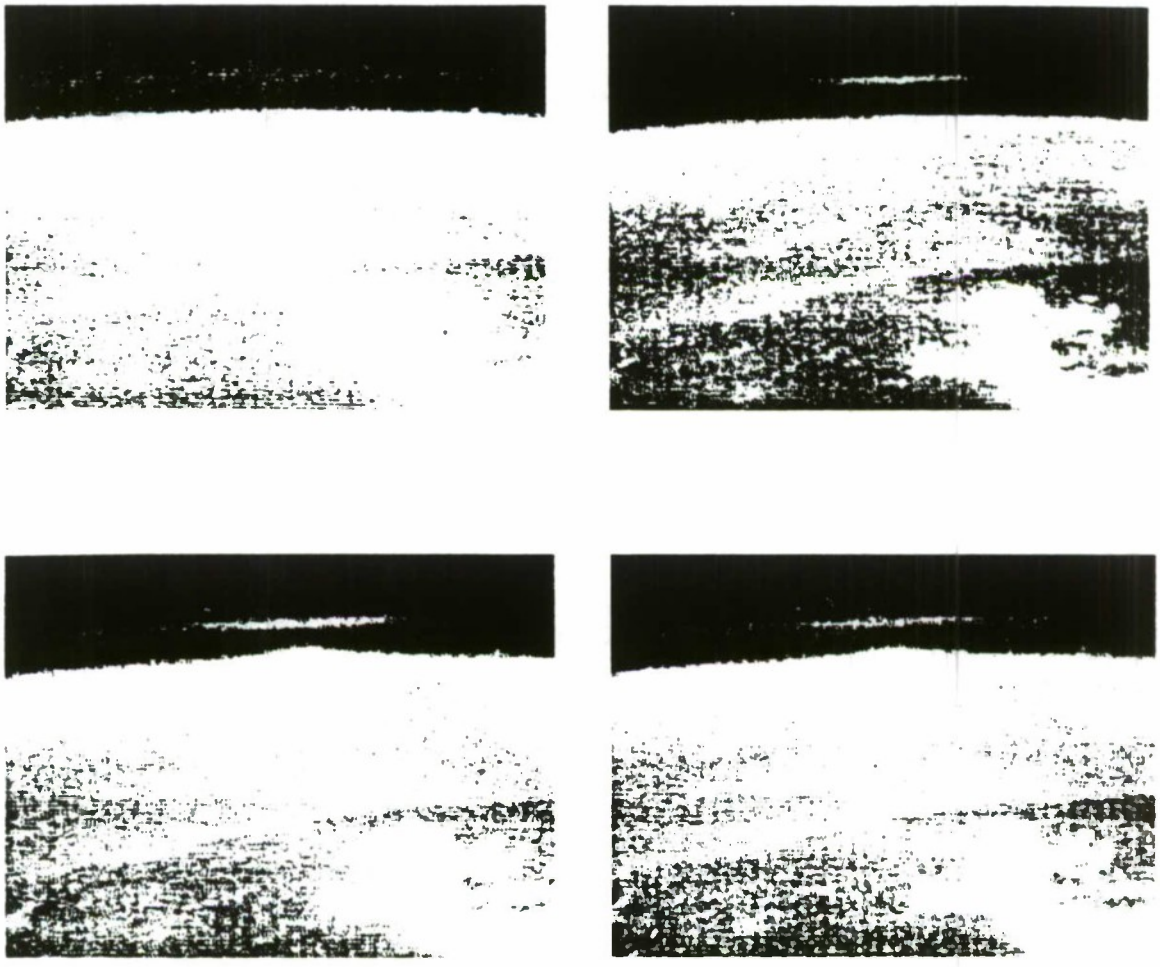

Fig. 1.3. Transient airglow brighting observed from the Space Shuttle [*Boeck et al.*, 1992]. The time sequence of frames is as follows: top left, top right, bottom left, and bottom right. See discussion in text for details.

heating by 28.5 kHz waves from a transmitter with 100 kW radiated power. However, it was noted that an additional mechanism producing density enhancements would be needed to explain the observed 'early' or 'fast' effects in view of their relatively long (10–100 s) recovery times [*Inan* 1990]. Generalization of the comparatively simple model of heating [*Inan,* 1990] to the parameters of lightning discharges and to include the production of ionization was undertaken by *Inan et al.* [1991]. Assuming a Maxwellian distribution of electrons to be maintained throughout the interaction process, and neglecting the reflection of the EM pulse from the lower ionosphere and processes such as the attachment of electrons to molecular oxygen, this first study concluded that significant new ionization can indeed be produced by strong CG discharges. According to their results, lightning-induced electron heating in the D region can reach energies of several eV and can produce extra ionization sufficient to cause the observed perturbations of subionospheric VLF signals.

An additional effect of lightning-induced heating of the lower ionsophere is the production of enhanced optical emissions by the heated electrons. The excitation of optical emissions should be a natural consequence of lightning induced heating of ambient D region electrons to energies of several eV [*Inan et al.,* 1991; *Rodriguez et al.,* 1992]. *Taranenko et al.* [1992] used the temperature profile of heated electrons from [*Inan et al.,* 1991] and assumed a Maxwellian distribution of the heated electrons to consider the intensities of optical emissions excited in the D region by the heated electrons.

The results of *Taranenko et al.* [1992] suggest that lightning-induced heating of ionospheric electrons leads to the excitation of emission lines from atomic oxygen (O), molecular oxygen (O_2), molecular nitrogen (N_2), ions of molecular oxygen (O_2^+), and nitrogen (N_2^+) with intensities ranging from 10 to 10^9 R. For example, the 5577 $\mathring{A}$ line from O emits ~60 Rayleigh (R) and lasts for ~350 ms while the 1st and 2nd positive bands of N_2 emit ~10^9 R but last only as long as the EM pulse, namely ~50–100μs. The brightest emissions from the D region above a thunderstorm are expected to be the allowed transitions, including the 1st and 2nd bands of N_2 and the 1st negative and Meinel bands

of N_2^+. The radiation time of these bands is approximately equal to the duration of the EM pulse (i.e., 50 to 100 μs). For the emissions of O and O_2 considered, the radiation time is limited by quenching and does not exceed a few seconds. Most of the emissions appear to be easily detectable with fast optical systems that have exposure times of 50 μs to several seconds and use the optical impulse from lightning to trigger the camera.

Hence, initial theoretical calculations [*Inan et al.*, 1991; *Taranenko et al.*, 1992] assuming a Maxwellian distribution of the heated electrons are in qualitative agreement with the phenomena of 'early' or 'fast' perturbations of subionospheric VLF transmitter signals and the excitation of a transient airglow brightening in the D region. The assumption of a Maxwellian distribution used in these calculations has little effect on the average quantities (e.g., energy of the distribution, conductivity, etc.). However, such quantities as the optical-excitation or ionization rates that depend on the number of electrons in the high energy ($\geq$ 10 eV) tail of the distribution are strongly influenced by its exact form. A Maxwellian distribution is not typical for electrons in a weakly ionized plasma under the influence of an electric field [*Gurevich*, 1978], and the knowledge of the detailed micro physical processes of field-particle interactions in the collision dominated ionospheric plasma is therefore essential for understanding the key factors that determine the vertical dimension and intensity of ionization and optical emissions in the heated region.

In this thesis , we undertake a fully kinetic description of the interaction of a lightning EM pulse with the lower ionosphere, using a self consistent solution of the Boltzmann equation for the electrons and Maxwell's equations for the EM fields.

1.3 SCIENTIFIC CONTRIBUTIONS

The purpose of this Ph.D. dissertation research was to theoretically investigate a new form of electrodynamic, thermal, and aeronomic coupling of energy originating in lightning discharges to the mesosphere and lower ionosphere. The specific scientific contributions resulting from these efforts are presented in Chapters 2–4. A brief summary of these contributions is provided below. Most of the results presented in this dissertation were previously published in [*Taranenko et al.,* 1992, 1993*a*, *b*]

Chapter 2 A new model has been developed which involves the self-consistent solution of the Boltzmann equation for electrons and Maxwell's equations for the EM fields and which simulates the interaction with the lower ionosphere of lightning radiated 50–150 μs EM pulses.

Chapter 3 A detailed quantitative assessment was made of electron density changes in the lower ionosphere caused by heating of the ionospheric electrons by the EM pulses. Our results provide the first detailed estimates of the absolute values and altitude distributions of electron density changes for different intensities of EM pulses and ambient electron density profiles and form a basis for quantitative explanation of all known features of 'early' and/or 'fast' VLF perturbation events which occur nearly simultaneously with lightning.

Chapter 4 A detailed assessment was made of optical emissions excited by heating of the ionospheric electrons by the EM pulses. Our results provide *(i)* the first estimates of the absolute values of major emissions and their altitude distributions for different intensities of EM pulses and ambient electron density profiles, and *(ii)* a quantitative explanation of Space Shuttle observations [*Boeck et al.*, 1992] of an enhanced airglow transient in the D region. We also provide a detailed evaluation of the atmospheric transparency for remote

sensing of the airglow transients for space-borne, aircraft-, and ground-based observations.

2

Electrodynamics and Kinetics of the Interaction

In this chapter, we describe the basic model of the electrodynamic interaction of an intense EM pulse from lightning with the collisional electron gas in the lower ionosphere.

2.1 AMBIENT PROFILES AND FIELD ORIENTATIONS

The altitude range of interest lies between 70 and 100 km, for which we use the U.S. Standard Atmosphere [1976] for the altitude profile of ambient neutrals and assume the composition to be $\sim$80% N_2, $\sim$20 % O_2, and a varying concentration of O which is $\simeq$ 0.0001% at 80 km and $\simeq$ 5% at 100 km in accordance with the MSIS neutral atmosphere model [*Hedin*, 1987]. Our results are only weakly dependent on the ambient neutral temperature, which is taken to be 250^o K throughout the region. The ambient neutral and electron density profiles are summarized in Figure 2.1. We conduct calculations for the ambient electron density profiles taken from *Barr et al.* [1985] and represent 'tenuous' nighttime (a), 'intermediate' or 'dense' nighttime (b), and daytime (c), profiles. 'Tenuous' and 'dense' profiles respectively represent somewhat more tenuous and more dense D region than the one used in [*Taranenko et al.*, 1992] which is also shown in Figure 2.1 for comparison.

In principle, the angles between the wave electric field $\vec{E}$, the ambient magnetic field $\vec{B}_o$, and the plane of the ionosphere can be expected to influence the details of the

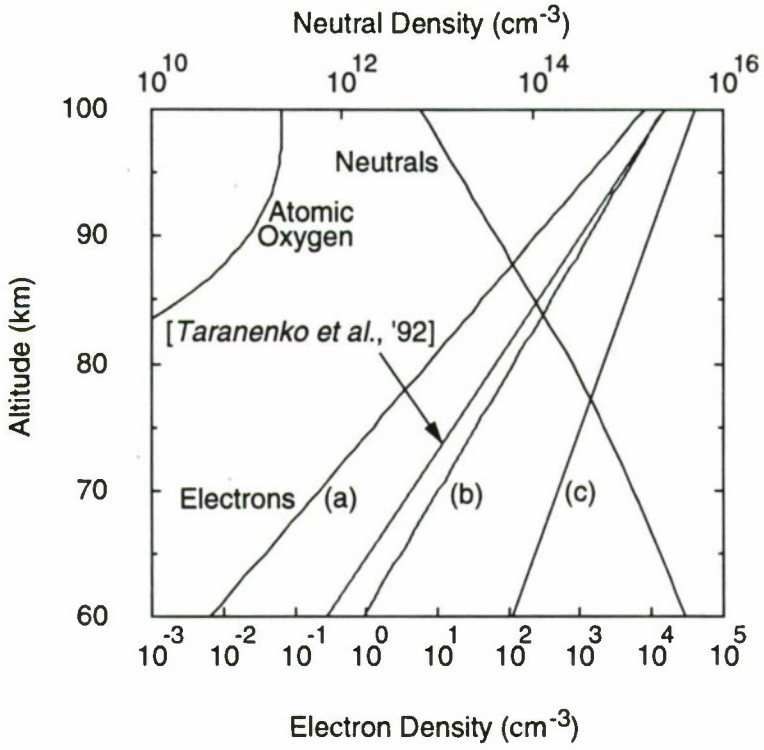

Fig. 2.1. Ambient profiles of electron and neutral densities. Electron density profile (a) represents a 'tenuous' nighttime D region, profile (b) represents a 'dense' nighttime profile for 'disturbed' geomagnetic conditions and (c) represents daytime conditions. The electron density profile used in our earlier paper [*Taranenko et al.*, 1992] is also shown for comparison.

interaction. For simplicity we assume that the ambient magnetic field lies in the plane of the lower ionospheric boundary (i.e., horizontal) and the incident EM wave is planar. We consider two extreme cases with $\vec{E} \parallel \vec{B}_0$ and $\vec{E} \perp \vec{B}_0$. With these assumptions, our model results are most directly applicable to the interaction of lightning EM fields with the ionosphere near the geomagnetic equator. It is shown in Section 3.4 by comparing results for $\vec{E} \parallel \vec{B}_0$ and $\vec{E} \perp \vec{B}_0$ that, due to the intense nature of the heating for typical cases, the plasma is collision dominated so that the general characteristics of the coupling do not depend critically on the orientation of the magnetic field.

2.2 DESCRIPTION OF THE EM FIELDS AND THE ELECTRON DISTRIBUTION

The propagation of EM fields is described by the one dimensional (1-D) Maxwell's equations:

$$\begin{aligned} &\frac{\partial B_z}{\partial x} + \frac{1}{c}\frac{\partial E_y}{\partial t} = -\frac{4\pi}{c}J_y, \quad \frac{\partial B_y}{\partial x} - \frac{1}{c}\frac{\partial E_z}{\partial t} = \frac{4\pi}{c}J_z \\ &\frac{\partial E_z}{\partial x} - \frac{1}{c}\frac{\partial B_y}{\partial t} = 0, \quad \frac{\partial E_y}{\partial x} + \frac{1}{c}\frac{\partial B_z}{\partial t} = 0 \end{aligned} \tag{2.1}$$

where c designates the velocity of light in a vacuum, x is the vertical, z is the horizontal axis directed along the ambient magnetic field $\vec{B}_o$, and y is the horizontal axis directed in accordance with a right handed x, y, z coordinate system. The electron distribution function $f(\vec{r}, \vec{v}, t)$ is related to the electric current $\vec{J}$ and electron density N_e via the subsidiary equations:

$$\vec{J} = -e\int \vec{v} f(\vec{r}, \vec{v}, t) d\vec{v}; \qquad N_e = \int f(\vec{r}, \vec{v}, t) d\vec{v} \tag{2.2}$$

where e is the electron charge. Since, as will be seen later (Section 2.4), the random electron velocity is much larger than its average directional velocity, we expand $f(\vec{r}, \vec{v}, t)$ in spherical functions of zero order keeping only the first two terms [*Allis*, 1956]

$$f(\vec{r}, \vec{v}, t) \simeq f_0(\vec{r}, v, t) + \frac{\vec{v} \cdot \vec{f}_1(\vec{r}, v, t)}{v} + \ldots \tag{2.3}$$

where $f_0(\vec{r}, v, t)$ is the symmetrical part, whereas $\frac{\vec{v} \cdot \vec{f}_1(\vec{r}, v, t)}{v}$ is the directional part. For our case (2.3) is a good approximation as long as $e^2E^2/m\bar{\varepsilon}\nu^2 \ll 1$ which is satisfied for all parameters considered here (see Appendix A), and throughout the process of the interaction, where m is the electron mass, $\nu(\bar{\varepsilon})$ is the total effective electron collision frequency with neutrals, and $\bar{\varepsilon}$ is the average energy of the electrons. Substitution of (2.3) into (2.2) gives:

$$\vec{J} = -\frac{4\pi e}{3}\int_0^\infty v^3 \vec{f}_1(\vec{r}, v, t) dv; \qquad N_e = 4\pi \int_0^\infty v^2 f_0(\vec{r}, v, t) dv$$

which explains the physical meaning of first two expansion terms in (2.3): $f_0(\vec{r}, v, t)$ can be used to calculate the electron density whereas $f_1(\vec{r}, v, t)$ is useful for calculating the particle flow in configuration space. For a weakly ionized plasma, the Boltzmann equation for the electron distribution function can be reduced to the following system of equations (see Appendix A)

$$\frac{\partial f_0}{\partial t} = \frac{e}{3mv^2}\frac{\partial}{\partial v}\left(v^2\vec{E}\cdot\vec{f}_1\right) + \frac{1}{2v^2}\frac{\partial}{\partial v}\left[v^2\delta\nu_{el}\left(\frac{T}{m}\frac{\partial f_0}{\partial v} + vf_0\right)\right] + S_{0in} \tag{2.4}$$

$$\frac{\partial \vec{f}_1}{\partial t} = \frac{e\vec{E}}{m}\frac{\partial f_0}{\partial v} + \frac{e}{mc}\left[\vec{B}\times\vec{f}_1\right] - \nu\vec{f}_1 \tag{2.5}$$

$$S_{0in} = S_{0in}^{rot} + S_{0in}^{vib} + S_{0in}^{opt} + S_{0in}^{dis} + S_{0in}^{att} + S_{0in}^{ion} \tag{2.6}$$

The second term on the right hand side of (2.4) describes contributions from elastic collisions of the electrons with neutrals, with δ being the fraction of electron energy lost per collision, $\nu_{el}(v)$ being the frequency of elastic collisions, and T being the temperature of neutrals. S_{0in} is the part of the Boltzmann collision integral representing inelastic collisions consisting of rotational, vibrational, optical, dissociative, dissociative with attachment, and ionization losses. The rotational term can be represented as [*Gurevich,* 1978; p. 53]

$$S_{0in}^{rot} = \frac{\partial}{\partial v}\left[\frac{8\beta N v\sigma^{rot}}{m}\left(\frac{T}{m}\frac{\partial f_0}{\partial v} + vf_0\right)\right] \tag{2.7}$$

where β is the rotational constant for a specific molecule (see Appendix B), N is the density of molecules, and σ^{rot} is the rotational cross section (see Appendix B). For a weakly ionized plasma the vibrational, optical, and dissociative losses are represented in a similar manner [*Holstein,* 1946]

$$S_{0in} = \frac{2N}{mv}\sum_j\left[(\epsilon+\epsilon_j)f_0(\epsilon+\epsilon_j)\sigma_j(\epsilon+\epsilon_j) - \epsilon f_0(\epsilon)\sigma_j(\epsilon)\right] \tag{2.8}$$

where $\epsilon = \frac{mv^2}{2}$, ϵ_j is the energy difference between the ground and j levels, and σ_j is the corresponding cross section (see Appendix B for numerical values). The attachment

term is given as [*Gurevich*, 1978; p. 79]

$$S_{0in}^{att} = -N_{O_2}\sigma_{att}(v)vf_0 \tag{2.9}$$

where N_{O_2} is the density of O_2 molecules, and σ_{att} is the attachment cross section (see Appendix B). Ionization processes are described by the following equation [*Gurevich*, 1978; p. 77]

$$\begin{aligned} S_{0in}^{ion} = 4\pi &\int_{v_{ion}}^{\infty} \nu_{ion}(v', v) f_0(v') v'^2 dv' \\ &+ \frac{2N_l}{mv}\left[(\epsilon + \bar{\epsilon}_k) f_0(\epsilon + \bar{\epsilon})\sigma^{ion}(\epsilon + \bar{\epsilon}) - \epsilon f_0(\epsilon)\sigma^{ion}(\epsilon)\right] \end{aligned} \tag{2.10}$$

where v_{ion} is the electron velocity corresponding to the ionization threshold for the particular molecule (O_2 or N_2), $\nu_{ion}(v', v)$ is the number of electron-ion pairs produced in one second by an electron having a velocity v' and leading to the appearance of a new electron having a velocity v, $\bar{\epsilon}_k(\epsilon)$ is the average energy lost by electrons in a single ionization as given in calculations using *Opal et al.* [1971] data on the secondary electron spectra and the ionization potential approximation used by *Richards and Torr* [1990]. The dissociative attachment of electrons ($O_2 + e \rightarrow O + O^-$) and ionization ($M_2 + e \rightarrow M_2^+ + 2e$, where M_2 designates a N_2 or O_2 molecule) are processes in the model that affect the electron density. We neglect existing spatial gradients of the distribution function since they are only important in the D region over time intervals longer than several hundred seconds [*Tomko et al.*, 1980] and the duration of the lightning EM pulse is typically <100 μs. The total electron energy loss function F, where

$$F = \sum_j C_j \delta\varepsilon_j v \sigma_j, \tag{2.11}$$

(where the summation is performed over all inelastic loss processes and C_j is the concentration of the particular sort of neutrals, $\delta\varepsilon_j$ is the energy loss) is shown as a function of energy in Figure 2.2 and is similar to that given in Figure 7 of *Tsang et al.* [1991]. We note that there are two major energy barriers. The first one is due to the N_2 vibrational

barrier, extending from 1.5 to 3 eV. Inelastic losses in the range 3 to 6 eV are much smaller than the vibrational losses of the first barrier. The second barrier appears in the range above ~6 eV, and is due to the optical, dissociative, and ionizational excitations of the ambient neutrals.

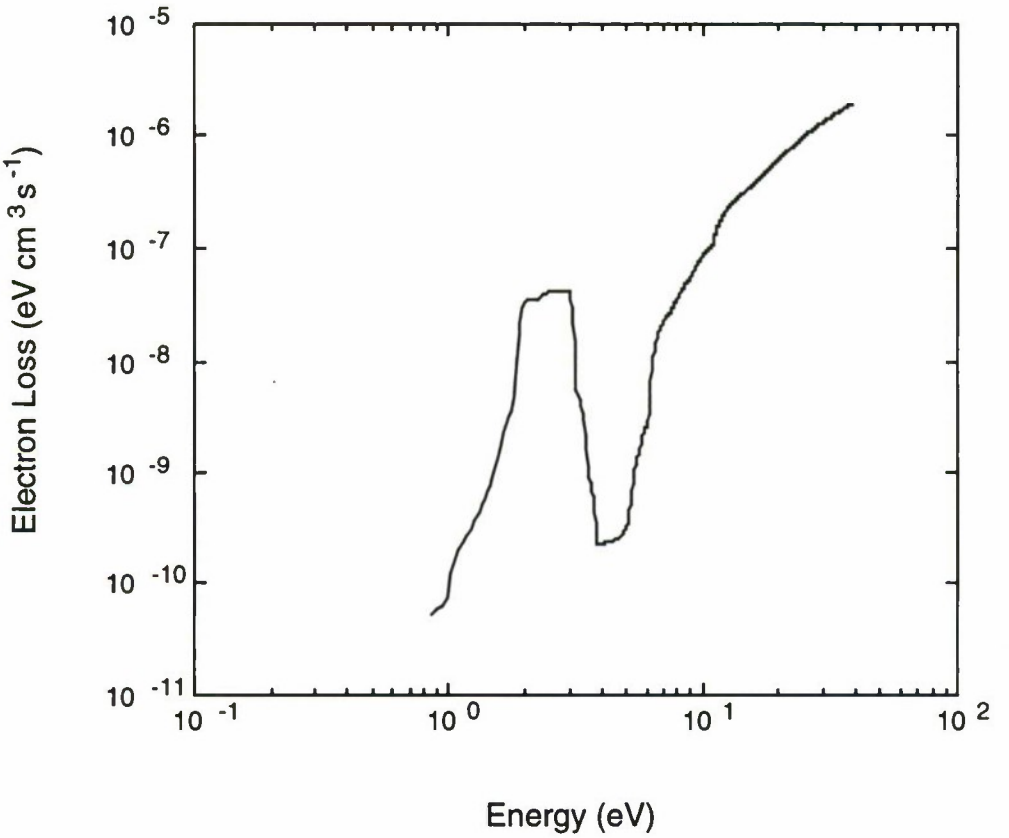

Fig. 2.2. Electron loss function in air. Equation (2.11) and numerous electron impact cross sections (Appendix B) were used to compile this function.

2.3 TIME EVOLUTION OF THE ELECTRON DISTRIBUTION FUNCTION IN A SINGLE SLAB

Even after the simplifying assumptions introduced in the previous section, the solution of the one dimensional Maxwell's equations (2.1) simultaneously with the equations (2.4) and (2.5) for the evolution of the electron distribution function as given by (2.3) for time varying fields over the altitude range of interest (70 to 100 km) requires extensive computer resources. It is thus useful to make additional simplifications by taking into account the parameters of our particular problem. For some insight, we first examine the time evolution of the distribution function in a single slab for a given applied electric field.

We solve equations (2.4) and (2.5) including all loss terms (2.6) under the assumption of a constant electric field using a numerical technique for the Boltzmann transport equation, as described for example by *Rockwood and Greene* [1980], which conserves energy and the number of particles. Details of the numerical technique are given in Appendix C.

The time evolution of the distribution function in a single slab located at 90 km altitude for a constant electric field of 15 V/m applied for 20 μs is shown in Figure 2.3 (b).

The distribution function is initially a Maxwellian with temperature equal to that of the neutrals ($\sim 250^o$ K). After the onset of the electric field, the energy of the electrons increases, reaching a constant value of $\sim$5.7 eV in about 5 μs (Figure 2.3 (a)), at which time the distribution function has reached its quasi-equilibrium state. This state is characterized by an almost flat distribution below $\sim$1.2 eV with a drop between 1.2 and 3 eV due to the vibrational excitations of N_2 (see Figure 2.2). A second flat region exists from 3 to 6 eV due to the gap in the electron loss function as can be seen from Figure 2.2 and as discussed above, followed by a precipitous drop as electrons reach energies above the major optical, dissociative, and ionization thresholds of the atmospheric constituents and the loss rate increases rapidly with energy as seen in Figure 2.2. The corresponding time evolutions of the electric current density, average energy, ionization and attachment rates

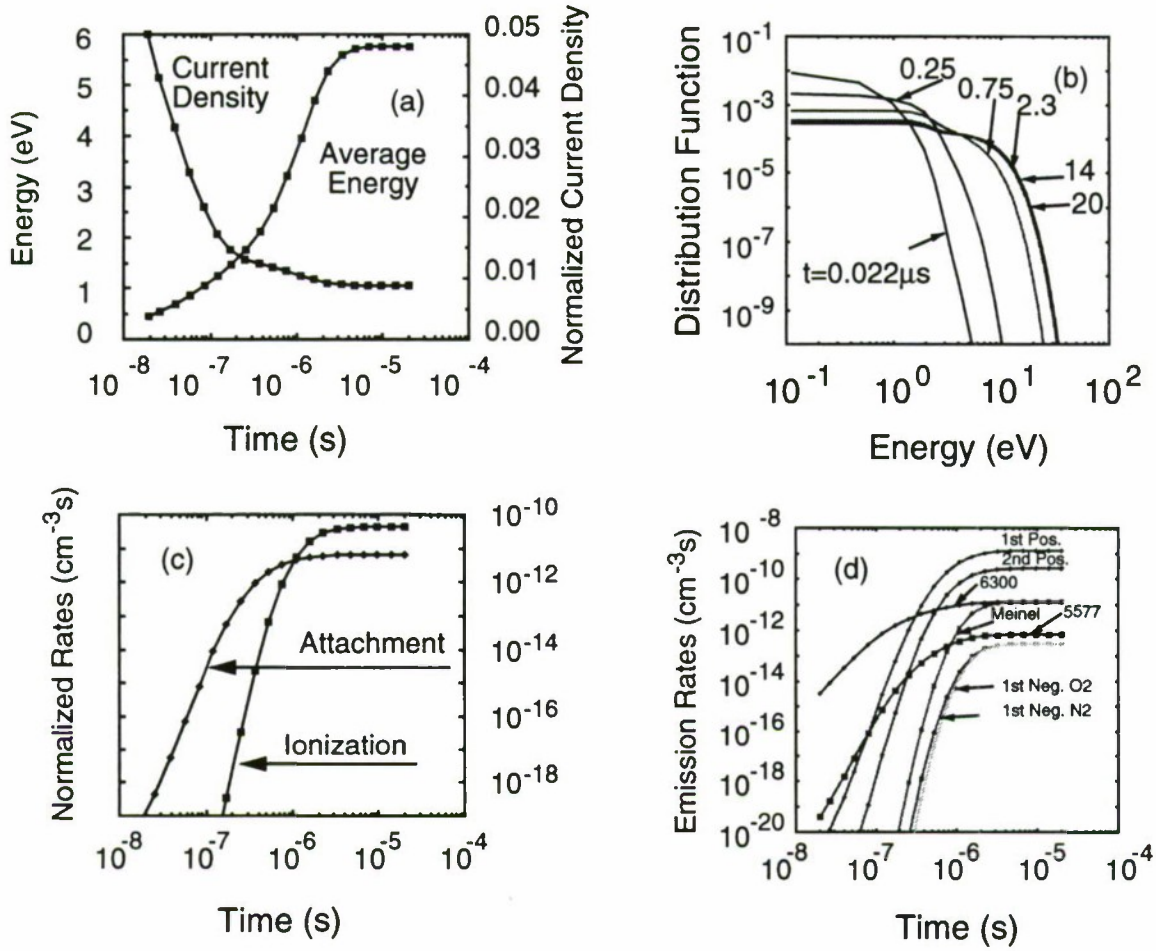

Fig. 2.3. Results of a single slab (at 90 km altitude) simulation for a fixed applied electric field of E = 15 V/m applied at time t = 0. *Top left:* Time evolution of the normalized electric current and average electron energy. *Top right:* Time evolution of the electron distribution function. The electron distribution function is shown at 0.022 μs, 0.25 μs, 0.75 μs, 2.3 μs, 14 μs, and 20 μs. *Bottom left:* Time evolution of the attachment and ionization rates. *Bottom right:* Time evolution of the optical emission rates for selected lines. The current density and excitation rates are normalized to one electron per cubic centimeter.

are shown in Figure 2.3 (a) and (c). It is seen from Figure 2.3 (c) that the attachment rate reaches its equilibrium value over a shorter time interval than the ionization rate. This behaviour is due to the lower threshold energy of attachment (~6 eV) in comparison with ionization (~16 eV). The excitation rates of selected optical emissions shown Figure 2.3 (d) behave in a similar manner with higher states (e.g., the 1st negative of N_2^+ and O_2^+, and Meinel of N_2^+) reaching equilibrium values at slightly later times compared to lines with lower thresholds (6300 and 5577 Å). The rational for selection of the particular emission lines and bands is given in Chapter 4.

Two other examples of single slab calculations for applied electric fields of 10 and 5 V/m are shown in Figure 2.4 and 2.5. We note that the system reaches equilibrium state over somewhat longer time for smaller electric field amplitudes. For example, 90 % value of the equilibrium ionization rate (see Figure 2.3 (c), 2.4 (c), and 2.5 (c)) is reached in ~3 μs for E = 15 V/m, in ~4 μs for E = 10 V/m, and in ~15 μs for E = 5 V/m. This behaviour is due to slower development of the high energy tail of the distribution (which determines the ionization rate) for lower electric field amplitudes. However, since the electric current is determined by the bulk of the electrons, the 110 % value (the current becomes smaller with time) of the equilibrium current is established in smaller time intervals (Figure 2.3 (a), 2.4 (a), and 2.5 (a)) ~2 μs for E = 15 V/m, ~3 μs for E = 10 V/m, and ~3 μs for E = 5 V/m. We note the more than three orders of magnitude difference in the equilibrium ionization rates for E = 15 and E = 5 V/m which underscore the highly nonlinear nature of the interaction and the resulting ionization process.

As will be seen from the results presented in Chapters 3 and 4, the major electron density changes and excitation of optical emissions for the electron profiles considered in this thesis occur at or below 90 km altitude. Hence, we have chosen to present our single slab simulation results for this altitude.

Concerning other altitudes and electric field amplitudes, we note that from equation

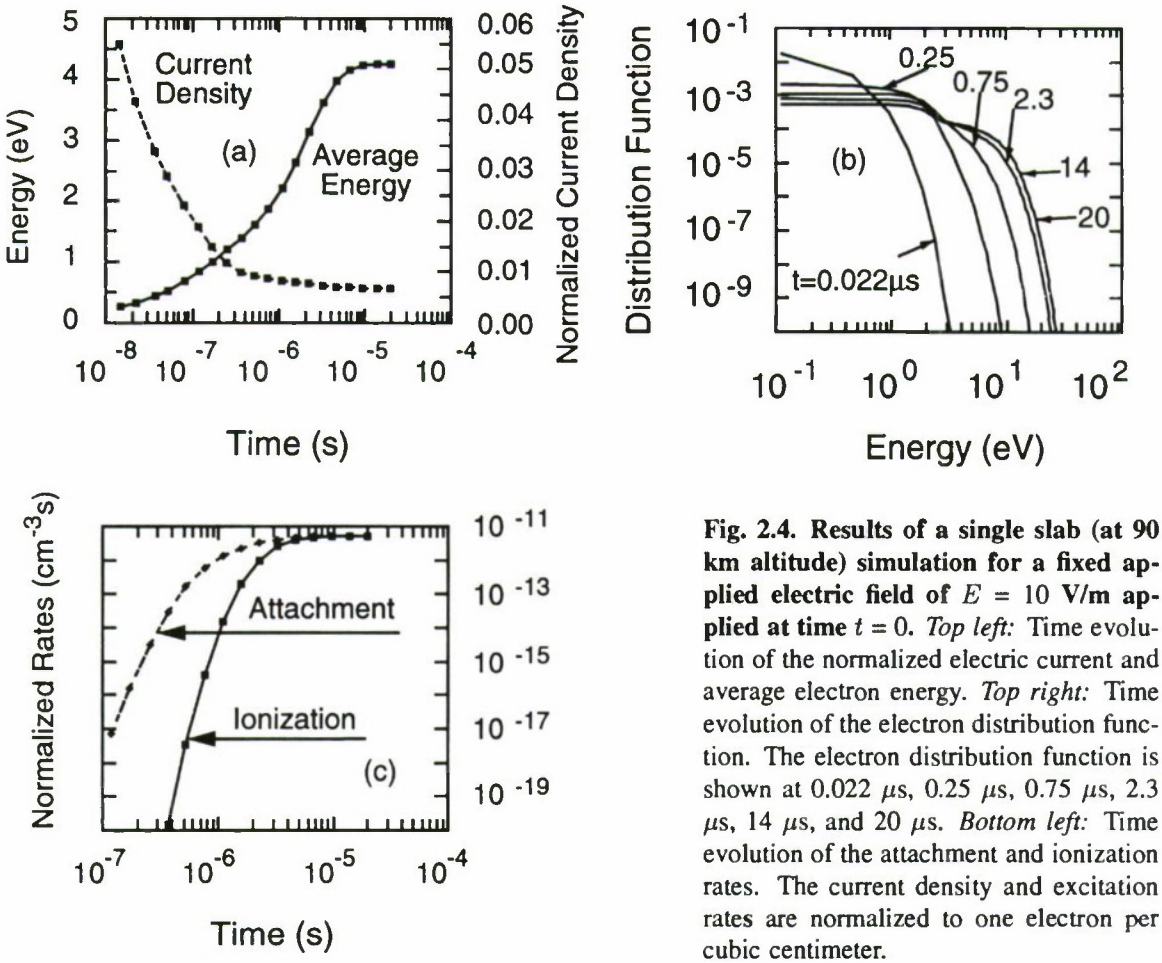

Fig. 2.4. Results of a single slab (at 90 km altitude) simulation for a fixed applied electric field of E = 10 V/m applied at time t = 0. *Top left:* Time evolution of the normalized electric current and average electron energy. *Top right:* Time evolution of the electron distribution function. The electron distribution function is shown at 0.022 μs, 0.25 μs, 0.75 μs, 2.3 μs, 14 μs, and 20 μs. *Bottom left:* Time evolution of the attachment and ionization rates. The current density and excitation rates are normalized to one electron per cubic centimeter.

(C.1) in Appendix C that the first term on the right hand side, namely the driving force F_E due to the electric field E, is

$$F_E \sim E^2/\nu \tag{2.12}$$

The diffusion time of the distribution function over a unit of velocity or energy space under the influence of the electric field is inversely proportional to this force and is estimated as $\sim \nu/E^2$. The collision frequency ν is proportional to the neutral density which changes by a factor of ~6 over a 10 km altitude span (see Figure 2.1). Also from Figures 2.3 (a) – 2.5 (a) we observe that the average energy changes only by a factor of ~1.4 (i.e., from ~4.1 to ~5.7 eV) with a change in the amplitude of the electric field of a factor of three (i.e., from 5 to 15 V/m). This slow dependence is due to the high value

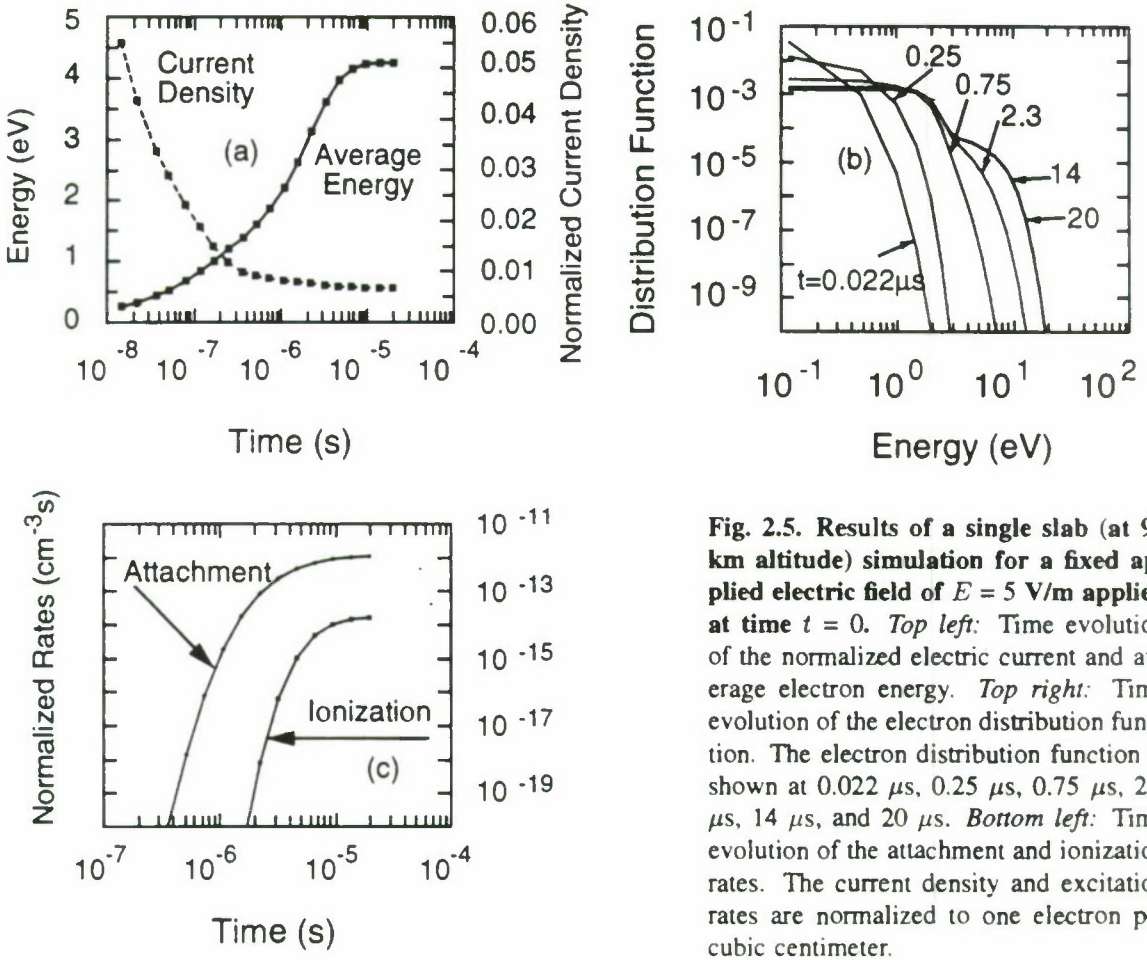

Fig. 2.5. Results of a single slab (at 90 km altitude) simulation for a fixed applied electric field of E = 5 V/m applied at time t = 0. *Top left:* Time evolution of the normalized electric current and average electron energy. *Top right:* Time evolution of the electron distribution function. The electron distribution function is shown at 0.022 μs, 0.25 μs, 0.75 μs, 2.3 μs, 14 μs, and 20 μs. *Bottom left:* Time evolution of the attachment and ionization rates. The current density and excitation rates are normalized to one electron per cubic centimeter.

of the second barrier starting at ~6 eV in the electon loss function shown in Figure 2.2. Hence, the average distance and time over which the electrons travel in energy space during the heating by the electric field starting from a cold state can be assumed constant for the electric field amplitudes discussed here. Consequently, we conclude that over the region of strong attenuation (80 to 95 km) of the EM pulses, the diffusion time for the electron distribution (i.e., the time for the distribution to reach equilibrium) varies only by a factor of ~6 due to the variation of the neutral density. We also note that equilibrium is reached over shorter time periods for the electric current, the attachment rate and optical excitations with low thresholds than for the ionization rate and optical excitations with high thresholds (see for example Figures 2.3, 2.4, 2.5 (a) and (c) for comparison). This

fact allows us to extend the validity of our assumption of achiving equilibrium over μs time scales to broader values of electric fields and altitudes as far as the relationship between the applied electric field and the electric current density is concerned; note that the latter is what is needed to propagate the EM pulses in accordance with equations (2.1). According to single slab calculations at other altitudes not shown here, and for electric field amplitudes of $\geq$5 V/m that are necessary to produce substantial electron density changes and optical emissions, equilibrium is reached over a several μs time scale for the current density, the optical excitation and ionization rates at the altitudes of interest (80 to 95 km).

For the case of small ($\leq$5 V/m) electric field amplitudes, and at altitudes $\leq$85 km, the average energy of the electrons in the electric field is $\leq$2 eV. For such a case, the most important factor which determines the distribution is inelastic collisions of electrons with excitation of rotational levels and low vibrational levels (see for example [*Gurevich*, 1978; pp. 70–73]). The distribution function f for such interactions is of the Druyvestein type and decreases with velocity more rapidly than a Maxwellian ($\ln f \sim -v^{\frac{8}{3}}/E^2$). The average energy of such a distribution is $\sim E^{\frac{15}{4}}$. Hence, the product of the electric field driving force (2.12) and the average energy (which determines the time needed to reach equilibrium) varies as $\sim E^{\frac{7}{8}}$. This analytical evaluation shows that the time needed to reach equilibrium decreases with electric field for the lower electric field amplitudes and allows us to state that the μs time interval is also sufficient for electrons to reach equilibrium in small electric fields.

2.4 MULTIPLE-SLAB MODEL OF THE INTERACTION AS A FUNCTION OF TIME AND ALTITUDE

The results of our full kinetic solution of the coupling for a single slab allow us to formulate a multi slab model of the interaction, to describe the coupling and its consequences as a function of altitude and time, as the EM pulse propagates upward and interacts with the increasingly dense lower ionosphere.

Subject to the caveats discussed above, the major conclusion we derive from the results of the single slab calculations is the fact that the form of the electron distribution function follows a quasi-equilibrium solution of equations (2.4), (2.5) and is established within a time interval <20 μs, so that if the applied electric field exhibited relatively 'slow' field changes over time scales of tens of μs then the quasi-equilibrium solution can be used to calculate the current density, ionization, and optical excitation rates.

Available data on the waveforms of lightning radiated EM pulses (e.g., [*Uman,* 1987; p. 113], also see Figure 1.1) indicate that they exhibit relatively slow time variations over a 10 μs time scale, with pulse durations of typically 50-150 μs. Hence, to simulate the propagation of the EM pulses from lightning through the lower ionosphere we do not need to follow the complete time evolution of the Boltzmann equations (2.4) and (2.5). The current density, ionization, attachment, and optical excitation rates can be approximated by their values derived from the equilibrium solution for a given electric field existing at a particular time, at a given altitude. For an electric field increasing (decreasing) with time such an approximation leads to an overestimate (underestimate) of the number of high energy electrons due to the fact that the equilibrium is reached from lower (higher) energies. However, as we discuss below, the error introduced in our results due to this approximation is typically less than 10 %.

Our practical realization of the approach described above was as follows. *First,* we prepared a table of equilibrium values (calculated using the single slab model) of current density, electron density variation rates, and optical excitation rates as a function of altitude and electric field values. This table covers the 70–100 km altitude range in 1 km increments and specifies the current density, electron density variation rate, and optical excitation rates over a 50-point grid of values of the electric field. The maximum value of the electric field over the grid is 70 V/m below 70 km altitude and is gradually reduced to 3 V/m at 100 km. For altitudes above 100 km the medium is approximated by its characteristics at 100 km. *Second,* we simulated the propagation of EM pulses solving Maxwell's equations (2.1) in a self consistent manner choosing appropriate values of

the electric current, density changes, and optical excitation rates from the table, using linear interpolation to find values between the tabulated points as shown in an example in Figure 2.6. Further details of our numerical method are given in Appendix C.

Due to the particular numerical scheme employed, the present version of the code has an upper limit for the electric field amplitude that does not allow the simulation of interactions with the lower ionosphere of EM pulses with amplitude $E_{inj} \geq 25.5$ V/m (observed $\sim$5% of the time) for a 'tenuous' D region and $E_{inj} \geq 37.5$ V/m (observed $\sim$1% of the time) for a 'dense' D region. Simulation of the interaction of such pulses with the lower ionosphere is the subject of future work (see Section 6.2).

To assess the validity of our numerical technique, we monitored the electric field, current density, and electron density values at fixed altitudes as the EM pulse propagated through the medium and then checked the resulting time dependences against single slab calculations.

Figure 2.7 (a) shows the variation of the electric field at 89 km calculated in the manner described above (i.e., using the grid values) for a single cycle sinusoidal pulse of 100 μs duration injected at 70 km with an initial peak intensity of E_{inj} = 20 V/m for the 'tenuous' nighttime profile (a) of Figure 2.1. Figure 2.7 (b) shows the corresponding current values as obtained from the same model (i.e., from the corresponding grid values), and Figure 2.7 (d) shows the current density as computed by a time dependent solution of (2.4), (2.5) for a single slab at this altitude and for the varying electric field value in effect as given in Figure 2.7 (a). The difference between the two is barely visible on the scale shown, confirming that, for the purposes of the propagation of EM pulses in the highly collisional lower ionosphere, our use of the equilibrium values is a reasonable assumption. The changes in the electron density, again calculated in the two different ways, are compared in Figure 2.7 (c). The difference between values calculated using the equilibrium solution and the single-slab time dependent solution with the varying electric field is $\sim$3.5%. This error is somewhat larger for smaller amplitudes of the electric fields

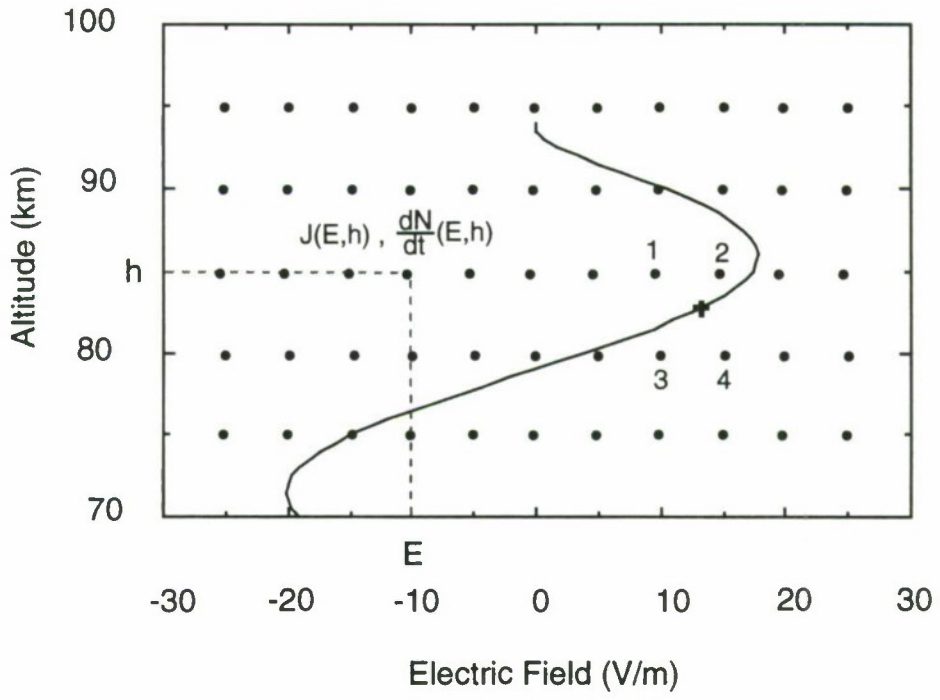

Fig. 2.6. Sketch of the grid used to propagate EM pulses in the collisional ionosphere. At each point shown with a dot the electric current density, the rate of change of electron density, and the optical excitation rates were pre-calculated using a single slab model similar to that described in Section 2.3 at different altitudes and for different applied electric fields. Linear interpolation is used between points to find the appropriate values of quantities in intermediate points (e.g., data from points 1 to 4 are used to perform calculations at the point designated with +). In the actual grid used for our model, the grid points are separated by 1 km in altitude (i.e., 30 points between 70 and 100 km) and the electric field was represented over a 50-point grid, with the maximum value varying from 70 V/m at 70 km to 3 V/m at 100 km.

since the system reaches equilibrium over a longer time intervals for weaker driving fields. However, since for injected electric field amplitudes $E_{inj} < 10$ V/m the resultant electron density changes are <1 % of the ambient we can safely use the approach described above for the range of parameters of interest. We note that during the calculations the ratio of the average directional electron velocity to the random electron velocity was 0.01 to 0.1 which confirms the validity of expansion (2.3).

Overall, the error introduced in our estimates of electron density changes because of our usage of the quasi-equilibrium solution and the method described above is <10

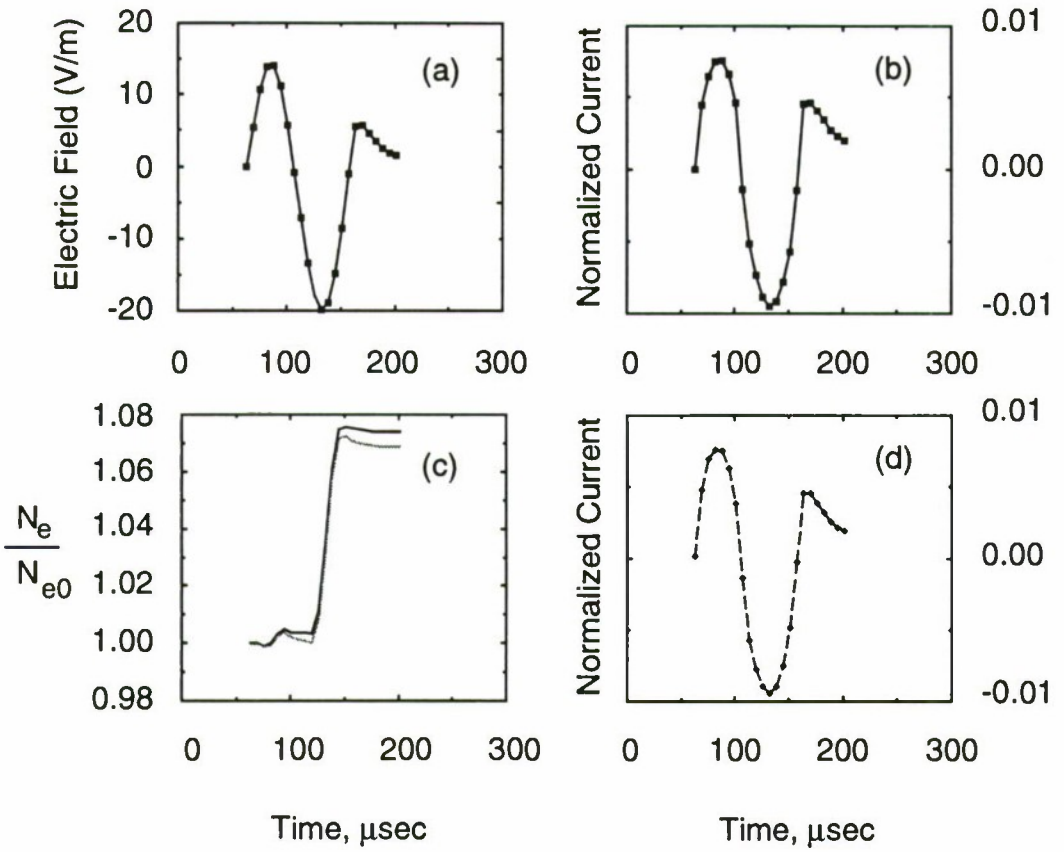

Fig. 2.7. Dynamic test of the numerical technique. Variations with time of the electric field (a) and the electric current density (b) at 89 km altitude for the 'tenuous' nighttime conditions (profile (a) of Figure 2.1) following the injection of a E_{inj} = 20 V/m EM pulse starting at t = 0 at 70 km. Single slab calculations of the electric current for the electric field varying as shown in (a) at 89 km are shown in plot (d). Plot (c) shows a comparison of the electron density changes as calculated from the grid model (solid line) and from the single slab calculations (lighter line) at 89 km for the electric field varying as shown in (a).

%. Due to a monotonic decrease in the electron distribution function with energy (see e.g., Figure 2.3 (b)) and the similarity of the single peaked dependences of the electron impact excitation cross sections of optical electronic states and dissociative attachment and ionization processes, the error in optical excitation rates would be similar (<10 %). Such accuracy is quite acceptable for the problem at hand, especially in view of the fact that the absolute magnitudes of the input radiation fields from lightning exhibit a much wider dynamic range, and that the ambient nighttime D region electron density is also highly variable and not well known [*Friedrich and Torkar*, 1992; *Mitra*, 1981].

2.5 REPRESENTATION OF INJECTED EM PULSES FROM LIGHTNING

To put the input electric field amplitudes E_{inj} in the right context, it suffices to remember that the mean amplitude for CG flashes as observed at 100 km distance on the ground is $E_{100} \simeq$8.8 to 11.2 V/m, with amplitudes >20 V/m occuring ~3 to 8 % of the time [*Krider and Guo*, 1983].

Since there is no significant attenuation below 80 km for parameters of interest (Chapter 3) and since we use a plane wave model in our calculations, it is useful to refer the injected EM pulse amplitude (E_{inj}) to this altitude. The lack of spherical spreading losses due to the plane wave assumption introduces ~10 % error in our calculations, which is comparable with other uncertainties due to other assumptions introduced in the model, especially in view of the fact that the absolute magnitudes of the input radiation fields from lightning exhibit a much wider dynamic range and that practically all the data on the lightning electric field amplitudes come from the ground based measurements [*Uman*, 1987; p. 110]. We note that there is reason to believe that lightning radiation fields above the ground may be substantially different [*Krider*, 1992].

Assuming a spherically spreading wave, and leaving aside directional aspects of the radiation from CG versus IC discharges [e.g., see *Rodriguez et al.*, 1992] (i.e., assuming an isotropic radiator), an electric field amplitude of E_{100} would be related to an injected field amplitude E_{inj} at 80 km as $E_{inj} \times \frac{80}{100}$. In accordance with this, the plane EM wave can be injected at any altitude below 80 km with the same amplitude E_{inj} without significant error (note that there is no spherical spreading factor in our model); for results presented in this thesis, we adopt an injection altitude of 70 km. We emphasize that moving the injection altitude to any other altitude below 70 km does not change any of the results of our simulations due to the plane wave model and lack of attenuation at those altitudes.

The optical emission intensities and the altitude distribution and absolute magnitude of ionization changes are highly sensitive to the time duration of the lightning EM pulse, its

shape and intensity. Each of these lightning characteristics exhibits great variability for both CG and IC discharges; see examples in Figure 1.1. For example, the time duration of the first return stroke varies by an order of magnitude with $\sim$100 μs being the average [*Uman*, 1987; p. 110], and the amplitude of the radiated EM field can reach E_{100} >25 V/m with the mean value E_{100} $\sim$10 V/m [*Krider and Guo*, 1983]. The shape of the pulse is also highly variable, including both single and double polarities, which produce different extremes of the maximum electric field amplitude in the lower ionosphere when the upgoing tail of the pulse interferes with the ionospherically reflected front part of the pulse. In this thesis our objective is to accurately determine the intensities of optical emissions and electron density changes for EM pulses with a time duration and shape for typical lightning waveform; investigation of the coupling of the full range of possible waveforms is the subject of future work (see Section 6.2). For this purpose, we represent the injected EM pulses by a single period oscillation of a 10 kHz sinusoid. The largest electric field amplitudes (E_{inj} = 25.5 V/m (observed $\sim$5% of the time) for profile (a) and E_{inj} = 37.5 V/m (observed $\sim$1% of the time) for profile (b)) that are used in our calculations are limited by the particular numerical model employed.

3

Electron Density Changes

To study the effect on the ionosphere of radiation from a single lightning discharge we inject a 100 μs long EM pulse at the lower boundary (70 km altitude) represented by a single period oscillation of a 10 kHz sinusoidal wave. We simulate the propagation of the EM pulse solving Maxwell's equations (2.1) and its evolution as it interacts with the ionosphere as determined by equations (2.2)–(2.6) for a time duration of ~260 μs, which allows the injected pulse to be reflected from the lower ionospheric boundary (~90 km) and to propagate back through the interaction region on its way to the ground. We maintain zero field boundary conditions* at the upper boundary (120 km) consistent with strong attenuation and reflection in the lower layers. The resulting density perturbations are shown at the end of the interaction for a variety of field amplitudes and ambient electron density profiles. We also illustrate a time sequence of events with snap-shots of altitude distributions of electric field, electron density changes, and average energy of electrons for the interaction of a E_{inj} = 20 V/m pulse with the 'tenuous' nighttime ionosphere.

Often the time period between consecutive discharges from thunderstorm centers is less

* We also note that due to the quasi-steady ($\partial/\partial t \simeq 0$) approach to the solution of the Boltzmann equations (2.4)–(2.6) our model does not account for whistler-mode waves (for any orientation of the electric field) which penetrate to the upper ionosphere and propagate to the weakly collisional magnetized plasma of the magnetosphere [e.g., *Helliwell*, 1965]. We note however, that leaving the whistler-mode out of our model has no significant impact on our modeling of the interaction of EM pulses with the highly collisional plasma of the lower ionosphere.

than a second [*Uman*, 1987, p. 19], which is much less than the relaxation time (10 to 100 s) of the density perturbations at D-region altitudes [*Glukhov et al.*, 1992]. In such cases, the ionization produced by consecutive strokes would accumulate as previously suggested [*Inan et al.*, 1991]. In modeling this accumulation we neglect relaxation during the time between strokes and supply incident EM energy for ~2.2 ms, a time that corresponds to ~20 consecutive lightning strokes. The resulting density perturbations are also presented for different electron densities and field strengths ($\vec{E} \parallel \vec{B}_0$). First we present the results for the electric field of the pulse oriented parallel to the ambient magnetic field. At the end of the chapter we compare these results with results for the perpendicular orientation ($\vec{E} \perp \vec{B}_0$).

3.1 ELECTRON DENSITY CHANGES FOR A 'TENUOUS' AMBIENT PROFILE

We start with the ambient electron density profile (a) in Figure 2.1 corresponding to a relatively 'tenuous' nighttime ionosphere. Figure 3.1 shows snapshots covering the 80 to 180 μs time interval in 20 μs increments following the injection of the EM pulse showing the altitude distribution of the electric field, average electron energy, and normalized electron density perturbations ($\delta N_e/N_{e0}$).

The injected wave amplitude at 70 km was taken to be E_{inj} = 20 V/m with the electric field polarized parallel to the ambient magnetic field (assumed horizontal). At 80 μs the wave front reaches 94 km altitude. As the wave propagates it becomes progressively attenuated and is partially reflected. We see from Figure 3.1 at 80 μs that at 85 km the amplitude has decreased to ~17.5 V/m. However, due to the partial reflection from the lower ionospheric boundary the amplitude of the pulse in the medium can exceed the initial amplitude (E_{inj} = 20 V/m in this case) as a result of constructive interference. An example of this effect is seen at 120 μs as the amplitude reaches ~27 V/m at ~83 km. Examination of Figure 3.1 shows that the lightning EM fields which penetrate above 97 km are strongly attenuated. The average energy of the electrons at ~90 km altitudes

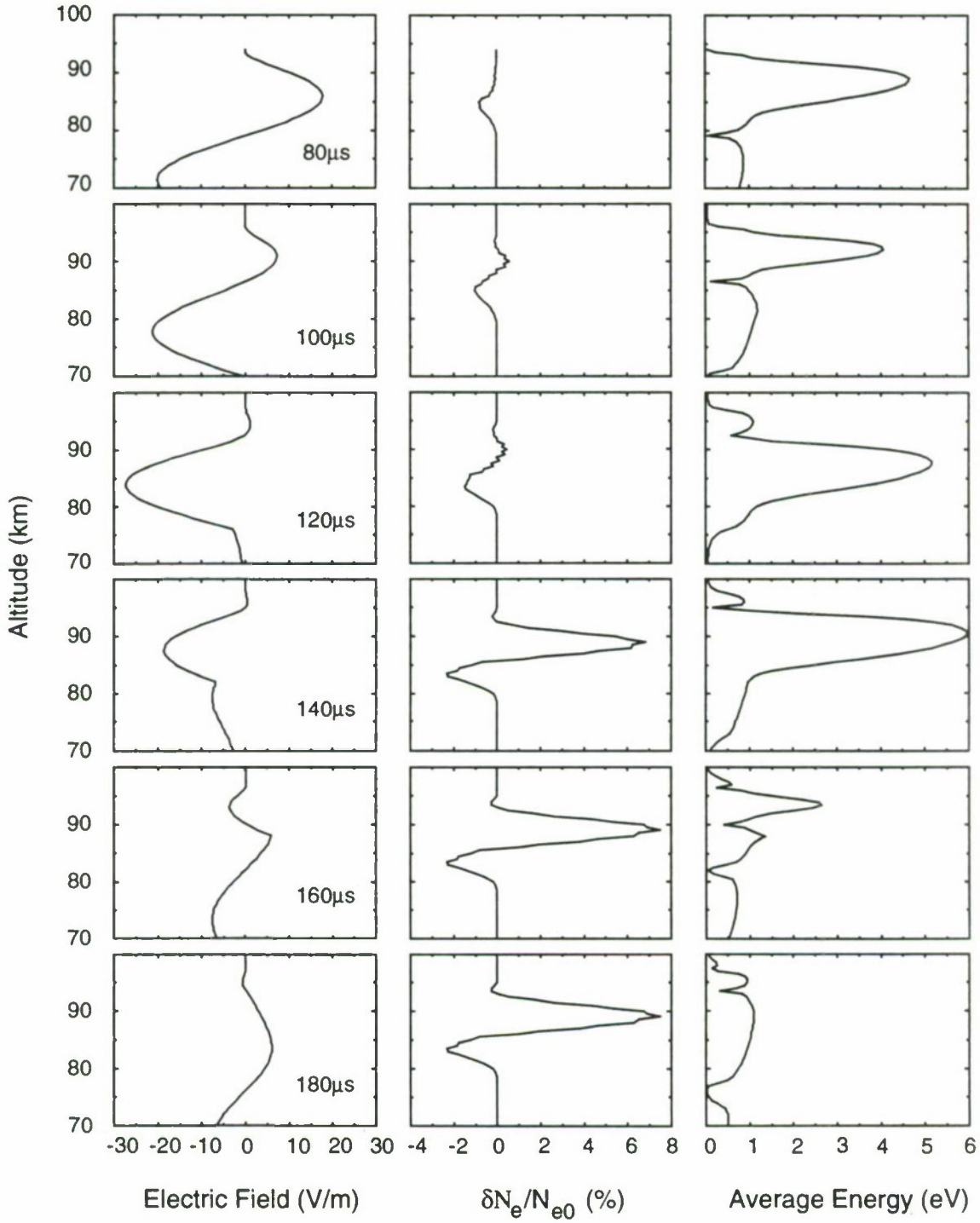

Fig. 3.1. Dynamics of the interaction of an EM pulse with the ionosphere. Snapshots of the electric field, normalized electron density change, and average electron energy covering the 80 to 180 μs time interval in 20 μs increments following the injection of a E_{inj} = 20 V/m EM pulse at 70 km under the 'tenuous' nighttime conditions (Figure 2.1 (a)).

at times exceeds 5 eV, providing a substantial number of electrons with energy higher than the thresholds for dissociative attachment (~6 eV) and ionization (~16 eV) and thus leading to changes in electron density. At lower altitudes (79 to 86 km) and at the end of the region penetrated by the fields (92 to 95 km) dissociative attachment prevails, causing decreases in electron density. At intermediate altitudes (86 to 92 km) the density is increased as ionization dominates. The major increase in density occurs at the time of constructive interference of the downgoing reflected first half of the pulse with the upgoing second half. The value of the density change reaches ~-3 % at 83 km and >+7 % at 89 km at the end of the interaction.

The resulting density changes for 6, 12, and 18 successive EM pulses with E_{inj} = 20 V/m are shown in Figure 3.2. The depletion evolves to ~48 % of the ambient at 83 km and the accumulated density increase is >150 % at 89 km.

A single 100 μs pulse with E_{inj} = 25 V/m causes up to a 27 % increase at ~89 km and a decrease of ~4 % at ~83 km as shown in Figure 3.3 (a). The resulting density changes for 8, 14, and 20 successive lightning strokes with E_{inj} = 25 V/m are shown in Figure 3.3 (b). The depletion evolves to ~55 % of the ambient at ~83 km and the density increase is >350 % at 89 km.

A summary plot of the resulting normalized density changes for single pulses of different strength is shown in Figure 3.4. Note for example that a pulse with 100 μs duration but with a smaller initial amplitude E_{inj}=10 V/m causes a substantially smaller (<1 %) negative density change with its maximum located at ~87 km, whereas a ~20 % density decrease occurs for 20 successive EM pulses of this strength. The drastic differences between the results for initial field intensities of 10, 20, and 25 V/m underscore the highly nonlinear nature of the interaction.

It is also interesting to note from the left hand panel of Figure 3.4that the altitude of maximum depletion moves lower with increasing input electric field intensity. This tendency is opposite to that found in earlier work, namely that the altitude of maximum

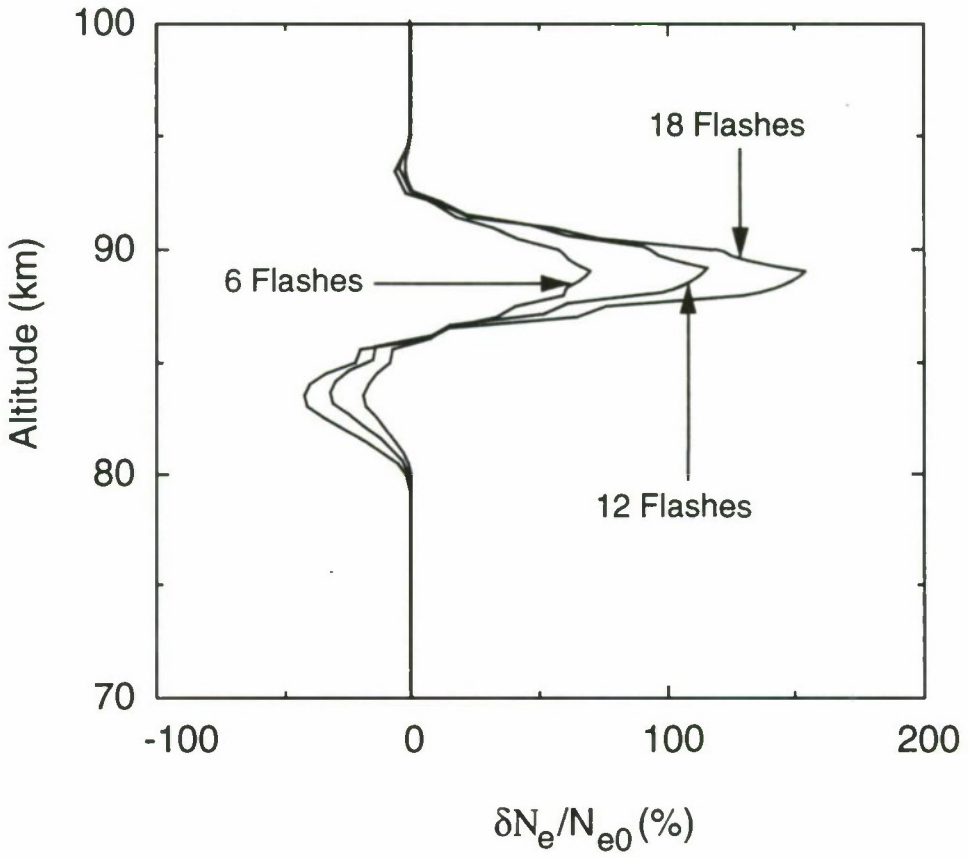

Fig. 3.2. Electron density changes. The resulting density changes produced by a sequence of 8, 14, and 18 EM pulses with E_{inj} = 20 V/m under 'tenuous' nighttime conditions (Figure 2.1 (a)).

heating increases with injected EM pulse intensity [*Rodriguez et al.*,1992], due to the increase in reflection height as a result of enhanced collision frequency (in the context of a WKB approximation the reflection of VLF waves occurs at the altitude at which $\omega_p^2 \simeq \omega\nu$ [*Ratcliffe*, 1959; p. 111] where ω_p is the plasma frequency, ω is the wave frequency, and ν is the effective electron collision frequency).

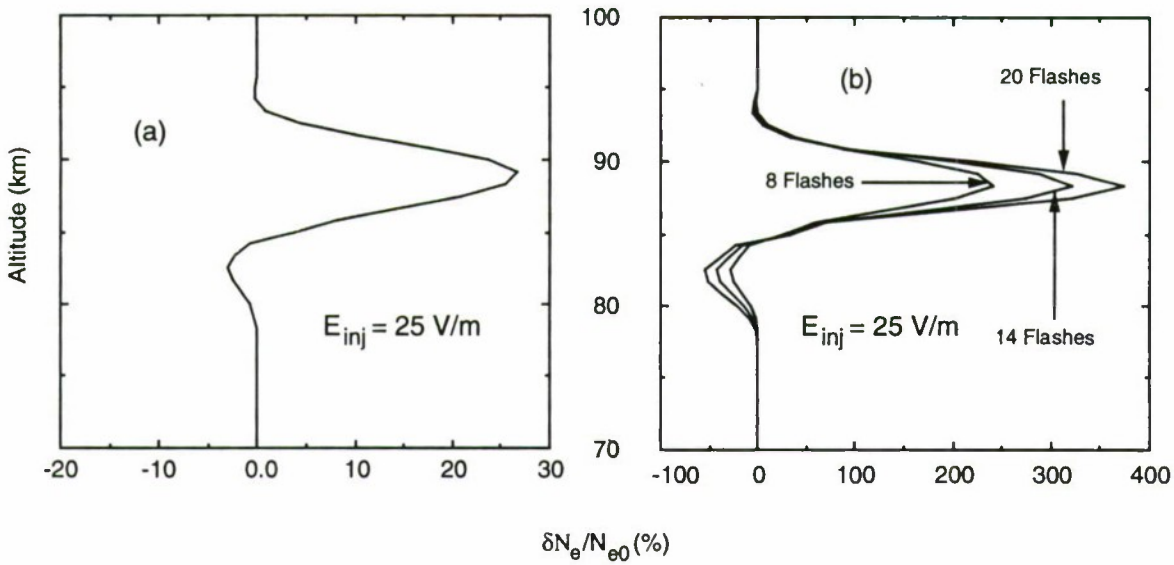

Fig. 3.3. Electron density changes. *(a):* The resulting density changes produced by a single EM pulse with E_{inj} = 25 V/m under 'tenuous' nighttime conditions (Figure 2.1 (a)). *(b):* The resulting density changes produced by a sequence of 8, 14, and 20 EM pulses with E_{inj} = 25 V/m under the same conditions.

3.2 ELECTRON DENSITY CHANGES FOR A 'DENSE' AMBIENT PROFILE

As an intermediate ambient density profile, we consider profile (b) in Figure 2.1, which may represent nighttime conditions during enhanced geomagnetic activity at midlatitude or in the auroral regions.

For a denser D region the reflection altitude for the EM pulse is lower, resulting in higher local neutral density and less electron heating compared to a tenuous D region. Thus, larger electric field amplitudes are needed to produce the same fractional density charges or to excite a given intensity of optical emissions.

For an EM pulse with E_{inj} = 35 V/m the density changes are shown in Figure 3.5. Negative changes (~-4 % at 81 km) are of larger magnitude than positive ones (~+2.3 % at 87 km). For pulses with E_{inj} <30 V/m, the density perturbations become single peaked and purely negative at ~83 km. The absolute value of $\delta N_e/N_e$ drops below 1 % for EM pulses with initial amplitudes smaller than 20 V/m.

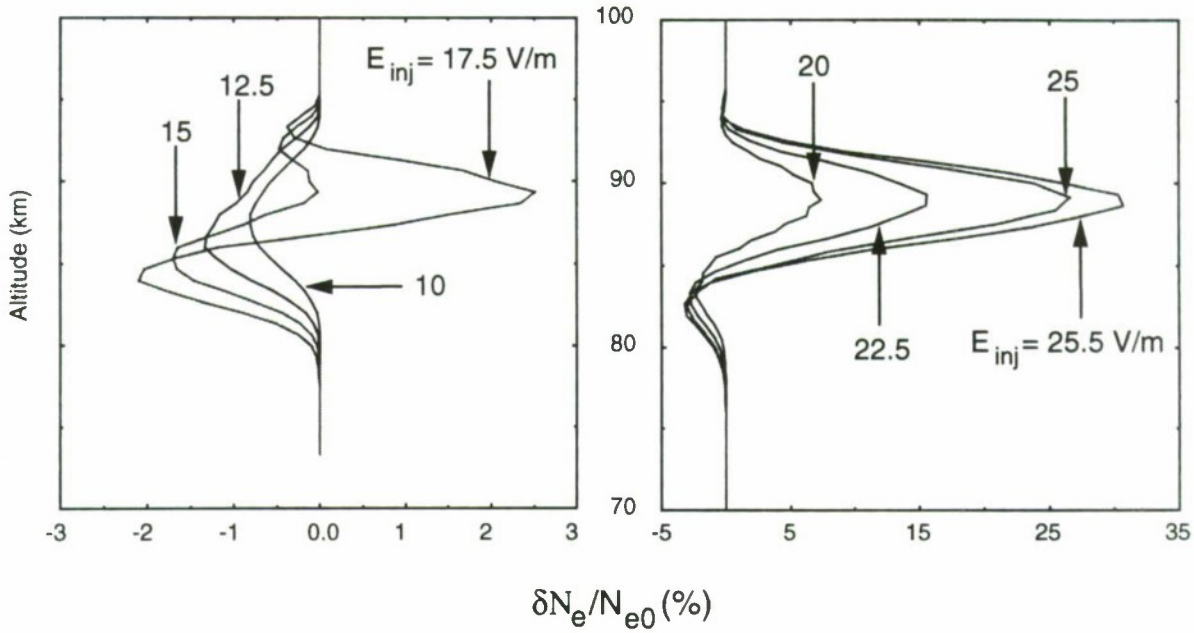

Fig. 3.4. Electron density changes. Summary of the resulting density changes produced by single EM pulses of E_{inj} = 10, 12.5, 15, 17.5, 20, 22.5, 25, 25.5 V/m under 'tenuous' nighttime conditions (Figure 2.1 (a)). Note the different scales for the abscissa for the left and right hand panels.

Successive EM pulses with initial amplitude E_{inj} = 35 V/m can produce quite prominent density changes as shown in Figure 3.6 for 8, 14, and 20 discharges. The positive and negative changes have about the same amplitude (~60 %) and peak at 85 km and 81 km respectively. For initial electric field amplitudes E_{inj} =30 V/m, the density perturbation is negative with a single peak at about 83 km and an amplitude of ~57 % for E_{inj} = 30 V/m, and ~20 % for E_{inj} = 20 V/m.

3.3 DAYTIME CONDITIONS

The daytime profile shown in Figure 2.1 as profile (c) was used to make calculations similar to those reported above. In general, we find that even for the strongest EM pulses (E_{inj} = 50 V/m) the density perturbation is negative with very small absolute value ($|\delta N_e/N_e| \leq 3 \times 10^{-3}$), whereas for 20 consecutive discharges of such intensity

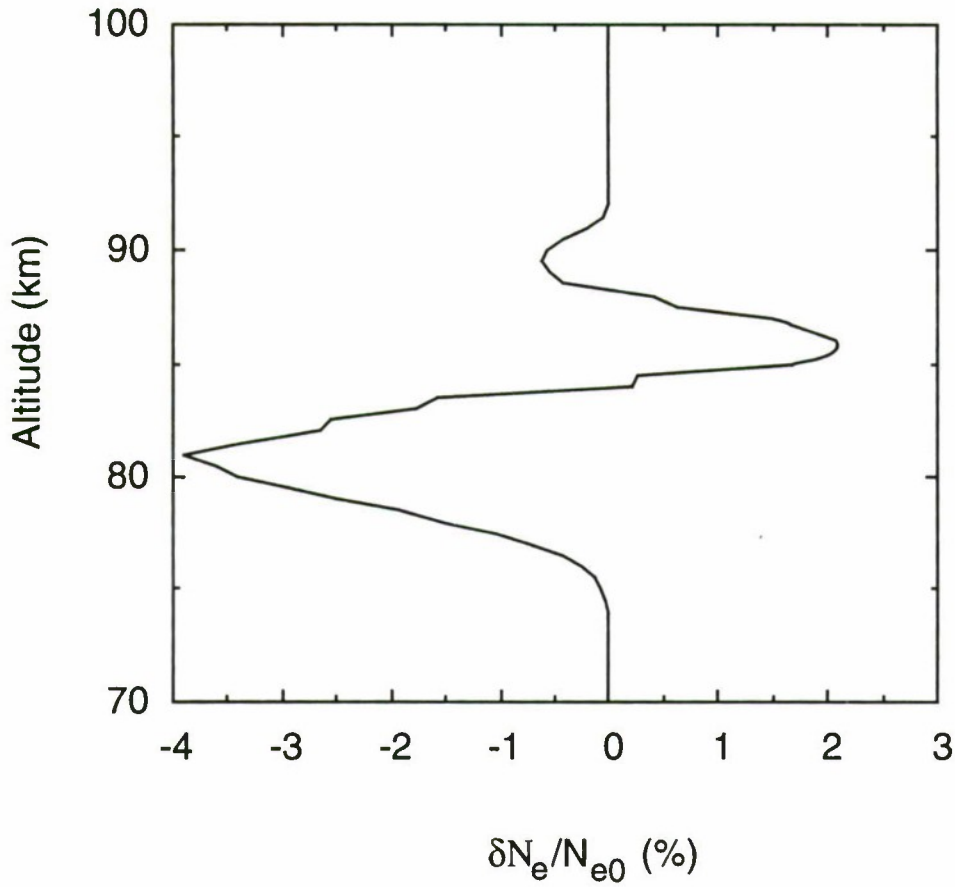

Fig. 3.5. Electron density changes. The resulting density changes produced by a single E_{inj} = 35 V/m EM pulse for a 'dense' electron density profile (Figure 2.1 (b)).

($|\delta N_e/N_e| \leq 5 \times 10^{-2}$). The minimum is located at ~76 km. Such perturbations are unlikely to be detectable and most probably do not play a significant role in the overall dynamics of the lower ionosphere. We therefore conclude that the phenomenon of lightning-induced ionization occurs predominantly under nighttime conditions.

The physical reason for the lack of significant ionization by lightning during daytime is the fact that the reflection altitude of the lightning EM pulses is at ~77 km, where the mean free path of the electrons is much shorter (~4 times) than at 85 km, and consequently, more of the electron energy goes into excitation of the molecular energy levels lower than those of ionization and dissociative attachment.

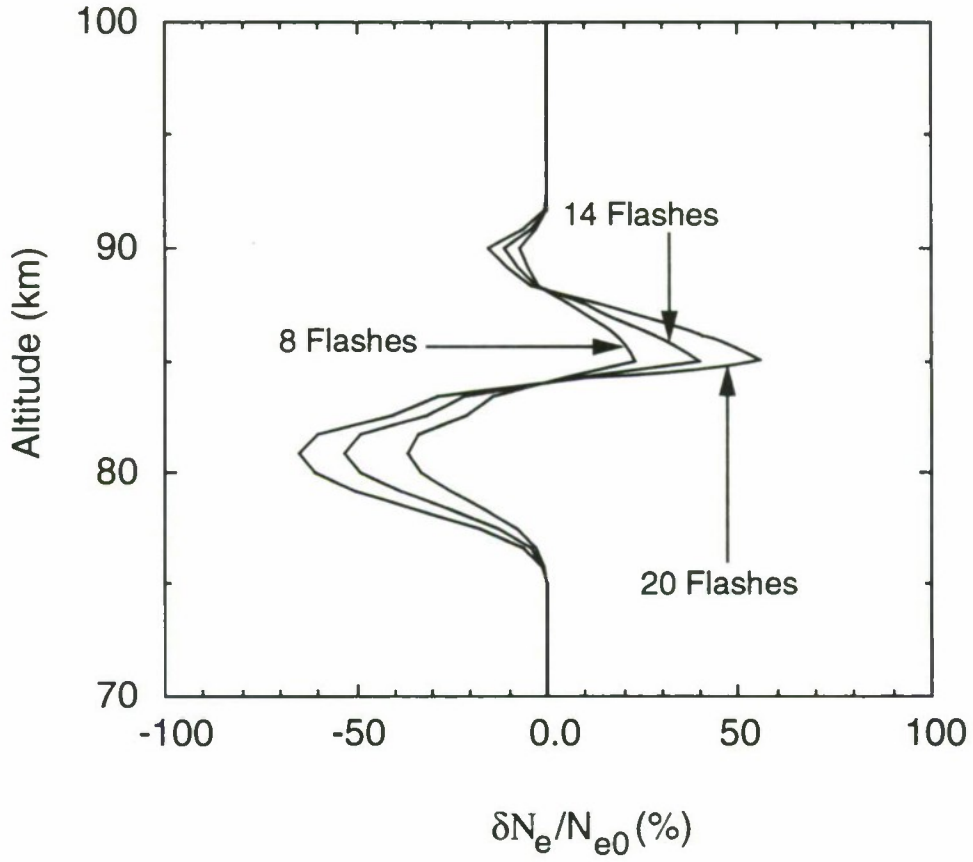

Fig. 3.6. Electron density changes. The resulting density changes produced by a sequence of 8, 14, and 20 E_{inj} = 35 V/m EM pulses under the 'dense' nighttime profile (Figure 2.1 (a)).

3.4 DEPENDENCE ON THE ORIENTATION OF THE ELECTRIC FIELD

The results reported so far were for an EM pulse with electric field assumed to be parallel to the ambient magnetic field ($\vec{E} \perp \vec{B}_0$), which in turn is taken to be horizontal. After performing similar calculations for the case of the perpendicular orientation of the electric field of the pulse with respect to the ambient magnetic field, we found two minor differences from the case of the parallel field orientation. *Firstly*, for the same electric field amplitudes and pulse duration, the maximum amplitudes of the *positive* density perturbations for the perpendicular orientation were 15 to 30 % smaller than for the case of parallel orientation. *Secondly*, the altitudes of the maximum *positive* density perturbations for the perpendicular orientation were 2 to 3 km higher than for the case of

parallel orientation. For example, a E_{inj} = 20 V/m 100 μs pulse with the perpendicular orientation for the nighttime conditions produced $\sim$6 % density increase located at $\sim$91 km in comparison to >7 % increase at 89 km for the parallel orientation (see Figure 3.1).

This comparatively weak dependence on the angle between the electric field of the wave and the ambient magnetic field is due to the high collision frequency of the heated electrons with the ambient neutrals which is much larger than the electron gyrofrequency in the ambient magnetic field in the altitude range of interest. For example, at 90 km the collision frequency of 5 eV electrons is $\sim 10^8$ s^{-1} which is about two orders of magnitude larger than the electron gyrofrequency at that altitude which makes the influence of the magnetic field completely negligible. However, for weaker heating (for example in the case of heating by VLF transmitters) $\vec{B}_o$ is important and leads to substantial asymmetry of the transverse shape of the heated region [*Inan et al.*, 1992; *Rodriguez*, 1993].

Overall, the results obtained in this study appear to be applicable with $\sim$10 % accuracy to any intermediate (between $\vec{E} \parallel \vec{B}_0$ and $\vec{E} \perp \vec{B}_0$) field orientation.

4

Optical Emissions

Airglow and auroral emissions have been used extensively to extract information about important ionospheric and magnetospheric processes. Excitation of a variety of optical emissions would be a natural consequence of lightning-induced heating of ambient electrons as suggested by *Inan et al.* [1991] and as discussed in Chapter 3. The experimental data that motivated the work of *Inan et al.* [1991] involved detection (via subionospheric VLF remote sensing) of lightning-associated ionization enhancements (as discussed in Chapter 3) that are produced at threshold energies of > 15.6 eV, which is well above the excitation thresholds of most optical emissions from neutral constitutients in the D region [e.g., *Rees*, 1989; Appendix 3]. The possibility of the excitation of optical emissions as a result of lightning-induced heating of the lower ionosphere was first recognized by *Inan et al.* [1991]. The first experimental evidence for such optical emissions via D region heating by lightning may be the recent observations from the Space Shuttle [*Boeck et al.*, 1992] of a transient airglow enhancement in the D region of the ionosphere that appeared to be associated with a tropospheric lightning discharge. These observations were discussed earlier in Section 1.2.

In this Chapter we use the same model for the electrodynamic interaction of a lightning EM pulse with the lower ionosphere as that used in Chapter 3 to calculate the radiation time constants and intensities of the emission lines of O, O_2, N_2, O_2^+, and N_2^+ most easily detectable in the natural aurora [*Vallance Jones*, 1974].

To study optical emissions from the D region excited by EM radiation from a single lightning stroke we inject, as before in Chapter 3, a 100 μs long EM pulse at the lower boundary (70 km altitude) represented by a single period oscillation of a 10 kHz sinusoidal wave. In accordance with the model described in Chapter 2, we simulate the propagation of the pulse solving Maxwell's equations (2.1) and its evolution as it interacts with the ionosphere as determined by equations (2.2)–(2.6) for a time duration of $\sim$260 μs, which allows the injected pulse to be reflected from the lower ionospheric boundary ($\sim$90 km) and to propagate back through the interaction region on its way to the ground. We maintain zero field conditions at the upper boundary (120 km) consistent with strong attenuation and reflection in the lower layers. In this Chapter we present time snapshots of the altitude distributions of electric fields, average electron energy and emission intensity, altitude distributions of the maximum intensities of optical emissions, and time and height integrated emission intensities.

The governing equation in our model for the impact excitation of neutral species is [e.g., *Sipler and Biondi*, 1972]

$$\frac{\partial n_i}{\partial t} = -\frac{n_i}{\tau_i} + \sum_j n_j A_j + N_i R_i \tag{4.1}$$

where n_i denotes the density of excited particles at i-th level, N_i is the ambient density of corresponding neutrals in the ground state, $\tau_i = (\sum_l A_l + k_{1i} N_{N_2} + k_{2i} N_{O_2} + k_{3i} N_O)^{-1}$ is the total lifetime of the i-th state, A_l is the radiation transition rate*, k_{ij} is the quenching rate†, and R_i is the excited state source term.‡ The first term on the right hand side of equation (4.1) describes the decrease of the density of the excited particles as a result of emissions and quenching by neutrals, the second term represents the increase in the population of excited particles as a result of cascading from higher states (e.g., population

* The transition rate is the inverse of the average time it takes for the spontaneous radiation of a photon.

† Quenching refers to the loss of energy by the excited particle due to collision processes with molecules or atoms.

‡ The source term describes excitation of the state by electron impact from the ground state.

of the $B^3\pi_g$ state of N_2 as a result of emissions of the 2nd positive band originating from the $C^3\pi_u$ level in Figure 4.1), and the third term describes the excitation of a particular state by electron impact from the ground state (e.g., $X'\Sigma_g^+$ state of N_2 in Figure 4.1).

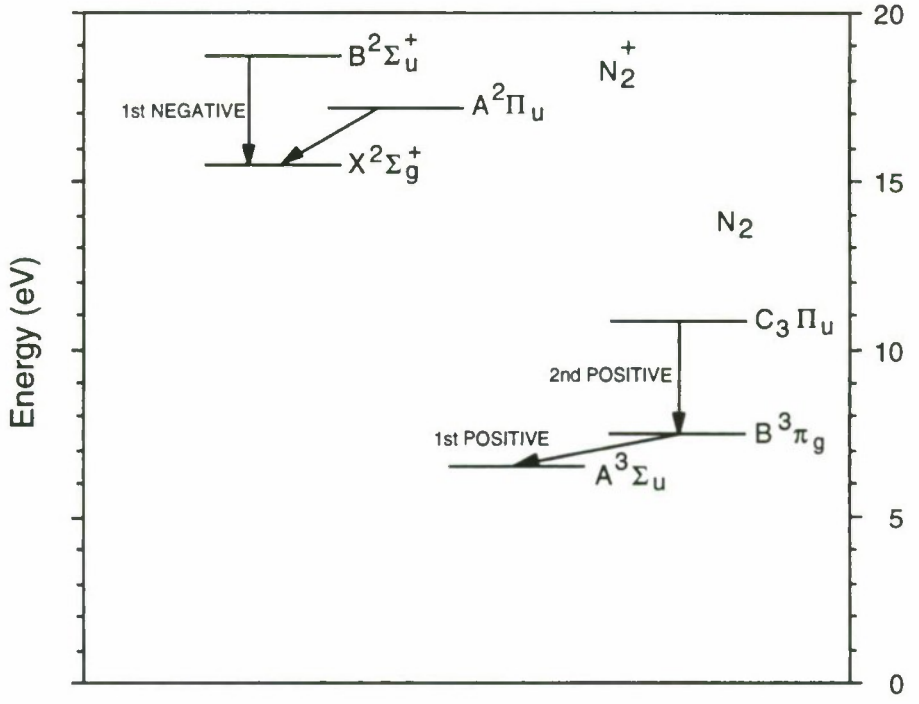

Fig. 4.1. Energy levels and electronic band systems for N_2 and N_2^+. The 1st and 2nd positive bands of N_2 and 1st negative and Meinel bands of N_2^+ are considered in our calculations. For a variety of different reasons, other bands of N_2 and N_2^+ (not shown here) are considered to be weak based on observed auroral spectra [*Vallance Jones*, 1974; p. 90].

The intensity of i-th line is given by [*Chamberlain*, 1978; p. 213]:

$$I_i = 10^{-6} \int A_i n_i dz \tag{4.2}$$

where the integration is performed along the line of sight and the units of the resultant intensity I_i are in Rayleighs (R), (i.e., photons/s emitted in a column with 1 cm^2 cross sectional area along the line of sight multiplied by 10^{-6}).

Differences between the time duration of EM pulses ($\sim$100 μs) and the time intervals of spontaneous radiation and quenching allow us to consider the process of excitation in a relatively simple manner. The fact that the 100 μs time interval is much shorter than the emission and quenching times for the 'forbidden'* [*Vallance Jones*, 1974; p. 95] transitions (e.g., 6300, 5577 $\AA$ of O with the quenching times being 1.5 ms and 0.35 s at $\sim$95 km, emission times being 107 s and 1 s (Appendix D) respectively), allows us to neglect emission and quenching losses during the time interval of the excitation process and to integrate the number of excited molecules over the time of excitation. The resulting number of excited atoms is used to calculate the maximum intensities of the lines. For all molecular bands (which constitute 'allowed'† [*Vallance Jones*, 1974; p. 95] transitions), the fact that the 100 μs time interval is much longer than the time intervals (the longest is 14 μs for Meinel band of N_2, see Appendix D) of spontaneous radiation of these emissions and much shorter than the quenching time intervals $\sim$1 ms (Appendix D) at altitudes of interest allows us to assume that $\sim$100 % of the excited molecules emit photons at about the excitation rates in effect during the time of the heating.

The three major constituents for which we estimate the optical emission characteristics are N_2, O_2, and O. We also consider O_2^+ and N_2^+ ions produced as a result of the electron impact ionization of the neutral species. Energy level diagrams of O, O_2, N_2, O_2^+, and N_2^+ are well known and are widely available in literature (e.g., see *Vallance Jones* [1974], pp. 85-91). The N_2 energy diagram is given as an example in Figure 4.1.

Each of the neutral and ionized species under consideration has emission lines ranging from far infrared (IR) to extreme ultraviolet (UV) which are commonly observed in auroral and airglow emission spectra. Emissions to be studied here were selected upon

---

* The term 'forbidden' is used to indicate the fact that these states have a zero electric and/or magnetic dipole moment as a consequence of the symmetry properties of the quantum wave function.

† The term 'allowed' is used to indicate the fact that these states have a electric or magnetic dipole moment not equal to zero as a consequence of the symmetry properties of the quantum wave function.

consideration of the following factors: *i)* amplitudes of electron impact excitation cross-sections (electron impact transfers kinetic energy of the electrons to optical excitations of ambient molecules; the individual cross sections are summarized in Appendix B), *ii)* emission rates (which determine the average time intervals of spontaneuous emissions summarized in Appendix D), *iii)* branching ratio of different lines originating from the same level (e.g., the ratio of the number of 5577 $\mathring{A}$ ($^1S \rightarrow ^1D$ transition) and 2972 $\mathring{A}$ ($^1S \rightarrow ^3P$ transition) photons originating from the same ^1S level of O; see Appendix D), *iv)* cascade effects (e.g., population of the $B^3\pi_g$ state of N_2 as a result of emissions of the 2nd positive band originating from the $C^3\pi_u$ level as can be seen from Figure 4.1), *v)* radiation trapping effects (i.e., resonant absorption of emitted photons by the same type of atoms or molecules, e.g., 1304 and 1356 $\mathring{A}$ lines of O [*Donahue and Strickland*, 1970]), *vi)* quenching rates by neutral species (upon collision of an electronically excited molecule with another molecule (or atom) in a ground state the former can lose its energy to the excitation of a vibrational state or to the translational energy of the latter [*Vallance Jones*, 1974; p. 114]; the quenching rates are summarized in Appendix D), *vii)* transparency of the atmosphere at the wavelength of the emission (after elimination of lines resonantly absorbed in the atmosphere, the major factor determining the optical depth of the path is the Rayleigh molecular scattering discussed in Section 5.2.2), *viii)* comparison of the expected intensities to the nighttime airglow background (this aspect is discussed in Section 5.2.1).

The optical lines and bands considered here are regularly observed in the airglow and auroral spectra [*Vallance Jones*, 1974; *Chamberlain*, 1978], namely: the red 6300 (6364) $\mathring{A}$ ($^1D \rightarrow ^3P$ transitions), and the green 5577 $\mathring{A}$ ($^1S \rightarrow ^1D$ transitions) lines of O; the blue to UV 2nd positive band ($C^3\pi_u \rightarrow B^3\pi_g$ transitions) and the red to IR 1st positive band ($B^3\pi_g \rightarrow A^3\Sigma_u^+$ transitions) of N_2; the blue 1st negative band ($B^2\Sigma_u^+ \rightarrow X^2\Sigma_g^+$ transition) and IR Meinel band ($A^2\pi_u \rightarrow X^2\Sigma_g^+$ transition) of N_2^+ ions; and the red 1st negative band ($b^4\Sigma_g^- \rightarrow a^4\pi_u$) of O_2^+ ions. We exclude the Herzberg I band from our present analysis due to lack of reliable electron impact excitation cross sections for this band [*T.*

Slanger, private communication]. The O_2 atmospheric band is also excluded due to the weak emission intensities in comparison with the nighttime backgrounds [*Taranenko et al.*, 1992]. Plots of the cross-sections for excitation of the chosen emissions by electron impact as a function of electron energy are shown in Appendix B whereas quenching and emission rates are summarized in Appendix D.

4.1 RESULTS FOR A 'TENUOUS' NIGHTTIME D REGION

We start with the ambient electron density profile (a) in Figure 2.1 corresponding to a 'tenuous' nighttime D region and show the dynamics of the interaction of the EM pulse with the lower ionosphere.

Figure 4.2 shows snapshots covering the 80 to 180 μs time interval in 20 μs increments following the injection of the EM pulse. Each frame shows the altitude distribution of the electric field, average electron energy, and number of emissions per cc per second of the 5577 $\AA$ line of O and the 1st positive band of N_2. The left and right hand panels of Figure 4.2 are identical to those of Figure 3.1; the center panels in Figure 4.2 show optical emission intensities instead of density changes as in Figure 3.1.

The injected wave amplitude at 70 km was taken to be 20 V/m with the electric field polarized parallel to the ambient magnetic field (assumed horizontal). At 80 μs the wave front reaches 94 km altitude. As the wave propagates upward it becomes progressively attenuated and is partially reflected. The average energy of the electrons at times exceeds 5 eV, providing a substantial number of electrons with energy higher than the optical thresholds (ranging from 2 to 19 eV) and thus leading to stimulation of optical emissions. It is seen that the intensity of the 'forbidden' line (5577 $\AA$) grows throughout the process of interaction whereas the intensity of the 1st positive 'allowed' band is highly variable and reaches its largest amplitude at the time of constructive interference of the downgoing reflected first half of the pulse with the upgoing second half. The difference in their behaviour is due to the difference in their radiation time intervals, $\sim$0.1 s (due to

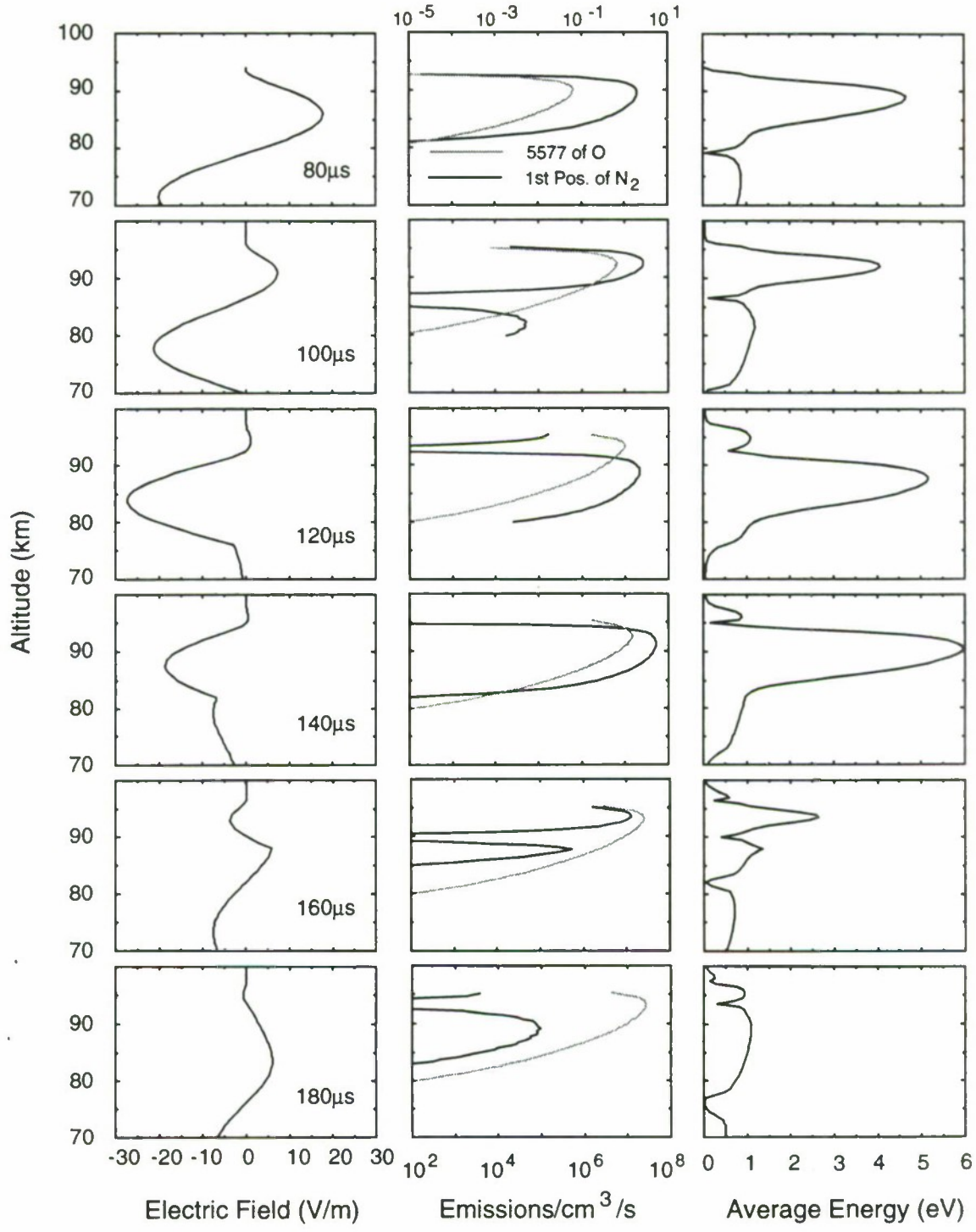

Fig. 4.2. Evolution of the interaction in space (altitude) and time. Snapshots of the electric field, optical excitation rates of the 5577 $\AA$ line of O (lighter line) and the 1st positive band of N_2 (solid line), and average electron energy shown for the 80 to 180 μs time interval in 20 μs increments following the injection of a E_{inj} = 20 V/m EM pulse at 70 km under 'tenuous' nighttime conditions (Figure 2.1 (a)).

quenching) at 90 km for the 5577 $\AA$ line and $\sim$6 μs (due to spontaneous radiation) for the 1st positive, for quenching and radiation rates see Appendix D.

The altitude distribution of maximum intensities of the various lines stimulated by an EM pulse with E_{inj} = 20 V/m is shown in Figure 4.3 (a). Note that the values plotted here represent the maximum emission intensity reached at that altitude sometime during the 260 μs interaction episode which was illustrated by means of space-time shapshots in Figure 4.2. The emission intensities of 'allowed' bands integrated over the 100 μs duration of the EM pulse* are shown in Figure 4.3 (b), whereas the temporal variations of the height integrated (70-100 km) intensities are shown in Figure 4.3 (c).

The altitude distribution of maximum intensities of the various lines stimulated by an EM pulse with E_{inj} = 25 V/m is shown in Figure 4.4 (a). Note that the values plotted here represent the maximum emission intensity reached at that altitude sometime during the 260 μs interaction episode. The emission intensities integrated over the duration of the emissions ($\sim$100 μs for the short lasting band emissions, $\sim$0.5 ms at 90 km for 6300 $\AA$ line of O, and $\sim$0.1 s at 90 km for 5577 $\AA$ line of O) are shown in Figure 4.4 (b), whereas the temporal variations of the height integrated (70-100 km) intensities are shown in Figure 4.4 (c).

For an EM pulse with E_{inj} = 10 V/m, the 1st and 2nd positive bands of N_2 have 10 to 12 times weaker maximum and time integrated intensities than those for a pulse with E_{inj} = 25 V/m. Emissions from molecular ions have $\sim$1,000 times weaker maximum and time integrated intensities. Intensities of 6300 and 5577 $\AA$ lines of O are lower by a factor of $\sim$10 in comparison with the E_{inj} = 25 V/m case.

Figure 4.5 shows the dependence of the maximum emission rates versus the electric

---

* Note that the duration of the optical emissions of the molecular bands is also $\sim$100 μs, although the 6300 and 5577 $\AA$ of O last longer ($\sim$0.5 ms and $\sim$0.1 s at 90 km respectively).

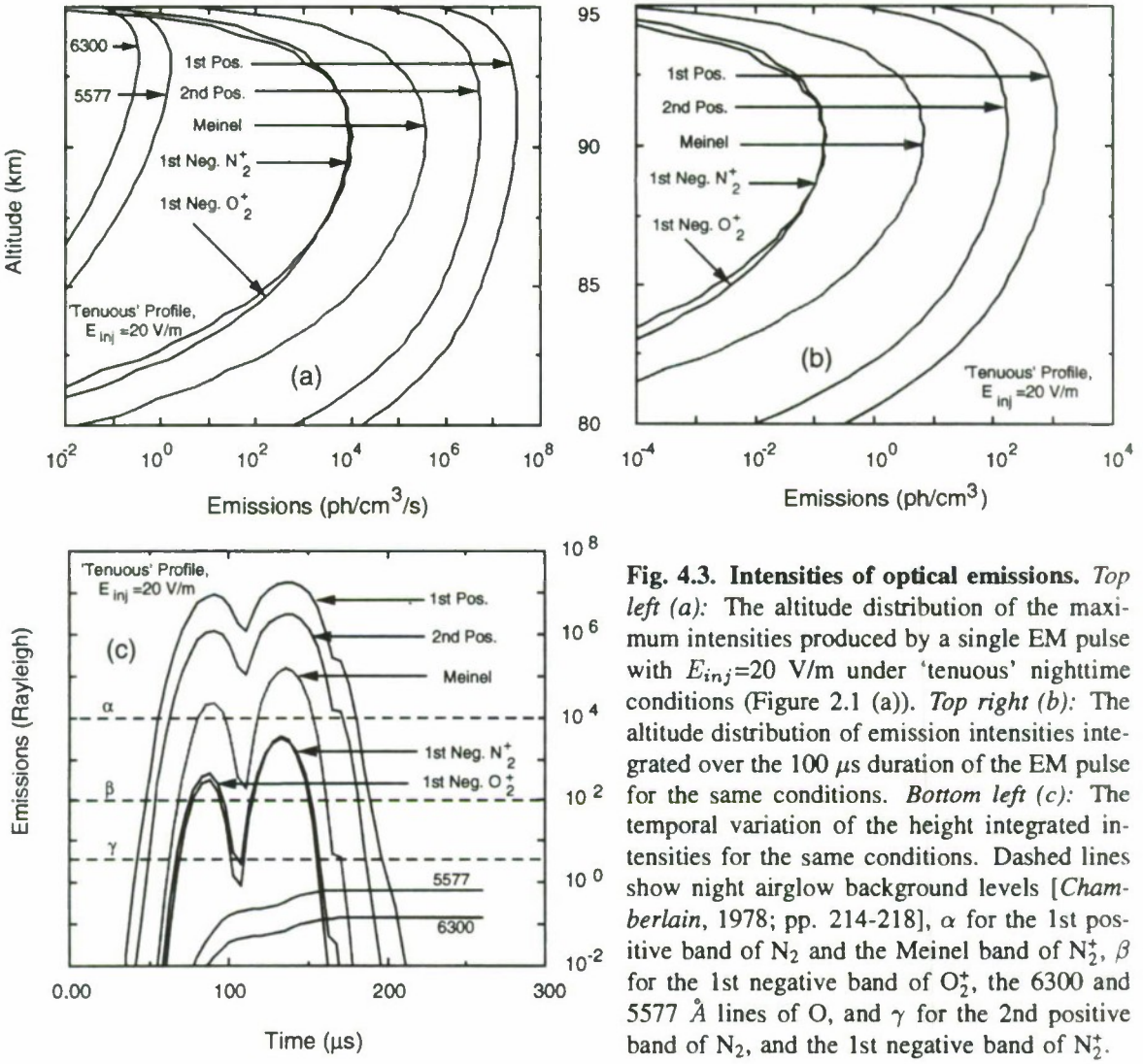

Fig. 4.3. Intensities of optical emissions. *Top left (a):* The altitude distribution of the maximum intensities produced by a single EM pulse with E_{inj}=20 V/m under 'tenuous' nighttime conditions (Figure 2.1 (a)). *Top right (b):* The altitude distribution of emission intensities integrated over the 100 μs duration of the EM pulse for the same conditions. *Bottom left (c):* The temporal variation of the height integrated intensities for the same conditions. Dashed lines show night airglow background levels [*Chamberlain*, 1978; pp. 214-218], α for the 1st positive band of N_2 and the Meinel band of N_2^+, β for the 1st negative band of O_2^+, the 6300 and 5577 $\AA$ lines of O, and γ for the 2nd positive band of N_2, and the 1st negative band of N_2^+.

field amplitude of the pulse, expressed in terms of E_{100}*. Also indicated are the percentages of occurence of CG discharges with E_{100} larger than the corresponding numbers in V/m, based on ground-based measurements [*Krider and Guo*, 1983].

We see from Figure 4.5 that due to the somewhat different dependence of the emission intensity of the various lines on E_{100}, the spectral content of the optical emissions from the D region vary in predictable manner. In particular, we note that the 1st and the 2nd positive bands of N_2 and 6300 and 5577 $\AA$ lines of O do not increase as rapidly with

* Note from Section 2.5 that $E_{100} = E_{inj} \frac{80km}{100km}$

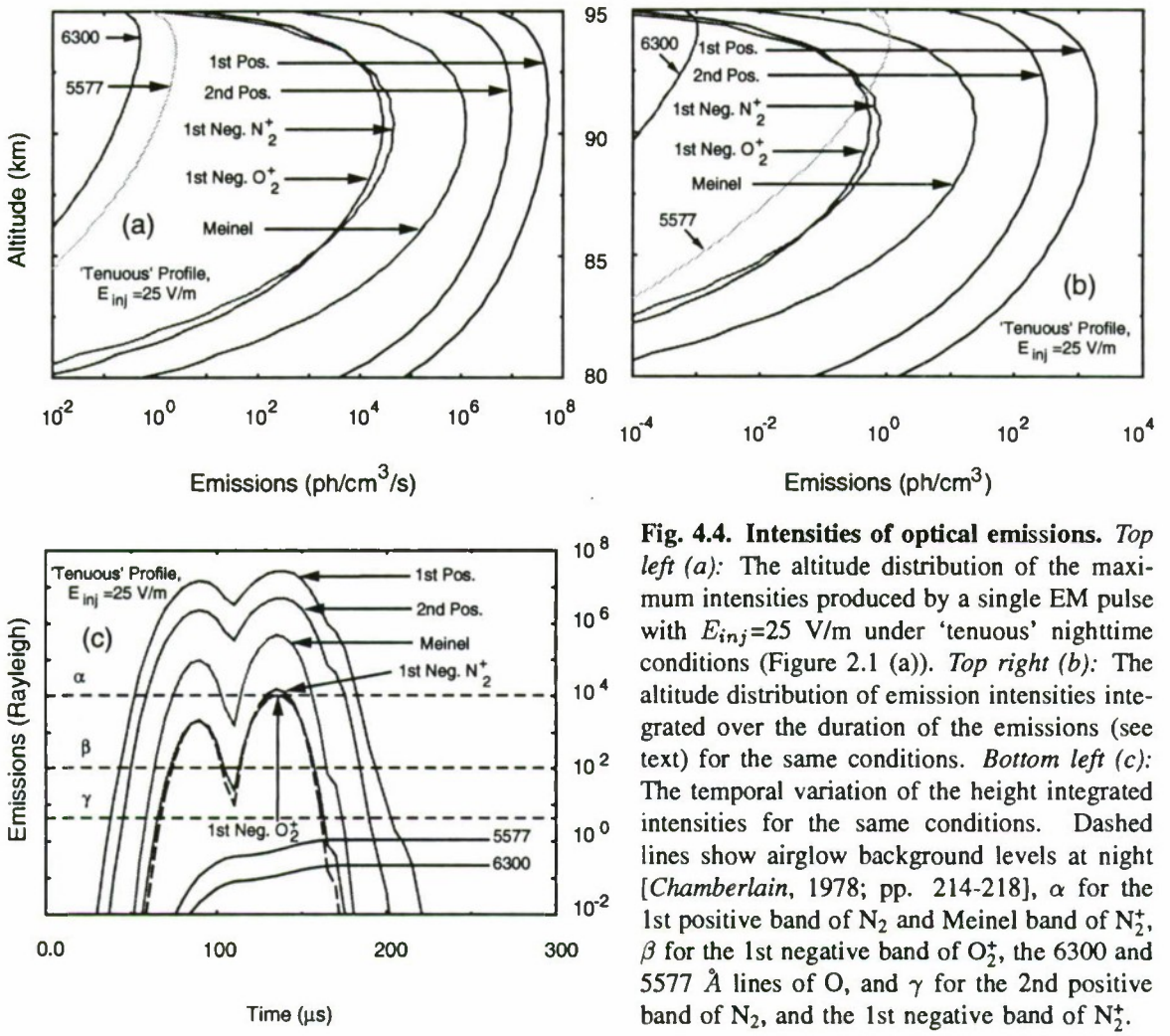

Fig. 4.4. Intensities of optical emissions. *Top left (a):* The altitude distribution of the maximum intensities produced by a single EM pulse with E_{inj}=25 V/m under 'tenuous' nighttime conditions (Figure 2.1 (a)). *Top right (b):* The altitude distribution of emission intensities integrated over the duration of the emissions (see text) for the same conditions. *Bottom left (c):* The temporal variation of the height integrated intensities for the same conditions. Dashed lines show airglow background levels at night [*Chamberlain*, 1978; pp. 214-218], α for the 1st positive band of N_2 and Meinel band of N_2^+, β for the 1st negative band of O_2^+, the 6300 and 5577 $\AA$ lines of O, and γ for the 2nd positive band of N_2, and the 1st negative band of N_2^+.

increasing E_{100} as the emission bands of the ionized molecules. For example, the ratio of emission rates of the 1st positive of N_2 and the 1st negative of N_2^+ for discharges with E_{100} = 20 V/m (stronger pulses occur ~5 % of the time) and E_{100} = 10 V/m (stronger pulses occur ~40 % of the time) is ~7 and ~400 respectively. This circumstance results from the generally higher excitation thresholds of the emissions for the ions and shows the potential use of spectroscopic measurements of airglow enhancements as a means to possibly assess the strength of the EM pulse, or if that is well known via other measurements, other quantities such as the ambient electron density (also see Figure 4.7 below).

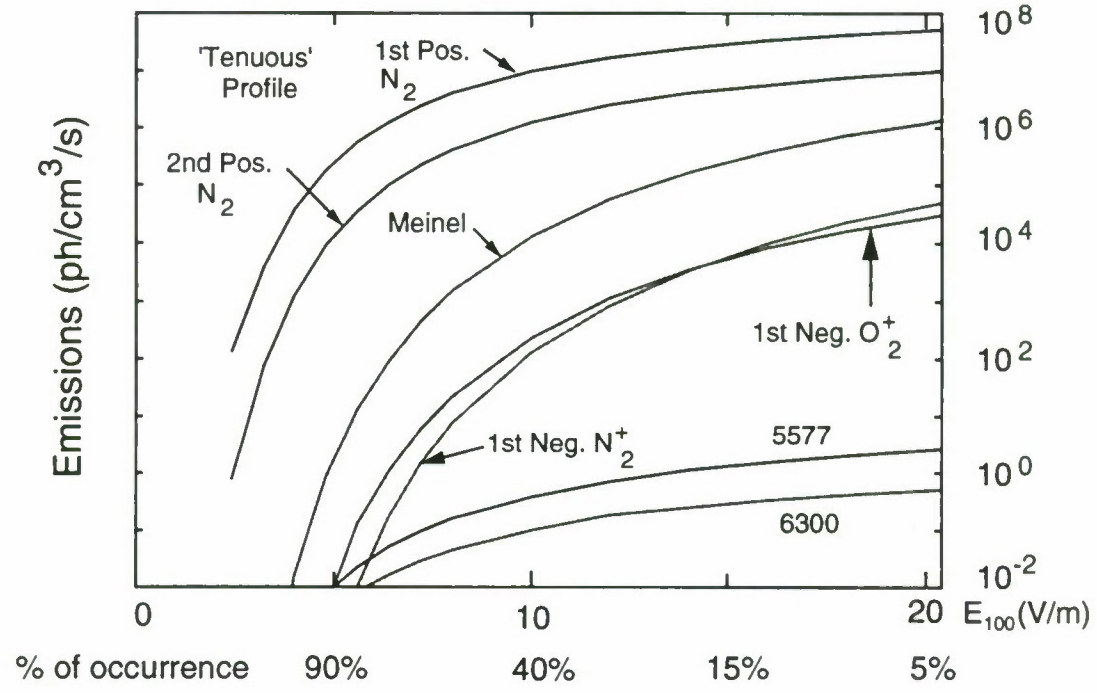

Fig. 4.5. Maximum emission rates as a function of the electric field amplitude E_{100}. The calculations were performed under 'tenuous' nighttime conditions (Figure 2.1 (a)). Also indicated are the percentages of occurrence of CG discharges with E_{100} larger than the corresponding numbers in V/m [*Krider and Guo*, 1983].

Although not shown here, altitude and time integrated intensities show similar dependences as a function of the input electric field amplitude since the peak intensities tend to dominate the averages over time and altitude.

4.2 RESULTS FOR A 'DENSE' NIGHTTIME D REGION

For a denser D region the reflection altitude of the EM pulse is lower (see Section 3.1 for a short discussion on reflection height), resulting in higher local neutral density and less electron heating compared to a 'tenuous' D region. Thus, generally larger electric field amplitudes are needed to produce the same levels of excitation of optical emissions.

As a 'dense' ambient density profile, we consider a profile (b) in Figure 2.1, which may represent nighttime conditions during enhanced geomagnetic activity or in the auroral

regions. In accordance with the above discussion the amplitudes of EM pulses that we consider in this section are larger than in Section 4.1 for a 'tenuous' D region. For an EM pulse with initial intensity E_{inj} = 35 V/m the altitude distribution of maximum intensities is shown in Figure 4.6 (a). The emission intensities integrated over the duration of the emissions ($\sim$100 μs for the short lasting band emissions, $\sim$0.5 ms at 90 km for 6300 $\AA$ line of O, and $\sim$0.1 s at 90 km for 5577 $\AA$ line of O) are shown in Figure 4.6 (b), whereas the temporal variation of the height integrated intensities is given in Figure 4.6 (c).

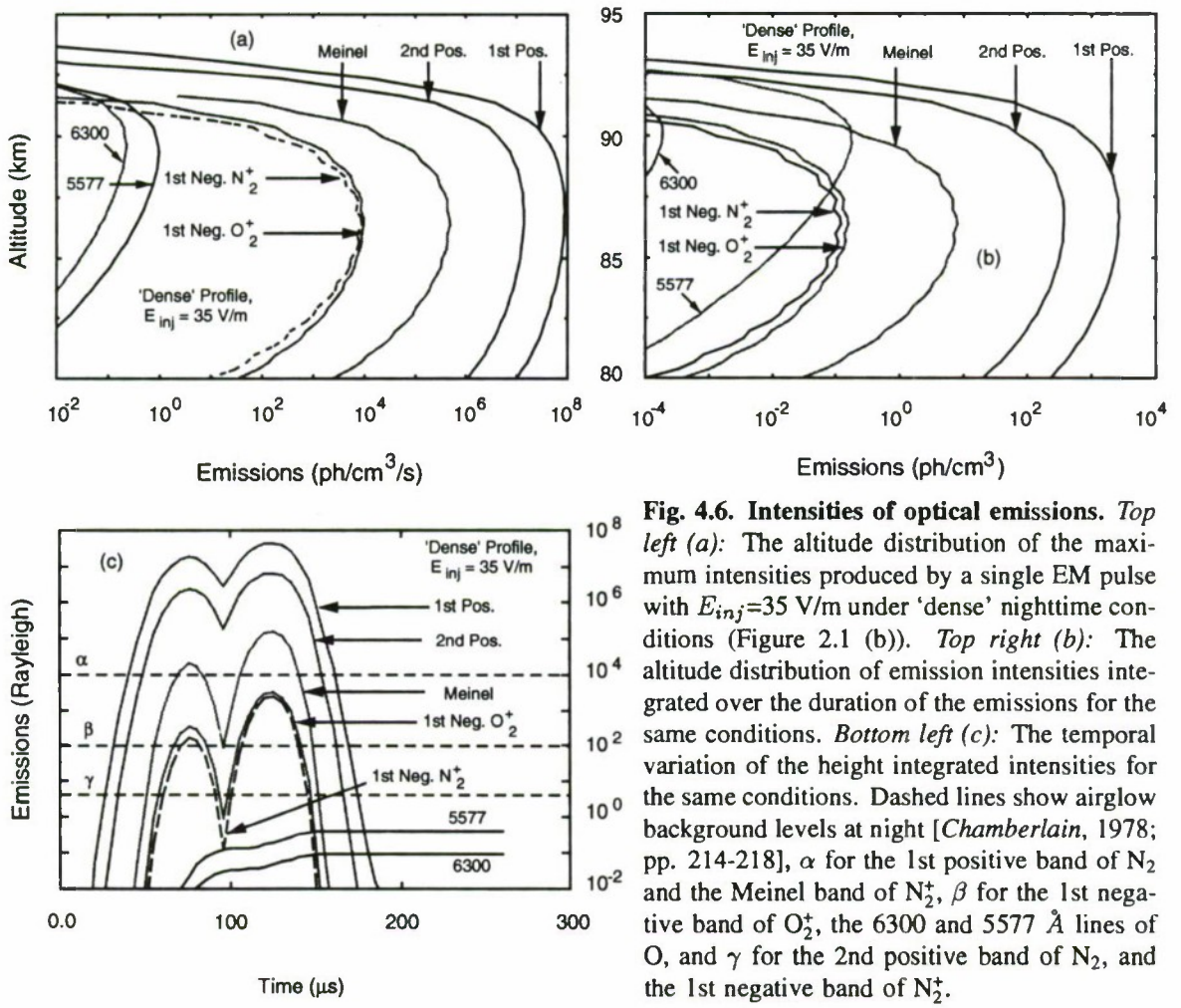

Fig. 4.6. Intensities of optical emissions. *Top left (a):* The altitude distribution of the maximum intensities produced by a single EM pulse with E_{inj}=35 V/m under 'dense' nighttime conditions (Figure 2.1 (b)). *Top right (b):* The altitude distribution of emission intensities integrated over the duration of the emissions for the same conditions. *Bottom left (c):* The temporal variation of the height integrated intensities for the same conditions. Dashed lines show airglow background levels at night [*Chamberlain*, 1978; pp. 214-218], α for the 1st positive band of N_2 and the Meinel band of N_2^+, β for the 1st negative band of O_2^+, the 6300 and 5577 $\AA$ lines of O, and γ for the 2nd positive band of N_2, and the 1st negative band of N_2^+.

For E_{inj} = 30 V/m, the intensities of the 1st and 2nd positive band of N_2 are ~1.5 times smaller than for a E_{inj} = 35 V/m pulse. Emissions from molecular ions have 2 to 3 times weaker maximum and time integrated intensities. Intensities of the 6300 and 5577 $\AA$ lines of O are lower by a factor of ~1.5 in comparison with the E_{inj} = 35 V/m case.

For E_{inj} = 20 V/m, the intensities of the 1st and 2nd positive bands of N_2 have ~10 times weaker maximum and time integrated intensities than those for a E_{inj} = 35 V/m pulse. Emissions from molecular ions have ~200 times weaker maximum and time integrated intensities. Intensities of the 6300 and 5577 $\AA$ lines of O are lower by a factor of ~10 in comparison with the E_{inj} = 35 V/m case.

Figure 4.7 shows the dependence of maximum emission rates on the electric field amplitude of the pulse, expressed in terms of E_{100}.

Also indicated are the percentages of occurence of CG discharges with E_{100} larger than corresponding numbers in V/m, based on ground-based measurements [*Krider and Guo*, 1983]. The dependences on E_{100} are similar to the 'tenuous' case but with important quantitative differences in the the relative amplitudes of the emission lines for a given E_{100}. For example, for E_{100} = 20 V/m, the ratio of the intensity of the 1st positive band of N_2 to that of the 1st negative of N_2^+ is $\sim 10^3$ for the 'tenuous' case (Figure 4.5) but $\sim 2 \times 10^5$ for the 'dense' D region case (Figure 4.7). Comparison of Figures 4.5 and 4.7 show the potential application of spectroscopic measurements of lightning-induced enhanced airglow to determine the ambient D region electron density profile.

4.3 COMPARISON WITH EARLIER WORK [*TARANENKO ET AL.*, 1992]

In this section, we compare our results with those presented in an earlier paper, which was based on a simplified model of the interaction neglecting reflection of the pulse and assuming a Maxwellian distribution of electrons and which used somewhat different ambient density profiles.

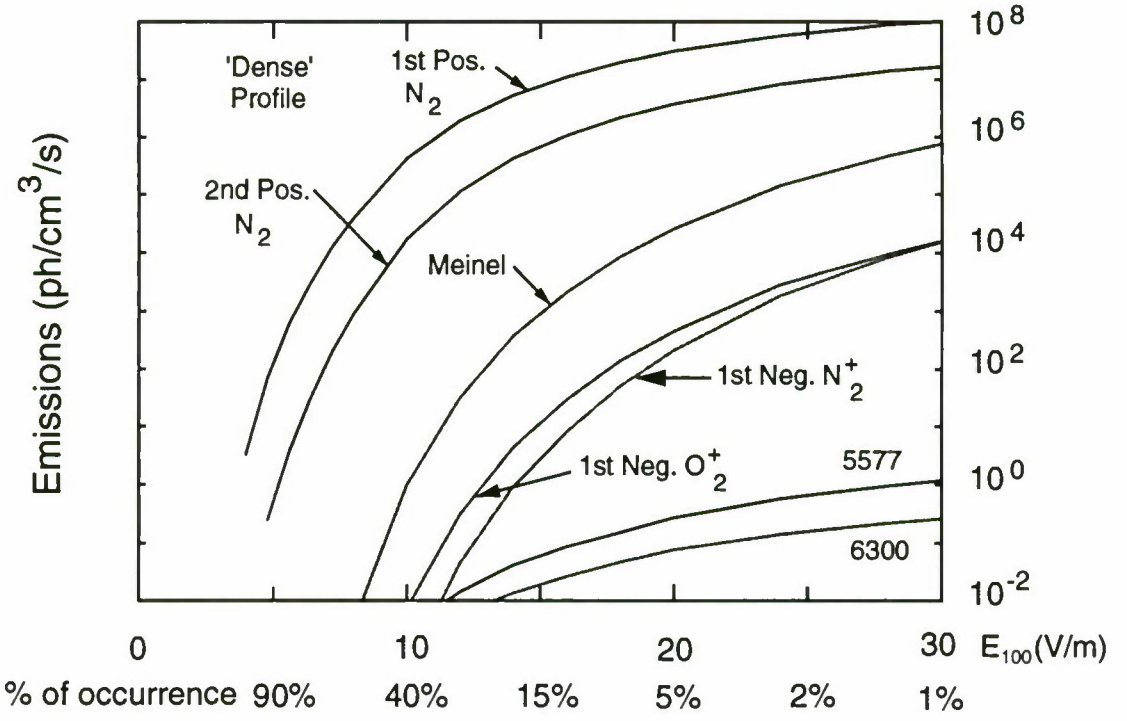

Fig. 4.7. Maximum emission rates as a function of the electric field amplitude E_{100}. The calculations were performed under 'dense' nighttime conditions (Figure 2.1 (b)). Also indicated are the percentages of occurence of CG discharges with E_{100} larger than corresponding numbers in V/m [*Krider and Guo*, 1983].

Results presented in Figures 3 to 6 of *Taranenko et al.* [1992] for the so-called Case A correspond to a E_{100} = 20 V/m pulse, which in turn corresponds in our case to a E_{inj} = 25 V/m pulse (Section 2.5). To make a comparison of the two models we used our new model described in this thesis for E_{inj} = 25 V/m with the electron density profile used by [*Taranenko et al.*, 1992]. Results indicate that the kinetic calculations give substantially lower emission intensities for the same EM pulse amplitude compared with the simple model of *Taranenko et al.* [1992]. Namely, the maximum intensity of the 1st positive band of N_2 is 5.2×10^7 cm^{-3} sec^{-1}, i.e. 30 times lower. The corresponding numbers for other lines are: the 2nd positive band of N_2 is 90 times lower, Meinel band of N_2^+ is 500 times lower, the 1st negative band of N_2^+ is 2,700 times lower, the 1st negative band of O_2^+ is 600 times lower, the 6300 Å line of O is 25 times lower, and the 5577 Å line of O is 30 times lower. These differences come about due to several factors. Firstly,

due to reflection of the pulse, the maximum heating occurs at ~88 km (5 km lower than in the old model) where the collision frequency is much higher, resulting in less heating (6 eV average energy instead of 9 eV) and therefore a reduced number of electrons above the excitation thresholds of most emissions. Secondly, the precipitous drop (due to high energy losses for energies above the thresholds of vibrational, optical, dissociative, and ionizational excitations; see Figure 2.3 (b)) of the electron distribution function decreases the number of energetic electrons in the tail of the distribution compared with a Maxwellian distribution of the same average energy.

For optical emissions with low excitation thresholds the latter factor is not as important. For example, for the 5577 $\AA$ line of O, the 5 km decrease in the altitude of maximum heating results in ~5.75 times less electrons and ~2.75 times less oxygen atoms, and the decrease in average energy gives a factor of ~2 decrease in intensity. Alltogether this results in ~31.6 times lower emission rate for this line which matches the 30 times difference between the new and old models.

We also note also that in [*Taranenko et al.*, 1992] a slightly different excitation cross section was used for the 2nd positive band of N_2 (see Appendix B). The usage of the different cross sections does not play an important factor in the difference between the emission intensities reported here and in [*Taranenko et al.*, 1992].

5

Discussion

In this chapter, we discuss the various implications of our results and compare them with available experimental data.

5.1 ELECTRON DENSITY CHANGES AND ASSOCIATED EFFECTS

5.1.1 Perturbation of VLF Subionospheric Signals

As was described in Chapter 1, the first experimental evidence for direct upward coupling of lightning energy to the lower ionosphere was in the form of 'early' and/or 'fast' perturbations (sometime called 'early' or 'fast' Trimpi events) of subionospheric VLF transmitter signals [*Inan et al.,* 1988; 1993]. Detailed theoretical investigation of such effects needs to be based on an adequate three dimensional model of the interaction to determine three dimensional parameters (most importantly the transverse extent) of the region of electron density changes which can in turn be used in a computer-based model of subionospheric VLF propagation [*Poulsen et al.,* 1993] to calculate the resultant VLF amplitude and phase changes. Such modeling is beyond the scope of our present one dimensional model. However, some first order estimates of the expected VLF perturbations due to the electron density changes produced by EM lightning pulses as calculated with the one dimensional model can be made on the basis of geometrical factors.

Since the source of the EM waves (i.e., lightning) is typically located at a distance of about 80 to 90 kilometers from the region of heating, it is reasonable to assume that its radiation pattern is not well directed, hence the transverse extent of the distributed region can be expected to be of the same order as the distance from the source (80 to 90 km). On this basis, [*Inan et al.,* 1991] used a computer-based model of subionospheric VLF propagation [*Poulsen et al.,* 1990] to calculate the amplitude and phase changes due to electron density increases produced by an EM pulse ionizing the D region. They found that a 150 km radius ionization patch with ~10 % maximum change in electron density at ~95 km altitude produces amplitude and phase changes of subionospheric VLF waves within the range of experimentally observed values [*Inan et al.,* 1988*b*]. Also, two dimensional modeling of heating based on a simple model assuming a Maxwellian electron distribution [*Rodriguez et al.,* 1992] showed widths at half-maximum of the ionized regions of 90 km (for a E_{100} = 20 V/m pulse from a vertical radiator at 0 km altitude) to 260 km (for E_{100} = 40 V/m), consistent with the arguments above.

In comparing our results with those of *Inan et al.* [1991], we see that although the general conclusions, such as the fact that lightning-induced heating of the electrons leads to impact ionization, are borne out, there are striking differences. The results of [*Inan et al.,* 1991] were based on a simplified model of coupling, which assumed a Maxwellian distribution to be maintained during the heating and which neglected the reflection of the EM pulse from the lower ionosphere. The estimation of the resulting ionization was also handled in terms of a first approximation by assuming that secondary production occurred only for electrons with average energy >35 eV. It is interesting to note that the relatively simple model of *Inan et al.* [1991] appears to have roughly predicted the magnitude of the density enhancements (a few percent to a few tens of percent) that we find for the higher altitudes. However, the earlier model predicted only density enhancements while our results also show a reduction in density at the lower altitudes due to attachment, which produces a general sharpening of the density profile. Also,

the altitude of maximum perturbation is found to be somewhat lower than in the earlier model due to the reflection of the pulse from the ionosphere.

In terms of the relevance of our results to the interpretation of experimental data, we note that disturbances at lower altitudes and with a more drastic change from ambient (i.e., both an increase at highter altutudes and a reduction at lower heights) would in general be more likely to lead to subionospheric VLF signal perturbations. Thus, the predicted modifications in electron density of 1–30 % of the ambient produced by single strokes should be quite sufficient to produce detectable amplitude and phase changes of subionospheric VLF signals. In this sense, our results reaffirm the conclusions of [*Inan et al.,* 1991], in that this heating and ionization mechanism appears to explain all known features of the 'early' and/or' fast' subionospheric VLF signal changes which occur at night nearly simultaneously with lightning discharges.

Our results show that the phenomenon of lightning-induced ionization and attachment occurs predominantly under conditions of a 'tenuous' D region which are realized during nighttime. Physically, this effect is due to the fact that for a 'dense' D region the reflection altitude of the lightning EM pulses is located at lower altitudes where the mean free path of electrons is short so that more of the energy goes into excitation of the molecular energy levels which require smaller amounts of energy than ionization and dissociative attachment. Due to the exponential dependence of the electron mean free path versus altitude, the critical amplitude of the electric field above which appreciable perturbations are produced is a strong function of the D region electron density profile. For example, in accordance with the results of Chapter 3, during daytime (profile (c) of Figure 2.1) even the strongest individual pulses (initial intensity E_{inj} = 50 V/m) do not produce substantial changes in the electron density ($|\delta N_e/N_e| \leq 3 \times 10^{-3}$), whereas during nighttime (profile (a) of Figure 2.1) an EM pulse with E_{inj} = 10 V/m ($E_{100} \simeq 8$ V/m) is expected to produce measurable electron density changes of $|\delta N_e/N_e| \simeq 1\%$. The strong dependence of the interaction on ambient electron density may explain recent nighttime observations of 'fast'/'early' VLF perturbation events [*Inan et al.,* 1993] as

associated with CG flashes with electric field amplitudes as low as E_{100} = 6 V/m, as possibly being a consequence of an unusually tenuous D region.

5.1.2 Formation of Ionization 'Bubbles' over Thunderstorms

An important prediction of [*Inan et al.*, 1991] was the possible formation of ionization 'bubbles' over thunderstorm centers due to the accumulation of ionization produced by successive strokes. This is reminiscent of sporadic E layers occasionally observed in the lower ionosphere [e.g., *Fenn et al.*, 1987; p. 21-55], sometimes in association with lightning [*Isted*, 1954]. Our kinetic model shows that this is indeed the case, with the added caveat that the density is depleted at lower altitudes and that the density profile is substantially sharpened as the 'bubble' builds up, e.g., the scale height decreases by a factor of ~2 at ~85 km for a single E_{inj} = 20 V/m EM pulse. An example of such a development of an electron density disturbance is shown in Figure 5.1. One would expect that such sharpened electron density profiles over thunderstorms would increase the reflectivity of VLF waves from the ionosphere and improve VLF transmission along the Earth-ionosphere waveguide. In this connection, it is interesting to note that all reported cases of 'early' VLF perturbations have been positive amplitude changes [*Inan et al.*, 1993], as expected from such a modification of the density profile as shown in Figure 5.1.

Increases in the electron density over a thunderstorm center produced in the initial stages of a thunderstorm may possibly lead to a denser D region and prevent production of appreciable changes in electron density by the lightning EM pulses occuring in later stages. Such an effect may occur due to the decrease in the reflection height of the EM pulses to the altitudes where most of their energy transfers to excitations other than dissociative attachment and ionization. Hence, observed characteristics of 'early' and/or 'fast' VLF perturbation events may evolve during a thunderstorm; one such example was observed in the case of a thunderstorm center which stayed active and centered on a VLF

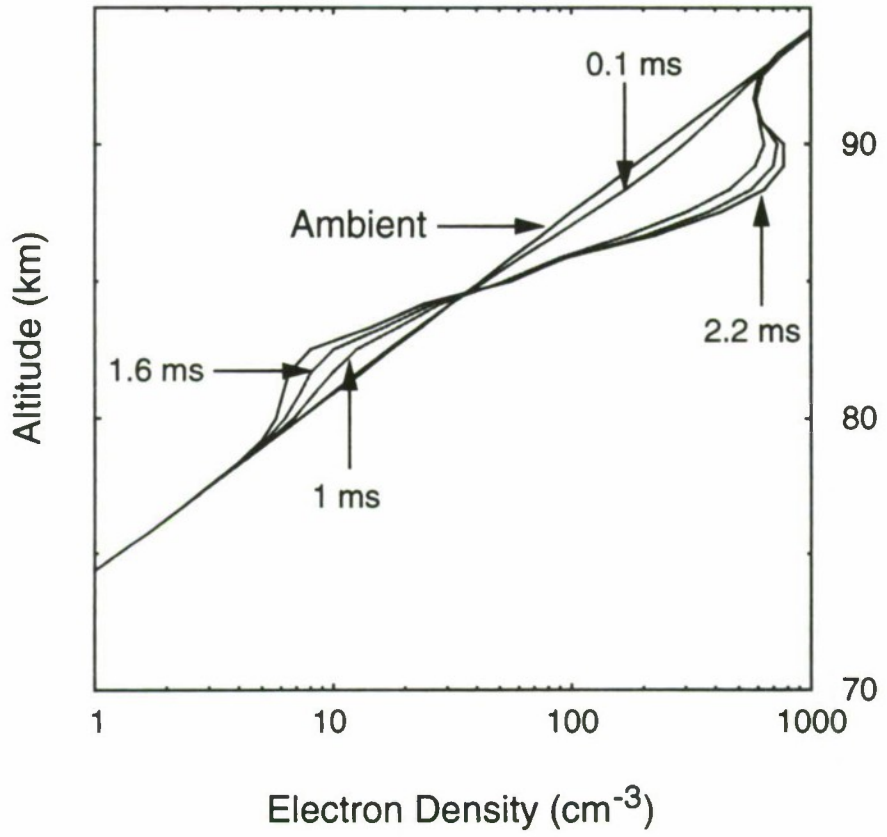

Fig. 5.1. Evolution of an electron density disturbance due to successive EM pulses from lightning. The disturbances were produced by an EM wave with E_{inj} = 25 V/m and different time durations of 0.1 ms (a single pulse), 1 ms (equivalent to a sequence of about 8 pulses), 1.6 ms (equivalent to a sequence of about 14 pulses), and 2.2 ms (equivalent to a sequence of about 20 pulses) under 'tenuous' nighttime conditions (Figure 2.1 (a)).

path for ~12 hours although 'early' VLF events were only observed during the first two hours [*Inan et al.*, 1988*b*].

5.1.3 Stimulation of ULF waves

The conductivity of a collisional magnetized plasma in a quasi-constant electric field is an anisotropic function of the electron and ion gyrofrequencies and the electron collision frequency [e.g., *Rees*, .1989; p. 202]. Since all three components of the ionospheric conductivity tensor are proportional to the electron density N_e, changes in the ionospheric electron density can modify the conductivity and lead to variations in ionospheric currents [e.g., *Bell*, 1976]. In the context of our results, slow variations of the electon density

above thunderstorms would be expected since typical flash rates [*Uman*, 1987, p. 49] are on the order of several flashes every ten seconds, and the density relaxation time is on the order of tens of seconds [e.g., *Glukhov et al.*, 1992]. Such slow variations occuring over few tens of second time scales can be expected to produce ionospheric current perturbations in the ULF range. Given the expected large horizontal scale (hundreds of kilometers, see discussion above and *Rodriguez et al.* [1992]) of the disturbed ionospheric regions, these current perturbations can result in increased ULF wave generation in the vicinity of thunderstorms. Recent experimental results [*Fraser-Smith*, 1993] showing increased ULF activity near thunderstorms may be experimental evidence for such effects.

5.2 EXCITATION OF OPTICAL EMISSIONS

In this section we discuss several issues related to remote detection and measurement of the optical signatures of lightning-induced heating. These are: *(i)* emission intensities compared to ambient airglow background; and *(ii)* radiative transfer. We also compare our model results directly with the observations of *Boeck et al.* [1992].

5.2.1 Emission Intensities Compared to Airglow Background

The comparison of the predicted optical emission intensities with the ambient airglow background is critically important for assessing their detectability in different experimental configurations. The intensities of emissions for vertical observations are shown in Figures 4.4 (c) and Figures 4.6 (c) together with the known ambient airglow levels for each line or band separately indicated. The comparison of the EM pulse stimulated emissions with the ambient levels can be summarized as follows.

The intensities of the 6300 and 5577 $\AA$ lines of O have low absolute values for all cases considered here and are more than one order of magnitude less than the ambient intensity of the night airglow for zenith observations, which is $\sim 10^2$ R [*Chamberlain*,

1978; p. 215] for vertical observations. This fact makes these emissions difficult to detect in practice.

The intensities of the transitions of N_2 (the 1st and 2nd positive bands), N_2^+ (the 1st negative and Meinel bands), and O_2^+ (the 1st negative band) are several orders of magnitude larger than typical background emissions in corresponding spectral regions (see Figures 4.3 (c), 4.4 (c), and 4.6 (c) and [*Chamberlain*, 1978; pp. 214-218]) for vertical observations. Hence, all of the molecular band emissions stimulated by EM pulses from lightning discussed in this thesis are substantially above the background levels at night and can be registered using specially designed high sensitivity photometers.

In terms of detectability with a typical auroral airglow photometer, we note that a good photometer would have a sensitivity of ~50 Rayleigh-seconds (R-s) [*S. Mende*, private communication]. In this context we note that the 1st and 2nd positive bands of N_2 have intensities of 1,200 and 200 R-s and should be detectable from the ground with conventional instruments. However, other emissions have lower than 50 R-s intensities and would have to be observed with specially designed instruments. Such considerations are important in the design of optical instruments aimed at detecting lightning-induced emissions from the D-region.

The fact that the longest radiation time of the strong allowed emissions considered above is ~14 μs indicates that relatively fast optical systems with 50–100 μs (about the time interval of emissions from a single EM lightning pulse) to several seconds time of exposure should be used in experiments aimed at observing the optical emissions from the D-region associated with lightning. In this context, we note that the intense radio impulse from lightning can be used to automatically trigger the camera. Since the radiation time of the brightest emissions is very small, it is important to take into account the size of the emitting region when one calculates the intensity and duration of the remotely observed optical pulse. This consideration is particularly important for limb observations and all-sky vertical observations and in view of the fact that the size of the

observed emitting region can reach 500 km [*Boeck et al.,* 1992]. In such cases, the light travel delay would spread out the duration of the impulse from ~50 μs to about 1.5 ms and consequently lower its intensity as compared to the case when the light travel time is negligible in comparison with the duration of the emissions.

5.2.2 Radiative Transfer

Radiative transfer of optical emissions in the atmosphere (i.e., the process of photon propagation in the atmosphere and processes of scattering, absorption, and re-emission that occur during such propagation) is important for remote sensing of the heated region, especially from ground-based platforms. The rigorous treatment of these processes is an area of active research by itself (see for example [*Fenn et al,* 1985; Chapter 18]), so in this section we merely make order of magnitude estimates that show optical extinction in the atmosphere for each band or line considered.

The 1st and 2nd positive bands of N_2 are not resonantly absorbed in the atmosphere. They originate from transitions between excited levels ($B^3\pi_g \rightarrow A^3\Sigma_u^+$ and $C^3\pi_u \rightarrow B^3\pi_g$ transitions respectively, as shown in Figure 4.1) with a minimum energy of ~6 eV. Hence, resonant absorbers for these emissions are practically not present in the cool (~250° K) atmosphere. In principle, these emissions could be resonantly absorbed in the heated region; however, the region is optically transparent due to low density of excited molecules (even in the extreme case of up to 10^9 excited particles per cc, with a cross section of $\sim 10^{-16}$ cm^2, and a 10^6 cm path we have optical depth of only 0.1, i.e. the radiation is attenuated by a factor of only $\exp(-0.1) \simeq 0.9$ after passing through the region). Rayleigh scattering (i.e., scattering by induced dipole moment of molecules) is the major mechanism that determines the optical thickness of the clear atmosphere for these bands and it results in intensity losses of up to 4 % for the red and up to 25 % for the blue spectral ranges per vertical traverse through the atmosphere [*Fenn et al.,* 1985]. Rayleigh scattering loss decreases to a few percent for observations from a high altitude (~20 km) aircraft.

Meinel and 1st negative bands of N_2^+ and the 1st negative band of O_2^+ also originate from transitions between excited levels with a minimum energy of ~15 eV [*Vallance Jones*, 1974; p. 90] so that the same arguments discussed above for the N_2 bands also apply to them.

5.2.3 Comparison with *Boeck et al.* [1992] Observations

We now show that recent observations of lightning induced brightening in the airglow layer from the Space Shuttle [*Boeck et al*, 1992] can be explained as electron impact induced emissions from the heated region above a powerful lightning stroke, produced in the manner described in this thesis.

Long lasting emissions from O and O_2 [*Taranenko et al.*, 1992] were not detected on the Space Shuttle for two reasons: (*i*) the brightest of them, Herzberg I band of O_2 lies outside of the camera wavelength sensitivity region, (*ii*) the expected excitation levels of the 6300 $\AA$ and 5577 $\AA$ lines of O, and the atmospheric band of O_2 is below the sensitivity of the camera [*Taranenko et al.*, 1992].

Each of the short lasting bands discussed above has transitions with wavelengths from 3600 to 7200 $\AA$ to which the TV camera on the Space Shuttle was sensitive with a peak sensitivity at 4400 $\AA$. However, transitions between states with low vibrational numbers of the 1st and 2nd positive bands of N_2, and Meinel band of N_2^+ have their wavelengths outside of the sensitivity region of the camera. Only two strong lines of the 1st negative band of N_2^+ (0-0 transition at 3914.4 $\AA$ and 0-1 transition at 4278.1 $\AA$) lie near the peak of the camera sensitivity. To obtain the intensity of the emissions for nighttime limb observations in Rayleighs one must multiply numbers on the ordinate scale of Figure 4.4 by the thickness of the emitting region given in units of 10 km (e.g., for a 500 km region as given in [*Boeck et al.*, 1992] the multiplier is 50). As is evident from Figure 4.4 (c), the time duration of the emissions for a 100 μs EM pulse with E_{inj} = 25 V/m is ~50 μs (resulting in 15 km thickness of the emitting region of simultaneously

registered photons) so that the side view intensity of this band averaged over 5 km of altitude is $\sim 5 \times 10^4$ R. The observed duration of the emissions for the 500 km thickness of the emitting region is ~1.5 ms. Hence, the observed effective intensity in R-s at the Space Shuttle would be ~10 times lower due to 1/60 s integration time of the camera. After this reduction, the intensity observed at the Shuttle would be $\sim 5 \times 10^3$ R. Emissions of the 1st negative band of O_2^+ are in the spectral region of the camera sensitivity (~5200–6500 Å). They have similar intensity and time duration to those of the 1st negative band of N_2^+ and make a comparable contribution to the total effective intensity $\sim 10^4$ R of the airglow transient over the visible spectrum range. For the E_{inj} = 20 V/m case at night the effective intensity of the emissions is ~10 times lower than for the case E_{inj} = 25 V/m (Section 4.3).

As has been mentioned in section 1.3, the intensity of the airglow transient observed from the Shuttle [*Boeck et al.*, 1992] was about twice that of the ambient, which is several kR over the visible spectral range at night [*Chamberlain*, 1978; pp. 214-218]. Hence, in accordance with the above estimates only EM pulses with $E_{inj} \geq 25$ V/m could produce such intensities. Emissions produced by EM pulses with $E_{inj} \leq 20$ V/m would not be distinguishable from the background, with the TV camera used in the *Boeck et al.* [1992] experiments.

To assess the lightning intensity that would lead to optical emissions at the detected level [*Boeck et al.*, 1992], we note that E_{100} corresponds to $E_{inj} \times \frac{80km}{100km}$ (see Section 2.5 for discussion), hence E_{inj} = 25 V/m corresponds to E_{100} = 20 V/m. According to *Krider and Guo* [1983] CG discharges with such intensities are expected to occur ~5 – 10 % of the time. Hence, one can conclude that the observed airglow transient [*Boeck et al.*, 1992] was due predominantly to emissions of the 1st negative bands of N_2^+ and O_2^+ excited by a relatively intense (and thus relatively rare) lightning discharge. The intensity of such emissions is a strong function of the EM field of the pulse due to the high excitation thresholds (~18.8 eV and ~18.2 eV respectively) and is expected to be below the background level at night for the EM pulses with $E_{100} \leq 16$ V/m. This

realization is consistent with the fact that the airglow enhancement reported by *Boeck et al.* [1992] was only observed once during the period of several hours of observation from the Space Shuttle (see Section 1.2) during that mission.

6

Summary and Suggestions for Future Research

6.1 SUMMARY

The thrust of this work has been the simulation of the interaction of lightning radiated EM pulses with the lower ionosphere by means of a self-consistent solution of the Boltzmann kinetic equation for electrons and Maxwell's equations for the electromagnetic (EM) fields. Our results indicate that attachment, ionization, and optical emissions produced in this interaction are sufficient to explain all heretofore known features of the 'early' and/or 'fast' VLF signal perturbations and airglow brightening observed simultaneously with lightning. Our model also provides the basis for quantitative evaluation of a wide variety of other electrodynamic and chemical processes (especially those that deal with the altered electron and negative ion densities) in the ionosphere which might occur in response to the EM energy released in the lightning discharges.

Under nighttime conditions, individual pulses of 10-20 V/m (normalized to 100 km distance) produce changes in electron density of 1-30 % of the ambient while a sequence of pulses leads to >100 % modification at altitudes <95 km. The nature of the density changes produced by lightning radiation are such that they lead to a 'sharpening' of the lower ionospheric boundary by causing a reduction in electron density at 75-85 km

(due to attachment) and a substantial increase at 85-95 km (due to ionization), e.g., the scale height decreases by a factor of ~2 at ~85 km for a single 20 V/m EM pulse (see Figure 5.1). The slow variations in the electron density resulting from ionization due to succesive flashes should lead to variations in the electrical conductivity of the lower ionosphere which in turn might also stimulate ULF waves. Also, intense electron heating in the D region over thunderstorms causes production of electron density 'bubbles' and may significantly alter the chemistry in that region.

Among the optical emissions the most promising for observations are determined to be the 1st (red) and 2nd (blue) positive bands of N_2, which emit at rates of $\sim 7 \times 10^7$ and $\sim 10^7$ $cm^{-3}s^{-1}$ at ~92 km respectively for a E_{100} = 20 V/m EM pulse. The height integrated intensities of the emissions reach $\sim 3 \times 10^7$ and $\sim 6 \times 10^6$ R, lasting for ~50 μs and producing ~1,200 and ~200 Rayleigh-seconds for zenith observations.

6.2 SUGGESTIONS FOR FUTURE RESEARCH

6.2.1 Dependence of the Lightning Generated Electron Density Changes and Optical Emissions on the Temporal Shape and Duration of Lightning EM Pulses

An immediate application of our one dimensional model is to extend it to a broader range of parameters of EM pulses from lightning.

As a first step, the current version of the computer code can be applied to study the response of the ionosphere to a variety of EM pulse shapes for CG and IC discharges (see Figure 1.1 for examples of pulse shapes). As a result of such a study some special features of the pulse shape that may enhance or suppress the interaction may be revealed. For example, the constructive interference that was seen to be very effective in Figure 3.1 would not occur for EM pulses which were dominantly positive or negative

(rather than alternating), thus leading to smaller perturbations even though the total EM energy of the pulse may be the same.

Another possible way to extend the model is the accomodation of larger amplitudes of injected EM pulses. This requires some modification of the code since, due to the particular numerical scheme employed, the present version has an upper limit for the electric field amplitude that does not allow the simulation of interactions with the lower ionosphere of EM pulses with amplitude $E_{inj} \geq 25$ V/m for a 'tenuous' D region. Although EM pulses with such intensities occur less than 5 % of the time, quantitative determination of the extent of their interaction would be very interesting, especially in view of the highly nonlinear nature of coupling, as is evident from Figure 3.4. In this context, we note that lightning EM pulses with intensities of as much as $E_{100} \simeq 100$ V/m are occasionally observed [e.g., *Turman*, 1977].

Investigation of the interaction of very short (≤ 10 μs) EM pulses with the lower ionosphere requires the removal of the quasi steady state assumption from the model. Such a development is essentially straightforward but would require two to three orders of magnitude more computer memory and time to perform the computations that are necessary.

6.2.2 Application of Model Results to Data on Subionospheric VLF Signal Perturbations

Thorough theoretical investigation of observed 'early' VLF perturbations requires an adequate three dimensional model of the interaction to determine the three dimensional parameters of electron density changes which can be used in a computer-based model of subionospheric VLF propagation [*Poulsen et al.*, 1990] to calculate the amplitude and phase changes due to the electron density changes. However, some first order estimates of the expected VLF perturbations due to electron density changes produced by lightning EM pulses can be made on the basis of geometrical factors as described in Section 5.1.1. Using such estimates, calculations similar to those using a computer-based model of

subionospheric VLF propagation [*Poulsen et al.,* 1993] can be made to calculate the amplitude and phase changes due to D region electron density changes produced by lightning EM pulses.

6.2.3 Three Dimensional Modeling of the Interaction of Lightning EM Pulses with the Ionosphere

Another obvious future development of our one dimensional model is to extend it to three dimensions using the quasi steady state distribution function technique for three dimensional values of electric currents, ionization and optical emission rates.

We expect that the dimensions of the disturbed electron density region will differ from that of the enhanced airglow region and will depend on the discharge strength, discharge orientation, dip angle, and ionospheric parameters. Also, the 3-D modeling would allow us to assess the best means of remote sensing of the regions among possible techniques such as: VLF remote sensing using earth-ionosphere waveguide signals; optical, infrared, or ultraviolet remote sensing of the enhanced airglow; radio interferometry using satellite beacons or natural radio sources; or ground-to satellite or ground-to-rocket radio beacons.

Results of the three dimensional modeling can provide detailed inputs to facilitate quantitative predictions for VLF subionospheric wave perturbations [*Poulsen et al.,* 1990], D region aeronomy models [*Glukhov et al.,* 1992], ULF wave generation [*Bell,* 1976], and for radiative transfer codes [*Fenn et al.,* 1985, p.18-37] that would describe optical signatures of the heated region as observed from a distance. Such modeling can also allow the determination of the total 3-D deposition of EM energy in the lower ionosphere and the dominant sinks for this energy.

6.2.4 Possible Effects of the Lightning EM Pulses on the Thermal and Chemical Balance of the Upper Atmosphere

Our results concerning the interaction of individual lightning EM pulses with the lower ionosphere bring to the fore the question of the significance of these effects on a global scale, in terms of the integrated effects of thunderstorms worldwide on the ionosphere. The buildup of an electon density 'bubble' in the lower ionosphere, expected from a sequence of EM pulses from a thunderstorm were mentioned in Section 5.1.2.

In further studies, the *Glukhov et al.* [1992] model of the D region chemistry can be applied to follow the evolution of such an electron 'bubble'. Preliminary applications of such a model to some previously modeled disturbances indicate that some of the least known chemical reaction rates in the nighttime D region altitudes may be measurable using subionospheric VLF data and in some cases new ionization layers are formed that represent a different attachment-detachment quasi-equilibrium value from that of the unperturbed ambient [*Pasko and Inan*, 1993]. Such new layers may exist for up to $\sim 10^5$ s following the disturbance. This is reminiscent of sporadic E layers occasionally observed in the lower ionosphere [e.g., *Fenn et al.*, 1987; p. 21-55].

There are some other indications that the lightning stimulated processes might change the lower ionosphere chemistry. For example, a three-body collision between electrons and two oxygen molecules

$$e + O_2 + O_2 \rightarrow O_2^- + O_2 + 0.45\text{eV} \tag{6.1}$$

is considered so far as the most important source of negative ions in the D region [*Banks and Kockarts*, 1973]. However, according to our results presented in Section 3.1 Figure 3.3 (b), EM radiation from lightning can create very substantial (on the order of 50 % of the electron density) depletion of the electron density due to dissociative attachment of electrons to O_2

$$e + O_2 \rightarrow O^- + O - 7\text{eV} \tag{6.2}$$

indicating that the population of negative atomic oxygen ions O^- in the D region above a thunderstorm can reach up to 50 % of the positive ion density in that region. Such production of negative ions by lightning-induced heating would thus effectively compete with reaction (5.2) in producing negative ions.

Once created, O^- is transformed into other negative ions by means of charge exchange, interchange, clustering, and cluster interchange reactions, involving a large variety of chemical reactions [*Banks and Kockarts*, 1973; p. 281]. Hence, appearance of negative atomic oxygen ions O^- in the D region above a thunderstorm can be expected to influence many channels of chemical reactions in that region.

6.2.5 Stimulation of ULF waves

As was discussed in Section 5.1.3, changes in the electron density in the lower ionosphere modify the natural conductivity tensor and therefore can generate ULF waves. To evaluate the importance of ULF waves generated in such a way one must make calculations of ULF currents and radiated ULF fields stimulated by the electron density changes and make comparison of the radiated fields to the natural magnetospheric and Earth-ionosphere waveguide backgrounds, and to ULF waves stimulated by other processes, such as electrons precipitated from the magnetosphere by whistlers [*Bell*, 1976].

A

Derivation of the Truncated Boltzmann Equations

In our derivation of (2.4) and (2.5) we follow the general pattern outlined in *Gurevich* [1978, p. 34]. We start with general form of the Boltzmann kinetic equation for the electron distribution function $f(\vec{r}, \vec{v}, t)$

$$\frac{\partial f}{\partial t} + \vec{v} \cdot \frac{\partial f}{\partial \vec{r}} - \frac{e}{m}\left\{\vec{E} + \frac{1}{c}\left[\vec{v} \times \vec{B}\right]\right\} \cdot \frac{\partial f}{\partial \vec{v}} + S = 0 \qquad \text{(A.1)}$$

where S is the Boltzmann collision integral, which describes, in our particular case, the change of the electron distribution function f under the influence of electron collisions with neutrals. The general expression for S is as follows

$$S = \int\int d\vec{v}_1 d\Omega q(u, \theta) u \{f(\vec{v})F(\vec{v}_1) - f(\vec{v}')F(\vec{v}_1')\} \qquad \text{(A.2)}$$

where $\vec{v}_1$ is the velocity of the neutral that collides with the electron, $u = |\vec{v} - \vec{v}_1|$, $q(u, \theta)$ is the differential effective scattering cross section, $\vec{v}'$ and $\vec{v}_1'$ are the velocity of the electron and of the neutral prior to their collision (their velocity after the impact are respectively $\vec{v}$ and $\vec{v}_1$); and F is the distribution function of the neutrals. The integration in equation (A.2) is over the velocities of the neutrals ($d\vec{v}_1$) and over the scattering angles $d\Omega = \sin\theta d\theta d\varphi$, where θ is the angle between the vectors $(\vec{v} - \vec{v}_1)$ and $(\vec{v}' - \vec{v}_1')$. All other variables in (A.1) and (A.2) were specified in Section 2.2.

The first simplification which we made in writing (A.1) deals with the spatial gradients ($\frac{\partial}{\partial \vec{r}}$) of the distribution function; we neglect such gradients since they are only important in the D region over time intervals longer than several hundred seconds [*Tomko et al.*, 1980].

If the electrons are under the influence of a weak electric field (the specific conditions are given below, equation (A.11)), such that their random velocity is much larger than their average directional velocity, then the distribution function depends mainly on the absolute value of the velocity and not on its direction. Under such an assumption, the Boltzmann equation can be simplified using an expansion of the distribution function in spherical functions of zero order (i.e. Legendre polynomials $P_k(\cos\theta)$ [*Hochstrasser*, 1972]) in velocity space [*Allis*, 1956].

For the sake of simplicity in the following analysis, we neglect the external magnetic field. A similar derivation in the presence of a constant ambient magnetic field was carried out by [*Davydov*, 1937]. Accordingly, we consider a uniform collisional plasma in the presence of an electric field $\vec{E}$ parallel to the z axis [*Gurevich*, 1978; p. 36], so that there is only one preferred direction in the medium, i.e., along the z axis. Consequently

$$f(\vec{v},\vec{r},t) = \sum_{k=0}^{\infty} P_k(\cos\theta) f_k(v,z,t) \tag{A.3}$$

where θ is the angle between the velocity vector and the z axis. Substitution of this expantion into equation (A.1) gives

$$\sum_{k=0}^{\infty} \left\{ P_k(\cos\theta)\frac{\partial f_k}{\partial t} - \frac{eE}{m}\cos\theta P_k(\cos\theta)\frac{\partial f_k}{\partial v} - \frac{eE}{mv}\sin^2\theta f_k \frac{\partial P_k}{\partial(\cos\theta)} \right\} + S = 0 \tag{A.4}$$

The last two of the terms inside the curly brackets result from the fact that

$$\vec{E}\cdot\frac{\partial f}{\partial \vec{v}} = E\frac{\partial f}{\partial v_z} = E\cos\theta\frac{\partial f}{\partial v} + \frac{E\sin^2\theta}{v}\frac{\partial f}{\partial(\cos\theta)}$$

Multiplying equation (A.2) by $P_k(\cos\theta)$ and integrating over the spherical solid angle $d\Omega = \sin\theta d\theta d\varphi$ we obtain the following

$$\frac{\partial f_k}{\partial t} - \frac{eE}{m}\left[\frac{k+1}{(2k+3)v^{k+2}}\frac{\partial}{\partial v}(v^{k+2}f_{k+1}) + \frac{kv^{k-1}}{(2k-1)}\frac{\partial}{\partial v}(v^{1-k}f_{k-1})\right] + S_k = 0 \qquad \text{(A.5)}$$

$$S_k = \frac{2k+1}{4\pi}\int S P_k(\cos\theta)d\Omega$$

Where we have taken into account the orthogonality of the polynomials [*Hochstrasser*, 1972]

$$\int_{-1}^{1} P_k(x)P_l(x)dx = \frac{2}{2k+1}\delta_{kl}$$

(where $\delta_{kl} = 1$ for $k = l$ and zero otherwise) and the recurrence relations

$$xP_k = \frac{k+1}{2k+1}P_{k+1} + \frac{k}{2k+1}P_{k-1},$$

$$(1-x^2)\frac{dP_k}{dx} = \frac{k(k+1)}{2k+1}[P_{k-1} - P_{k+1}]$$

Equations (A.5) represents a chain of equations for f_k

$$\frac{\partial f_0}{\partial t} - \frac{eE}{3mv^2}\frac{\partial}{\partial v}(v^2 f_1) + S_0 = 0 \qquad \text{(A.6)}$$

$$\frac{\partial f_1}{\partial t} - \frac{eE}{m}\left[\frac{\partial f_0}{\partial v} + \frac{2}{5v^3}\frac{\partial}{\partial v}(v^3 f_2)\right] + S_1 = 0 \qquad \text{(A.7)}$$

$$\frac{\partial f_2}{\partial t} - \frac{eE}{m}\left[\frac{2}{3}v\frac{\partial}{\partial v}\left(\frac{f_1}{v}\right) + \frac{3}{7v^4}\frac{\partial}{\partial v}(v^4 f_3)\right] + S_2 = 0 \qquad \text{(A.8)}$$

etc. This chain can be terminated after the first two equations if

$$\frac{\partial f_0}{\partial v} \gg \frac{2}{5v^3}\frac{\partial}{\partial v}(v^3 f_2) \qquad \text{(A.9)}$$

We neglect f_3 in (A.8) and using approximations*

$$\frac{\partial f_1}{\partial t} = -i\omega f_1, \quad \frac{\partial f_2}{\partial t} = -i\omega f_2$$

$$S_1 \simeq \nu f_1, S_2 \simeq \nu f_2$$

where ν is the collision frequency determined at the average electron energy $\bar{\varepsilon}$. We obtain from equations (A.8) and (A.9)

$$f_1 = \frac{eE}{m(-i\omega+\nu)}\frac{\partial f_0}{\partial v}, \quad f_2 = \frac{2eEv}{3m(-i\omega+\nu)}\frac{\partial}{\partial v}\left[\frac{eE}{m(-i\omega+\nu)v}\frac{\partial f_0}{\partial v}\right]$$

The condition for terminating the chain is therefore

$$|\partial f_0/\partial v| \gg \left|\frac{4}{15v^3}\frac{\partial}{\partial v}\left\{\frac{eEv^4}{m(-i\omega+\nu)}\frac{\partial}{\partial v}\left[\frac{eE}{m(-i\omega+\nu)v}\frac{\partial f_0}{\partial v}\right]\right\}\right| \tag{A.10}$$

For the average electron velocity $\bar{v}$, we have $\omega \ll \nu$† and assuming $\frac{\partial}{\partial v} \sim 1/v$‡ (A.10) reduces to

$$e^2E^2/m\bar{\varepsilon}\nu^2 \ll 1 \tag{A.11}$$

Note that this condition is satisfied for the problem at hand and for the parameters of interest. For example, at 90 km and for E = 10 V/m, $\bar{\varepsilon}$ = 4.1 eV (see Figure 2.4), $\nu(\bar{\varepsilon}) = 10^7$ s^{-1} so that the left hand side of (A.11) is $\sim 0.05 \ll 1$.

In the presence of a constant magnetic field, the same procedure can be applied with the additional term accounting for the presence of the magnetic field [*Davydov*, 1937]

$$\frac{\partial f_0}{\partial t} = \frac{e}{3mv^2}\frac{\partial}{\partial v}\left(v^2\vec{E}\cdot\vec{f}_1\right) + \frac{1}{2v^2}\frac{\partial}{\partial v}\left[v^2\delta\nu_{el}\left(\frac{T}{m}\frac{\partial f_0}{\partial v} + vf_0\right)\right] + S_{0in} \tag{A.12}$$

---

* These approximations are equivalent to an assumption that the higher order expansion terms of the distribution function vary with the same time scale ($\sim 1/\omega$) as the electric field.

† Holds true for EM pulses from lightning with VLF type spectra in the lower ionosphere (see Appendix C for numerical values and additional discussion).

‡ This approximation holds true for a Maxwellian distribution for $v \sim \bar{v}$, and is used only for illustrative purposes here.

$$\frac{\partial \vec{f}_1}{\partial t} = \frac{e\vec{E}}{m}\frac{\partial f_0}{\partial v} + \frac{e}{mc}\left[\vec{B} \times \vec{f}_1\right] - \nu \vec{f}_1 \tag{A.13}$$

The influence of the external magnetic field on the motion of energetic electrons in the lower ionosphere is weak (see Section 3.4 for details) and the equations (A.12) and (A.13) are valid to first order under the same conditions as (A.10) or (A.11).

B

Electron Impact Excitation Cross Sections

Plots of the electron impact cross sections for the excitation of the chosen optical emissions as a function of electron energy are shown in Figure B.1. The data on electron impact excitation from the ground states compiled in this figure were taken from the following sources: for ^1D and ^1S states of O [*Doering and Gulcicek*, 1989], for $b^1\Sigma_g^+$ and $A^3\Sigma_u^+$ states of O_2 [*Rees*, 1989, Appendix 4 and references therein], for $C^3\pi_u$ and $B^3\pi_g$ states of N_2 [*Cartwright et al.* 1977] with 30 % reduction in accordance with *Phelps* [1987] for the $C^3\pi_u$ state, for $A^2\pi_u$ and $B^2\Sigma_u^+$ states of N_2^+ [*Cartwright et al.* 1975], for $b^4\Sigma_g^-$ state of O_2^+ [*Watson et al.* 1967].

Plots of the electron impact cross sections for elastic, dissociative, dissociative with attachment, ionizing, and vibrational excitations of N_2 and O_2 are shown in Figure B.2. The data on electron impact cross sections compiled in this figure were taken from the following sources: for elastic and vibrational collisions of electons with N_2 and O_2 [*Phelps*, 1985], for the dissociative attachment of electrons to O_2 [*Schulz*, 1962], for the ionization [*Mark*, 1975], for the dissociation from [*Tsang et al.*, 1991].

The specific value of the rotational constant of N_2 is 2.48×10^{-4} eV= 2.9^o K and of O_2 is 1.79×10^{-4} eV= 2.1^o K [*Herzberg*, 1950].

Also [*Murphy*, 1988] is a good general reference concerning electron collision cross sections for O_2 and N_2.

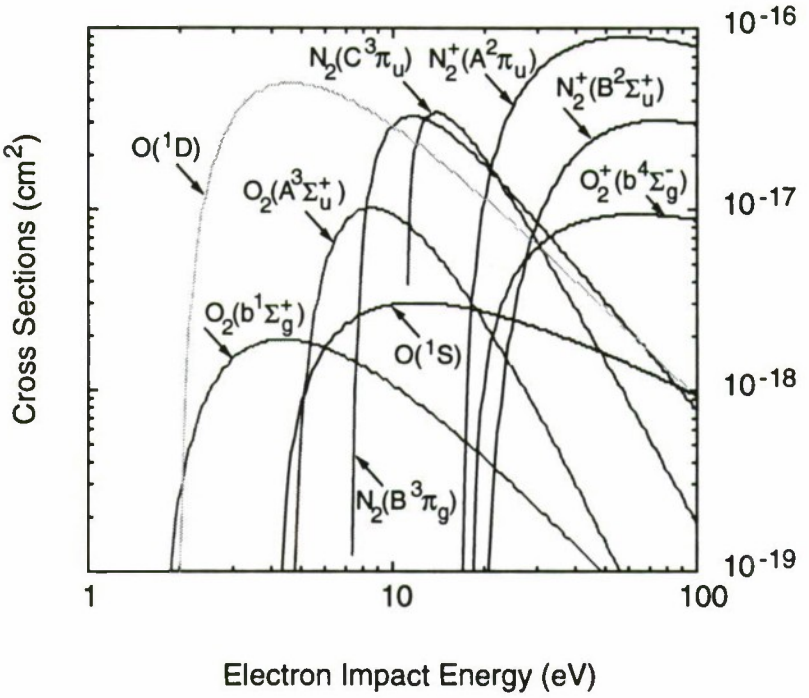

Fig. B.1. Electron impact cross sections for optical emissions. References for each particular line are given in the text.

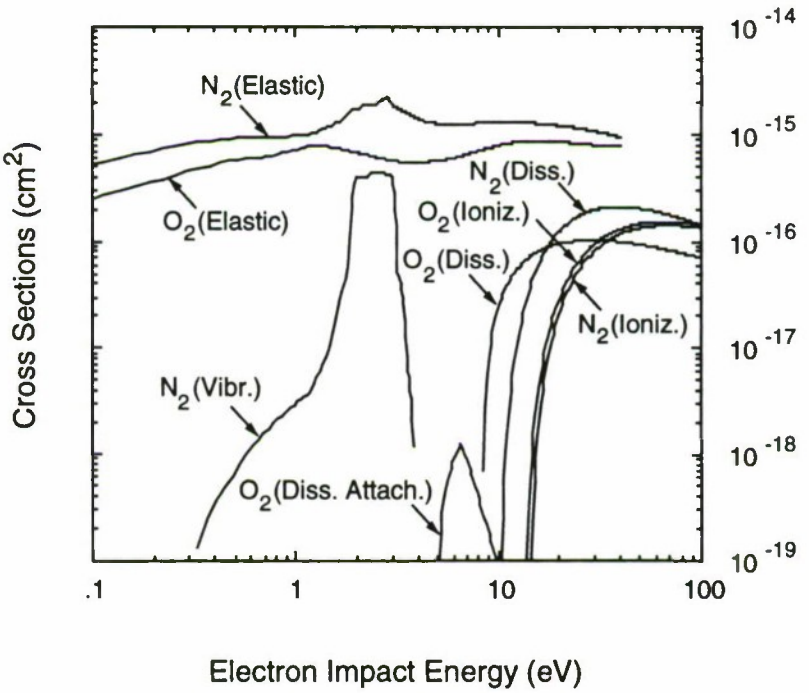

Fig. B.2. Electron impact cross sections. References for each particular line are given in the text.

C

Numerical Algorithms

C.1 THE BOLTZMANN KINETIC EQUATION

In the numerical solution of equations (2.4)-(2.6) we take into account the fact that the total collision frequency ν of electrons with neutrals is much larger than the typical characteristic frequency of the EM pulse ($\partial/\partial t$) and neglect the time derivative in equation (2.5). To support this assumption we note that even at 100 km altitude the collision frequency for cold ambient electrons is $\sim 3\times 10^4$ Hz (see for example Figure 1 in [*Taranenko et al.,* 1992]), which is still larger than 10 kHz, the value of the central frequency of the pulse used in our calculations. Also, the collision frequency increases substantially during heating and exponentially increases with decreasing altitude, so that this assumption is fully valid for the problem at hand over the altitude range of interest.

After neglecting the time derivative in equation (2.5), f_1 can be expressed in a straight forward way as a function of f_0 and such an expression can be substituted into (2.4) to give us an equation describing the evolution of f_0 under the influence of the electric field. For example, for $\vec{E} \parallel \vec{B}_o$ the procedure described above gives

$$\frac{\partial f_0}{\partial t} = \frac{e^2E^2}{3m^2v^2}\frac{\partial}{\partial v}\left(\frac{v^2}{\nu}\frac{\partial f_0}{\partial v}\right) + \frac{1}{2v^2}\frac{\partial}{\partial v}\left[v^2\delta\nu_{el}\left(\frac{T}{m}\frac{\partial f_0}{\partial v} + v f_0\right)\right] + S_{0in} \qquad \text{(C.1)}$$

Without S_{0in} this equation is a Fokker-Plank equation which appears in many branches of physical sciences [*Risken*, 1984]. Hence, one of the ways to treat (C.1) is to consider

it as a combination of the Fokker-Plank equation and an operator S_{0in} that transports electrons to lower energies due to inelastic loss processes at each time step (assuming discrete representation for the time and velocity variables). In our computer model we used the *Chang and Cooper* [1970] differencing scheme to represent the Fokker-Plank part of equation (C.1).

Another way to solve equation (C.1) is to convert it to the Boltzmann transport equation for electrons in energy space and represent it in discrete form [*Rockwood and Green*, 1980] as

$$\frac{dn_k}{dt} = \sum_l C_{lk} n_l \tag{C.2}$$

where n_k is the number of electrons per unit volume per unit energy in the energy interval $(\varepsilon_{k+1} - \varepsilon_k)$. The matrix elements C_{lk} are constants (for a given electric field) which represent the rate of transfer of electrons from energy ε_l to ε_k due to elastic and inelastic collisions.

It turns out that both of the two approaches are basically the same since in the discrete representation velocity derivatives describe transport of electrons between adjacent grid cells.

A FORTRAN computer code for solving equation (C.1) can be obtained from the VLF group of STAR Laboratory of Stanford University.

C.2 MAXWELL EQUATIONS

To describe the propagation of EM fields we numerically solve Maxwell's equations (2.1). Each of the two Maxwell equations can be treated as a parabolic equation in discrete space and time meshes and any of many different numerical methods for such equations can be applied. A good summary of such methods can be found in Table 3.1 of *Potter* [1973]. In our realization we used the Lax-Wedroff method. The mapping of the electric field amplitudes to the electric current density was done by solving equations (2.4)-(2.6) for

the electron distribution function in the way described above. The multi-slab technique that uses the steady state solution of the Boltzmann equation is described in Section 2.4.

A FORTRAN computer code for solving Maxwell's equations (2.1) as applicable to this particular problem can be obtained from VLF group of STAR Laboratory of Stanford University.

D

Quenching and Emission Rates

This appendix consists of a table of quenching and emission rates given on the next page. Each reaction in the Table that contains an $h\nu$ on its r.h.s. represent optical emissions while others represent quenching reactions. For convenience of readers the optical transitions are summarized as follows: 6300 (6364) $\mathring{A}$ ($^1D \rightarrow {}^3P$ transitions), and the green 5577 $\mathring{A}$ ($^1S \rightarrow {}^1D$ transitions) lines of O; the blue to UV 2nd positive band ($C^3\pi_u \rightarrow B^3\pi_g$ transitions) and red to IR 1st positive band ($B^3\pi_g \rightarrow A^3\Sigma_u^+$ transitions) of N_2; the blue 1st negative band ($B^2\Sigma_u^+ \rightarrow X^2\Sigma_g^+$ transition) and IR Meinel band ($A^2\pi_u \rightarrow X^2\Sigma_g^+$ transition) of N_2^+ ions; and the red 1st negative band ($b^4\Sigma_g^- \rightarrow a^4\pi_u$) of O_2^+ ions.

TABLE D1. Quenching and Emission Rates

Reaction	Rates ($cm^3\ s^{-1}$ or s^{-1})
$O(^1D) \rightarrow O + h\nu$	9.34×10^{-3}*
$O(^1D) + N_2 \rightarrow O + N_2$	$2.0 \times 10^{-11} \exp(107.8/T)$*
$O(^1D) + O_2 \rightarrow O + O_2$	$2.9 \times 10^{-11} \exp(67.5/T)$*
$O(^1D) + O \rightarrow O + O$	8×10^{-12}*
$O(^1S) \rightarrow O(^1D) + h\nu$	1.07*
$O(^1S) \rightarrow O + h\nu$	0.0444*
$O(^1S) + O_2 \rightarrow O + O_2$	$4.9 \times 10^{-12} \exp(-885/T)$*
$O(^1S) + O \rightarrow O + O$	2×10^{-14}*
$N_2(C^3\pi_u) \rightarrow N_2(B^3\pi_g) + h\nu$	2×10^7‡
$N_2(C^3\pi_u) + O_2 \rightarrow O_2 + N_2$	3×10^{-10}‡
$N_2(B^3\pi_g) \rightarrow N_2(A^3\Sigma_u^+) + h\nu$	1.7×10^5‡
$N_2(B^3\pi_g) + N_2 \rightarrow N_2 + N_2$	10^{-11}‡
$N_2^+(B^2\Sigma_u^+) \rightarrow N_2^+(X^2\Sigma_g^+) + h\nu$	1.4×10^6‡
$N_2^+(B^2\Sigma_u^+) + N_2 \rightarrow N_2 + N_2$	4×10^{-10}‡
$N_2^+(A^2\pi_u) \rightarrow N_2^+(X^2\Sigma_g^+) + h\nu$	7×10^4‡
$N_2^+(B^2\Sigma_u^+) + N_2 \rightarrow N_2 + N_2$	5×10^{-10}‡
$O_2^+(b^4\Sigma_g^-) \rightarrow O_2^+(a^4\pi_u) + h\nu$	8.5×10^4‡
$O_2^+(b^4\Sigma_g^-) + N_2 \rightarrow O_2 + N_2$	2×10^{-10}‡

* *Torr et al.* [1990]

‡ *Vallance Jones* [1974] (p. 115, 119)

Bibliography

Allis, W. P., Motions of ions and electrons, *Encyclopedia of Physics*, vol. 21, p. 404, Berlin: Springer-Verlag, 1956.

Appleton, E. V., and R. Naismith, Weekly measurements of upper-atmospheric ionization, *Proc. Phys. Soc.*, vol. 45, pp. 389-398, 1933.

Armstrong, W. C., Recent advances from studies of the Trimpi effect, *Antarctic Journal*, vol. 18, p. 281, 1983.

Bailey, M. A., and D. F. Martyn, The influence of electric waves on the ionosphere, *Phil. Mag.S.7,* vol. 18, pp. 369-387, 1934.

Banks, P. M., and G. Kockarts, *Aeronomy*, Academic Press, New York, 1973.

Barr, R., M. T. Rietveld, P. Stubbe, and H. Kopka, The diffraction of VLF radio waves by a patch of ionosphere illuminated by a powerful HF transmitter, *J. Geophys. Res.*, vol. 90, pp. 2861-2875, 1985.

Bell, T. F., ULF wave generation through particle precipitation induced by VLF transmitters, *J. Geophys. Res.*, vol. 81, pp. 3316-3326, 1976.

Boeck, W. L., O. H. Vaughan, Jr., R. Blakeslee, B. Vonnegut, and M. Brook, Lightning induced brightening in the airglow layer, *Geophys. Res. Lett.*, vol. 19, pp. 99-102, 1992.

Brook, M., R. W. Henderson, and R. B. Pyle, Positive lightning strokes to ground, *J. Geophys. Res.*, vol. 94, p. 13,295, 1989.

Burgess, W. C., and U. S. Inan, The role of ducted whistlers in the precipitation loss and equilibrium flux of radiation belt electrons, *J. Geophys. Res.*, vol. 98, pp. 15,643-15,665, 1993.

Cartwright, D. C., W. R. Pendleton, Jr., and L. D. Weaver, Auroral emission of the N_2^+ Meinel bands, *J. Geophys. Res.*, vol. 80, pp. 651-654, 1975.

Cartwright, D. C., S. Trajmar, A. Chutjian, and W. Williams, Electron impact excitation of the electronic states of N_2. II. Integral cross sections at incident energies from 10 to 50 eV, *Phys. Rev. A*, vol. 16, pp. 1041-51, 1977.

Chamberlain, J. W., *Theory of planetary atmospheres*, Academic Press, New York, 1978.

Chambers, J. A., *Atmospheric Electricity*, p. 307, Pergamon, London, 1967.

Chang, J. S., and G. Cooper, A practical difference scheme for Fokker-Planck equations, *J. Comp. Phys.*, vol. 6, pp. 1-16, 1970.

Davydov, B., On the theory of the motion of electrons in gases and semi-conductors. *Phys. Zeit. der Sow.*, vol. 12, pp. 269-300, 1937.

Doering, J. P. and E. E. Gulcicek, Absolute differential and integral electron excitation cross sections for atomic oxygen 7. The $^3P \rightarrow {}^1D$ and $^3P \rightarrow {}^1S$ transitions from 4.0 to 30 eV, *J. Geophys. Res.*, vol. 94, pp. 1541-1546, 1989.

Donahue, T. M. and D. J. Strickland, Excitation and radiative transport of OI 1304 Å resonance radiation – II, *Planet. Space Sci.*, vol. 18, pp. 691-697, 1970.

Fenn, R. W., S. A. Clough, W. O. Gallery, R. E. Good, F. X. Kneizys, J. D. Mill, L. S. Rothman, E. P. Shettle, and F. E. Volz, Optical and infrared properties of the atmosphere, in *Handbook of Geophysics and the Space Environment*, p. 18-1 to 18-80, AFGL, Hanscom, MA, NTIS, 1985.

Field, E. C. Jr., and M. Lewinstein, Amplitude - probability distribution model for VLF/ELF atmospheric noise, *IEEE Transactions on Communications*, vol. COM-26, pp. 83-87, 1978.

Fraser-Smith, A. C., ULF magnetic field generated by electrical storms and their significance to geomagnetic pulsation generation, *Geophys. Res. Lett.*, vol. 20, pp. 467-470, 1993.

Friedrich, M., and K. M. Torkar, An empirical model of the nonauroral D region, *Radio Science*, vol. 27, pp. 945-953, 1992.

Glukhov, V. S., V. P. Pasko, and U. S. Inan, Relaxation of transient lower ionospheric disturbances caused by lightning-induced electron precipitation bursts, *J. Geophys. Res.*, vol. 88, pp. 16,971-16,979, 1992.

Gurevich, A. V., *Nonlinear phenomena in the ionosphere*, Berlin: Springer-Verlag, 1978.

Hedin, A. E., MSIS-86 thermospheric model, *J. Geophys. Res.*, vol. 92, pp. 4649-46, 1987.

Helliwell, R. A., *Whistlers and related ionospheric phenomena*, Stanford, Stanford University Press, 1965.

Herzberg, G. *Spectra of diatomic molecules*, Princeton, Van Nostrand, 1950.

Hochstrasser, U. W., Ortogonal Polynomials, in *Handbook of mathematical functions with formulas, graphs, and mathematical tables*, pp. 773-802, United States Department of Commerce, National Bureau of Standards, 1972.

Holstein, T., Energy distribution of electrons in high-frequency gas discharges, *Phys. Rev.* vol. 70, p. 367, 1946.

Inan, U. S., Gyroresonant pitch angle scattering by coherent and incoherent whistler mode waves in the magnetosphere, *J. Geophys. Res.*, vol. 92, pp. 127-142, 1987.

Inan, U. S., VLF heating of the lower ionosphere, *Geophys. Res. Lett.*, vol. 17, pp. 729-732, 1990.

Inan, U. S., and D. L. Carpenter, Lightning-induced electron precipitation events observed at $L = 2.4$ as phase and amplitude perturbations on subionospheric VLF signals, *J. Geophys. Res.*, vol. 92, pp. 3293, 1987.

Inan, U. S., T. G. Wolf, and D. L. Carpenter, Geographic distribution of lightning induced electron precipitation observed as VLF/LF perturbation events, *J. Geophys. Res.*, vol. 93, pp. 9841-9853, 1988*a*.

Inan, U. S., D. C. Shafer, W. Y. Yip, and R. E. Orville, Subionospheric VLF signatures of nighttime D region perturbations in the vicinity of lightning discharges, *J. Geophys. Res.*, vol. 93, pp. 11,455-11,472, 1988*b*.

Inan, U. S., F. A. Knifsend, and J. Oh, Subionospheric VLF 'imaging' of lightning-induced electron precipitation from the magnetosphere, *J. Geophys. Res.*, vol. 95, pp. 17,217-17,231, 1990.

Inan, U. S., T. F. Bell, and J. V. Rodriguez, Heating and ionization of the lower ionosphere by lightning, *Geophys. Res. Lett.*, vol. 18, p. 705, 1991.

Inan, U. S., J. V. Rodriguez, S. Lev_tov, and J. Oh, Ionospheric modification with a VLF transmitter, *Geophys. Res. Lett.*, vol. 19, pp. 2071-2074, 1992.

Inan, U. S., J. V. Rodriguez, and V. P. Idone, VLF signatures of lightning-induced heating and ionization of the nighttime D-region, (in press) *Geophys. Res. Lett.*, 1993.

Isted, G. A., Irregularities in the E region caused by atmospheric electricity, in *Report of the Physical Society Conference on the Physics of the Ionosphere*, p. 105, Physical Society, London, 1954.

Krider, E. P., On the electromagnetic fields, poynting vector, and peak power radiated by lightning return strokes, *J. Geophys. Res.*, vol. 97, p. 15,913-15,917, 1992.

Krider, E. P., and C. Guo, The peak electromagnetic power radiated by lightning return strokes, *J. Geophys. Res.*, vol. 88, p. 8471, 1983.

Kucherov, K. I., and A. P. Nikolaenko, Heating of electrons in the lower ionosphere by horizontal lightning discharges, *Izvestiya Vysshikh Uchebnykh Zavedenii, Radiofizika,* vol. 7, pp. 894-896, 1979.

Lin, Y. T., M. A. Uman, J. A. Tiller, R. D. Brantley, W. H. Beasley, E. P. Krider, and C. D. Weidman, Characterization of lightning return stroke electric and magnetic fields from simultaneous two-station measurements, *J. Geophys. Res.*, vol. 84, pp. 6307-6314, 1979.

Mark, T. D., Cross section for single and double ionization of N_2 and O_2 molecules by electron impact from threshold up to 170 eV, *J. Chem. Phys.*, vol. 63, pp. 3731-3736, 1975.

Mitra, A. P., Chemistry of middle atmospheric ionization – a review, *J. Atmos. Terr. Phys.*, vol. 43, pp. 737-752, 1981.

Murphy, T., Total and differential electron collision cross sections for O_2 and N_2, *Los Alamos National Laboratory Report No. LA-11288-MS*, 1988.

Opal, C. B., W. K. Peterson, and E. C. Beaty, Measurements of secondary-electron spectra produced by electron impact ionization of a number of simple gases, *J. Chem. Phys.*, vol. 55, pp. 4100-4106, 1971.

Pasko, V. P., and U. S. Inan, Recovery signatures of lightning-associated VLF perturbations as a measure of the lower ionosphere, submitted to *J. Geophys. Res.*, 1993.

Phelps, A. V., Excitation and ionization coefficients, *Gaseous Dielectric*, vol. 5, 1987, pp. 1-9, 1987.

Potter, D., *Computational physics*, London, New York, J. Wiley, 1973.

Poulsen, W. L., T. F. Bell, and U. S. Inan, Three-dimensional modeling of subionospheric VLF propagation in the presence of localized D region perturbations associated with lightning, *J. Geophys. Res.*, vol. 95, p. 2355, 1990.

Ratcliffe, J. A., *The magneto-ionic theory and its applications to the ionosphere*, Cambridge at the University Press, 1959.

Reagan, J. B. et al, Modeling of the ambient and disturbed ionospheric media pertinent to ELF/VLF propagation, *Proc. of NATO-AGARD meeting on medium, long, and very long wave propagation*, Brussels, Belgium, September 1981.

Rees, M. H., *Physics and chemistry of the upper atmosphere*, Cambridge University Press, Cambridge, 1989.

Richards, P. G., and D. G. Torr, Auroral modeling of the 3371Å emission rate: dependence on characteristic electron energy, *J. Geophys. Res.*, vol. 95, pp. 10,337-10,344, 1990.

Risken, H., *The Fokker-Planck equation : methods of solution and applications*, Berlin, New York: Springer-Verlag, 1984.

Rodriguez, J. V., U. S. Inan, and T. F. Bell, D region disturbances caused by electromagnetic pulses from lightning, *Geophys. Res. Lett.*, vol.19, pp. 2067-2070, 1992.

Rodriguez, J. V., Modification of the Earth's ionosphere by very-low-frequency transmitters, *Ph.D. Thesis*, Stanford, 1993.

Rockwood, S.D. and A.E. Green, Numerical solutions of the Boltzmann transport equation, *Comp. Phys. Communic.*, vol. 19, pp. 377-393, 1980.

Schulz, G. J., Cross sections and electron affinity for O^- ions from O_2, CO, and CO_2 by electron impact, *Phys. Rev.*, vol. 128, pp. 178-186, 1962.

Sipler, D. P., and M. A. Biondi, Measurements of $O(^1D)$ quenching rates in the F region, *J. Geophys. Res.*, vol. 77, pp. 6202-6212, 1972.

Short, R., D. Lallement, K. Papadopoulos, T. Wallace, A. Ali, P. Koert, R. Shanny, C. Stewart, A. Drobot, K. Chang, and P. Vitello, Physics studies in artificial ionospheric mirror (AIM) related phenomena, *Tech. Report*, GL-TR-90-0038, Geophysics Laboratory, AFSC, USAF, Hanscom Air Force Base, MA, 1990.

Taranenko, Y. N., U. S. Inan, and T. F. Bell, Optical signatures of lightning-induced heating of the D region, *Geophys. Res. Lett.*, vol. 19, pp. 1815-1818, 1992.

Taranenko, Y. N., U. S. Inan, and T. F. Bell, Interaction with the lower ionosphere of electromagnetic pulses from lightning: heating, attachment, and ionization, *Geophys. Res. Lett.*, vol. 20, pp. 1539-1542, 1993*a*.

Taranenko, Y. N., U. S. Inan, and T. F. Bell, Interaction with the lower ionosphere of electromagnetic pulses from lightning: optical emissions, in press *Geophys. Res. Lett.*, 1993*b*.

Thomas, R. J., Analyses of atomic oxygen, the green line, and Herzberg bands in the lower thermosphere, *J. Geophys. Res.*, vol. 86, pp. 206-210, 1981.

Tomko, A. A., A. J. Ferraro, H. S. Lee, and A. P. Mitra, A theoretical model of D-region ion chemistry modifications during high power radio wave heating, *J. Atmos. Terr. Phys.*, vol. 42, pp. 275-285, 1980.

Torr, M. R, D. G. Torr, and R. R. Laher, The O_2 atmospheric 0-0 band and related emissions at night from Spacelab 1, *J. Geophys. Res.*, vol. 90, pp. 8525-38, 1985.

Torr, M. R., D. G. Torr, P. G. Richards, and S. P. Yung, Mid- and low-latitude model of thermospheric emissions 1. $O^+(^2P)7320\mathring{A}$ and $N_2(2P)3371\mathring{A}$, *J. Geophys. Res.*, vol. 95, pp. 21,147-21,168, 1990.

Tsang, K., K. Papadopoulos, A. Drobot, P. Vitello, T. Wallace, and R. Shanny, RF ionization of the lower ionosphere, *Radio Science*, vol. 26, pp. 1345-1360, 1991.

Turman, B. N, Detection of lightning superbolts, *J. Geophys. Res.*, vol. 82, pp. 2566-2568, 1977.

Tzur, I., and R. G. Roble, The interaction of a dipolar thunderstorm with its global electrical environment, *J. Geophys. Res.*, vol. 90, p. 5989, 1985.

Uman, M. A., *The lightning discharge*, Academic Press, Orlando, 1987.

Vallance Jones, A., *Aurora*, D. Reidel publishing company, Dordrecht-Holland, 1974.

Voss, H. D., W. L. Imhof, J. Mobilia, E. E. Gaines, M. Walt, U. S. Inan, R. A. Helliwell, D. L. Carpenter, J. P. Katsufrakis, H. C. Chang, Lightning-induced electron precipitation, *Nature*, vol. 312, p. 740, 1984.

U.S. Standard Atmosphere, 1976, NOAA-S/T 76-1562, U.S. Government Printing Office, Washington, D.C., 1976.

Watson, C. E., V. A. Dulock, Jr., R. S. Stolarski, and A. E. S. Green, Electron impact cross sections for atmospheric species. 3. Molecular oxygen, *J. Geophys. Res.*, vol. 72, pp. 3961-66, 1967.

Weidman, C. D., and E. P. Krider, The radiation field wave forms produced by intracloud lightning discharge processes, *J. Geophys. Res.*, vol. 84, pp. 3159-3164, 1979.

Wilson, C. T. R., The electric field of a thundercloud and some of its effects, *Proc. Phys. Soc.*, vol. 37, pp. 32D-37D, 1925.

Zipf, E. C., Dissociation of molecules by electron impact, in *Electron-molecular interactions and their applications*, vol. 1, pp. 335-401, Academic Press, Inc., 1984.